Low temperature and timing properties of SIPMs

G.Collazuol
INFN Padova

Overview
- Introduction
- Low T measurements & discussion
- Timing measurements & discussion
- Conclusions

Introduction: building block of a SiPM → GM-APD

Diode reverse-biased above $V_{breakdown}$

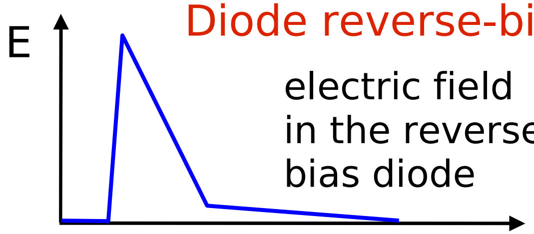

- t=0: carrier initiates the avalanche

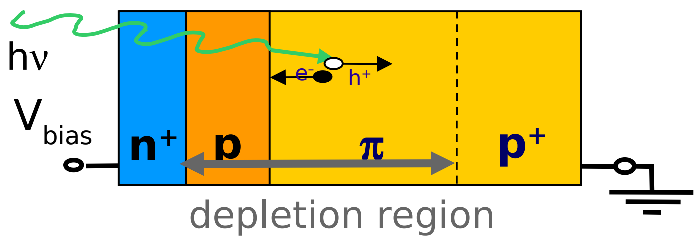

- $0<t<t_1$: avalanche spreading

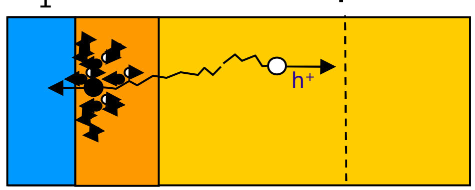

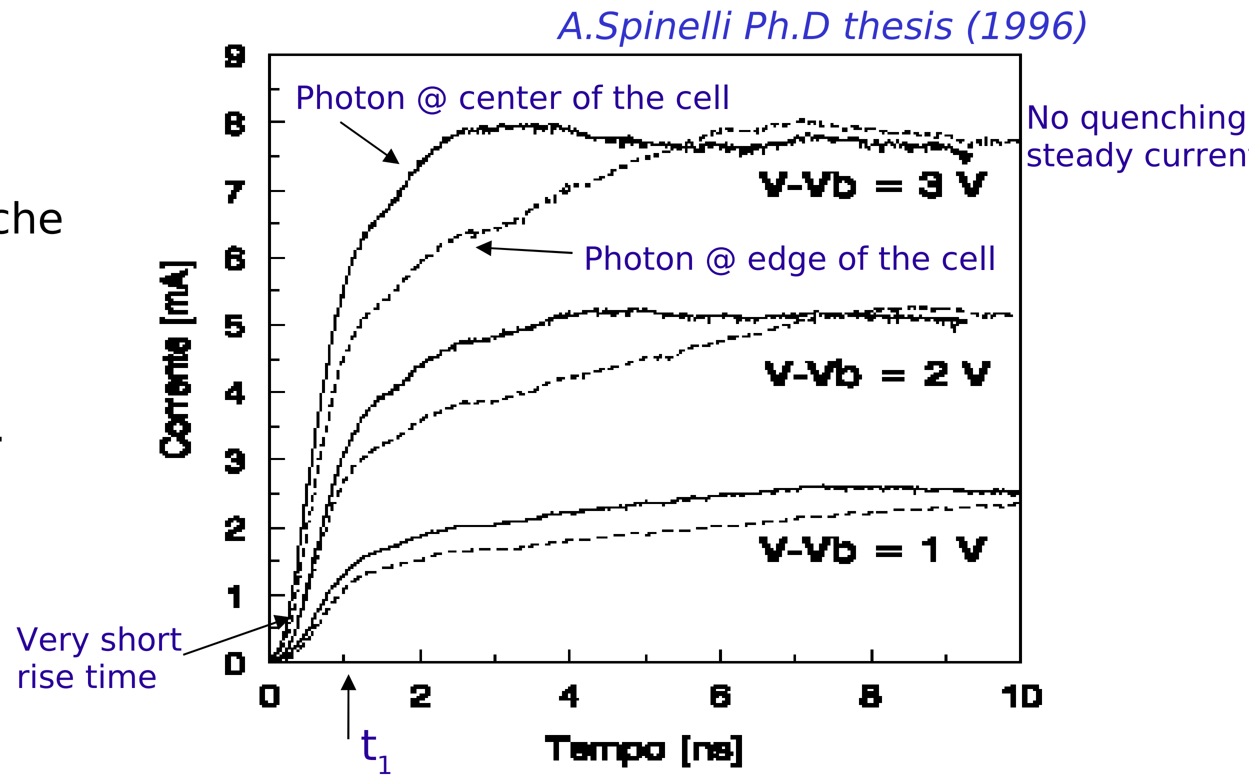

- $t_1<t$: self-sustaining current (limited by series R)

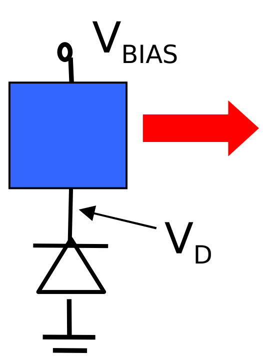

To detect another photon need a quenching mechanism. Two solutions:

- large resistance: passive quenching
- analog circuit: active quenching

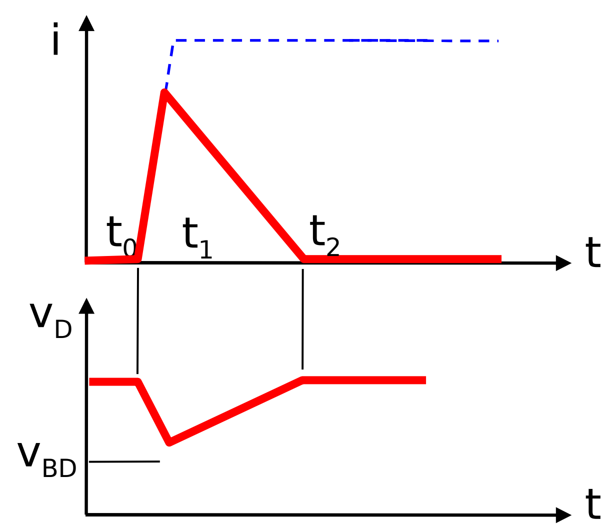

Operation principle of a GM-APD

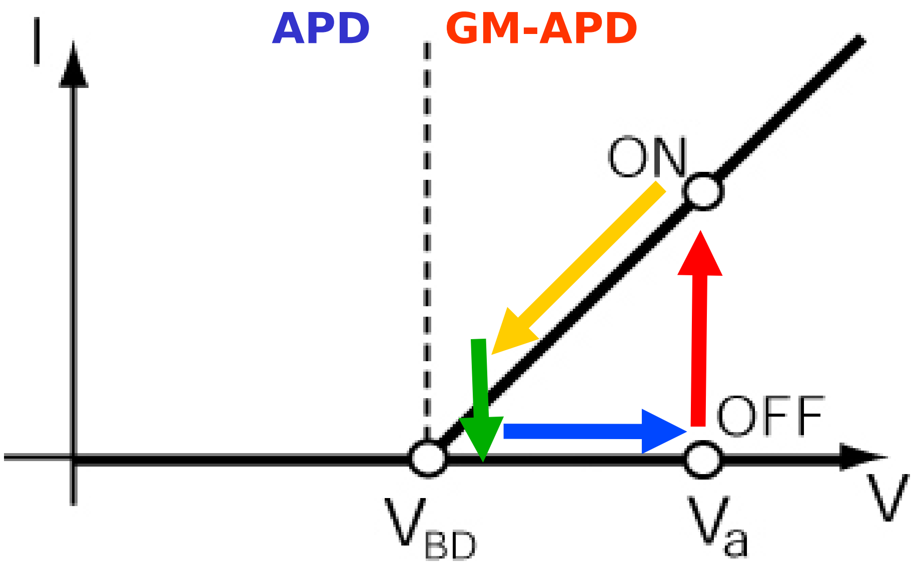

Haitz JAP 35 (1964)

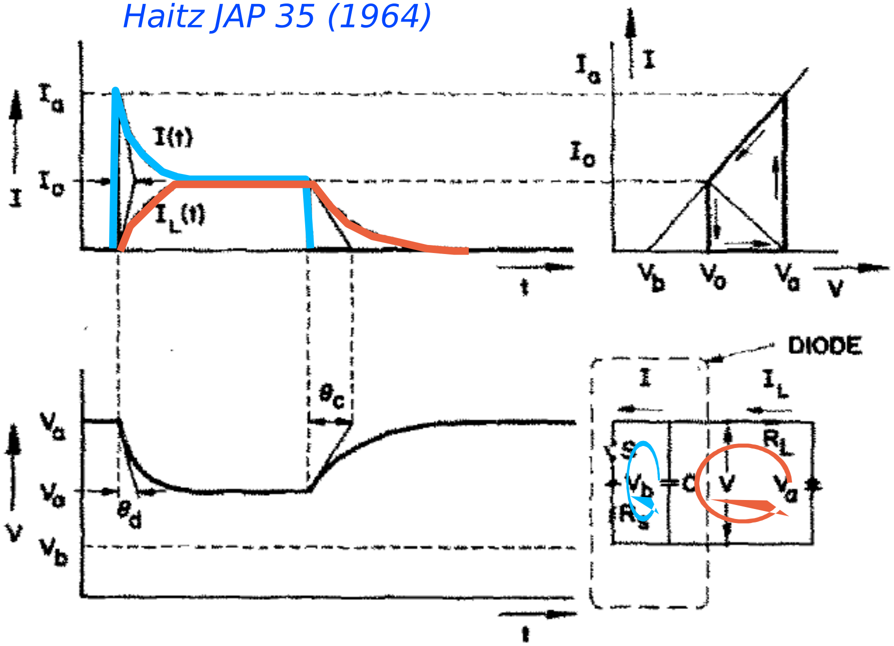

FIG. 3. Shape of current pulse for $\theta_d \ll \tau_1(I_0)$.

OFF condition: avalanche quenched, switch open, capacitance charged until no current flowing from V_{BD} to V_{BIAS} with time constant $R_q x C_d = \tau_{Quenching}$ (→ recovery time)

P_{01} = turn-on probability
probability that a carrier traversing the high-field region triggers the avalanche

P_{10} = turn-off probability
probability that the number of carriers traversing the high-field region fluctuates to 0

ON condition: avalanche triggered, switch closed
C_D discharges to V_{BD} with a time constant $R_S x C_D = \tau_{discharge}$,
at the same time the external current asymptotic grows to $(V_{BIAS}-V_{bd})/(R_q+R_s)$

Signal shape, Gain and Recovery time

Fast Capacitor (cell) discharge and slow recharge (roughly speaking)

If R_q is high enough the internal current decreases at a level such that statistical fluctuations quench the avalanche: need $i_{latch} \sim \Delta V/(R_q+R_d) \sim 10\mu A$

"Overvoltage" $\Delta V \equiv (V_{bias}-V_{Breakdown})$

With usual R_q values turn-off time is very short O(1ns)

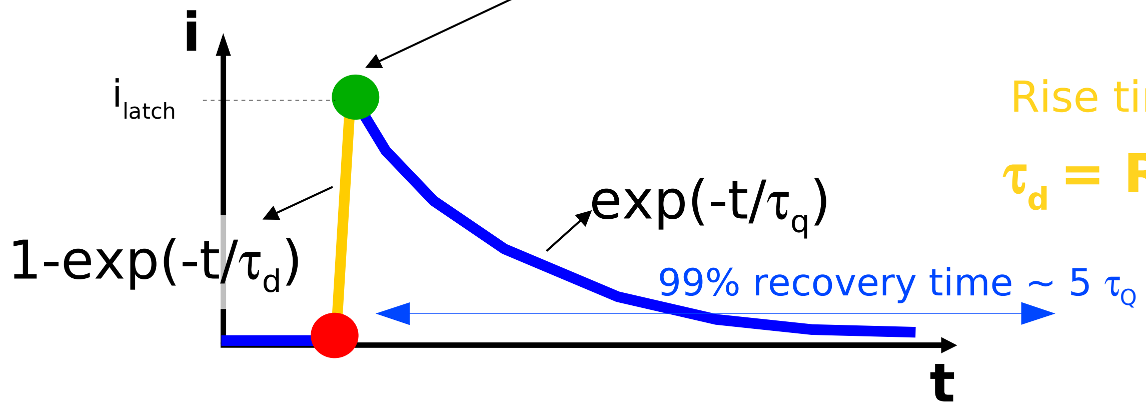

Rise time $\tau_d = R_d C_d$ $\ll$ Falling time (recovery) $\tau_q = R_q C_d$

Recovery time: increases at low T due to polysilicon R_q while C_d is independent of T

also rise time expected to be T dependent (silicon R_d vs T)

Gain~$C_d\,\Delta V$ → independent of T

at fixed Over-Voltage (ΔV)

G.Collazuol - DIRC2011 4/6/2011

SiPM equivalent circuit (detailed model)

Single cell model → $(R_d||C_d)+(R_q||C_q)$

SiPM + load → $(||Z_{cell})||C_{grid} + Z_{load}$

Signal = slow pulse ($\tau_{d\ (rise)}, \tau_{q\text{-}slow\ (fall)}$) +

+ fast pulse ($\tau_{d\ (rise)}, \tau_{q\text{-}fast\ (fall)}$)

- $\tau_{d\ (rise)} \sim R_d(C_q+C_d)$
- $\tau_{q\text{-}fast\ (fall)} = R_{load}\ C_{tot}$ (fast; parasitic spike)
- $\tau_{q\text{-}slow\ (fall)} = R_q\ (C_q+C_d)$ (slow; cell recovery)

F.Corsi, et al. NIM A572 (2007)

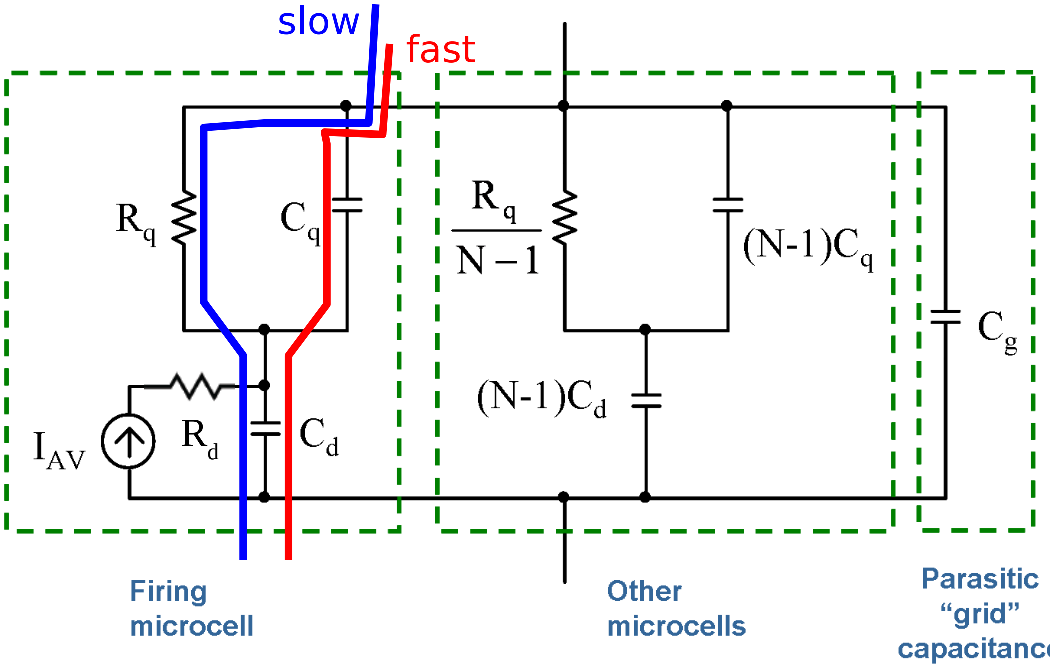

→ Rise time degraded by parasitic inductance

Pulse shape

- Exponential rise
- Sum of two exponential fall

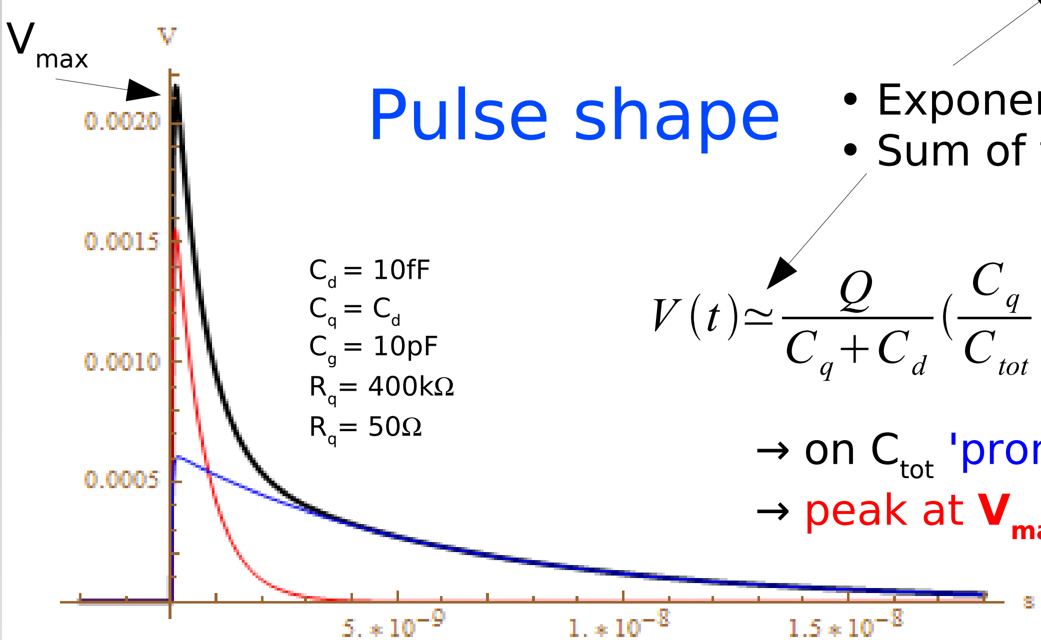

$$V(t) \simeq \frac{Q}{C_q+C_d}\left(\frac{C_q}{C_{tot}} e^{\frac{-t}{\tau_{FAST}}} + \frac{R_{load}}{R_q}\frac{C_d}{C_q+C_d} e^{\frac{-t}{\tau_{SLOW}}}\right)$$

→ on C_{tot} 'prompt' charge $\mathbf{Q_{fast} = Q\ C_q/(C_q+C_d)}$

→ peak at $\mathbf{V_{max} \sim Q_{fast}/C_{tot}}$ **is independent of R_{load}**

Pulse shape: dependence on Temperature

Single cell model → $(R_d||C_d)+(R_q||C_q)$
SiPM + load → $(||Z_{cell})||C_{grid} + Z_{load}$

Signal = slow pulse ($\tau_{d\ (rise)}, \tau_{q\text{-slow}\ (fall)}$) +
+ fast pulse ($\tau_{d\ (rise)}, \tau_{q\text{-fast}\ (fall)}$)

- $\tau_{d\ (rise)} \sim R_d(C_q+C_d)$
- $\tau_{q\text{-fast}\ (fall)} = R_{load}\ C_{tot}$ (fast; parasitic spike)
- $\tau_{q\text{-slow}\ (fall)} = R_q\ (C_q+C_d)$ (slow; cell recovery)

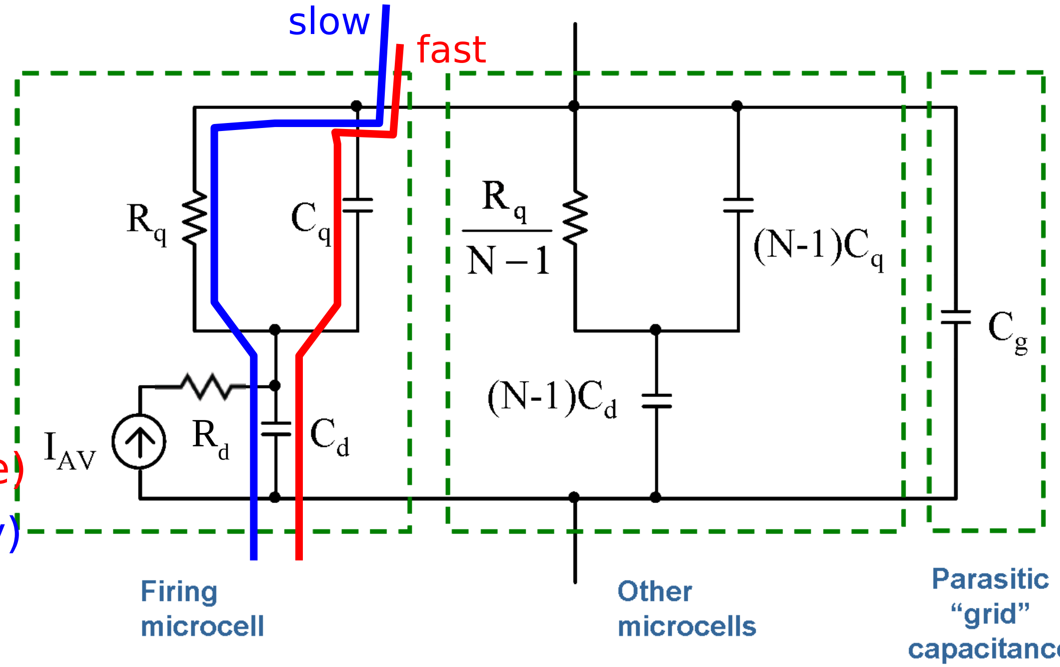

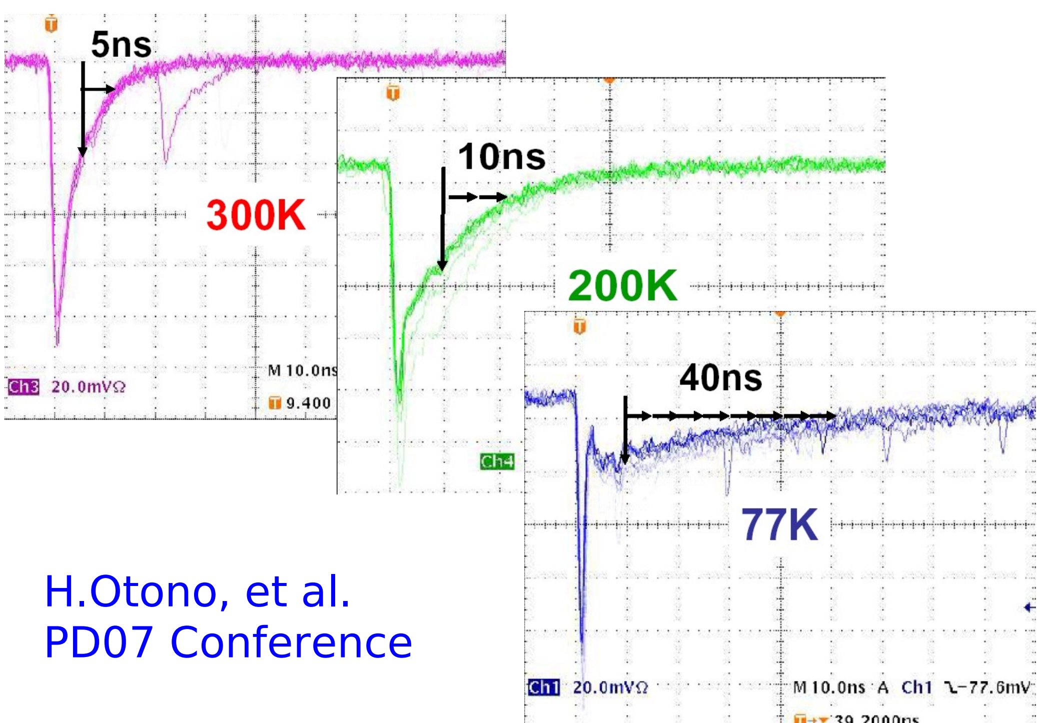

H.Otono, et al.
PD07 Conference

Pulse shape:

The two current components show different behavior with Temperature

→ fast component is independent of T because stray C_q couple with external R_{load} (no dependence on T) while R_q is strongly dependent on T

(we used low light level, BW filters against noise and AC coupling → difficult to disentangle the two components)

Overview – SiPM properties at low T

Complete characterization of FBK SIPM in the temperature range 50K<T<320K

1) junction characteristics: forward and reverse (breakdown)
2) gain, dark current, after-pulses, cross-talk
3) photon detection efficiency (PDE)

G.C. et al NIM A628 (2011) 389

→ Improved SiPM performances at low temperature (w/ respect to T room):

1) lower dark noise by several orders of magnitude
2) after-pulsing probability constant down to ~100K (then blow up)
3) PDE variations up to ±50% (depending on λ) down to ~100K
4) better timing resolution
5) better $V_{breakdown}$ stability against variations of T

→ SiPM is an excellent alternative to PMT at low T

...even more than at room temperature !!!

Experimental Setup

Vacuum vessel (P < 10^{-3} mbar)

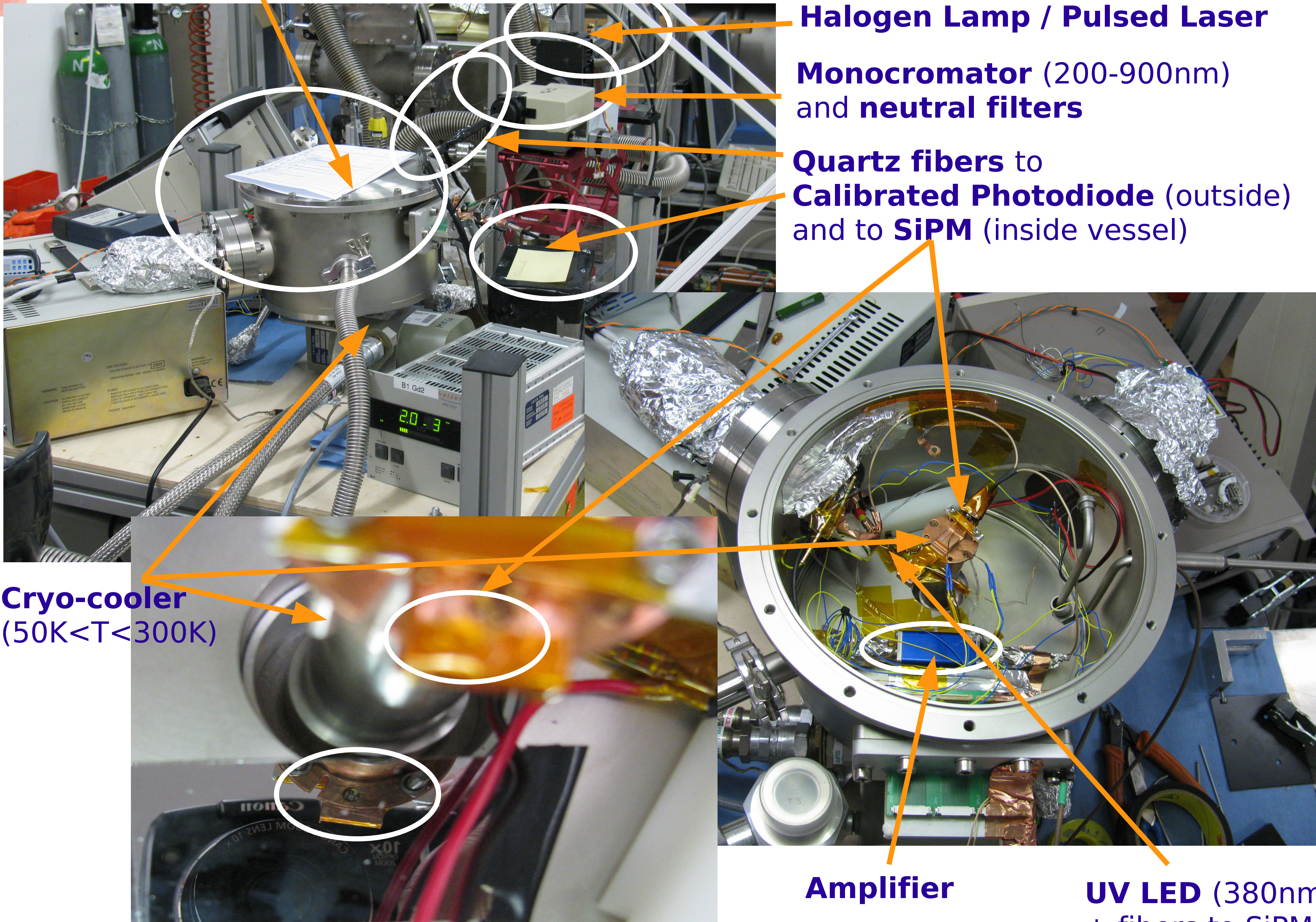

Halogen Lamp / Pulsed Laser

Monocromator (200-900nm) and **neutral filters**

Quartz fibers to **Calibrated Photodiode** (outside) and to **SiPM** (inside vessel)

Cryo-cooler (50K<T<300K)

Amplifier

UV LED (380nm) + fibers to SiPM

Experimental setup

Temperature control/measurement

- Close cycle, two stages, He cryo-cooler and heating with low R resistor
- Vacuum with P< 10^{-3} mbar
- thermal contact (critical) with cryo-cooler head: SIPM within a copper rod + kapton (electrical insulation)
- T measurement with 3 pt100 probes
- Measurements on SiPM carried after thermalization, ie all probes at the same T
- check junction T with forward characteristic

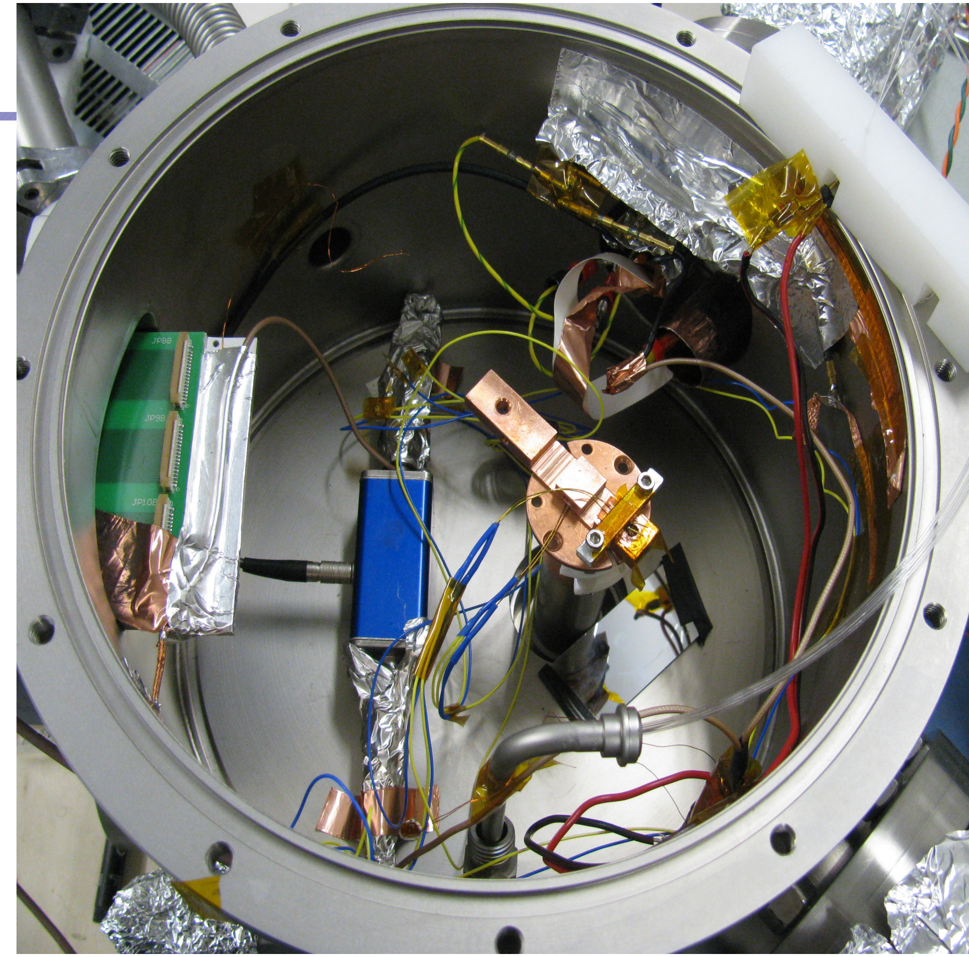

Light sources

- CW: halogen lamp and UV LED (λ~380nm)
- Pulsed: laser (30ps rms, λ~405nm)

V_{bias} and current measurements

- Keytley 2148
  Voltage/Current source/meter

Pulse/Waveform sampling

- Care against HF noise
  → feedthroughs !!!
- Amplifier Photonique/CPTA (gain~30, BW~300MHz)
- Lecroy o.scope, 1GHz, 20GS/s

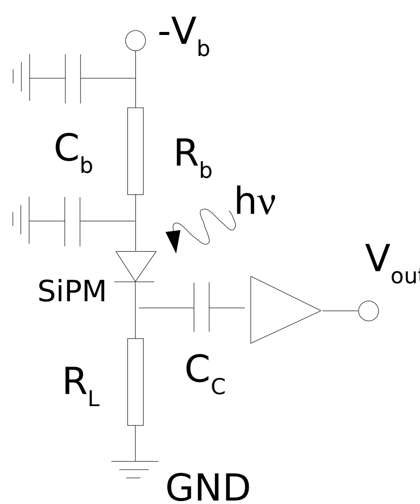

SiPM samples

FBK SiPM (2008) – 1mm²
(Vbr~33V, fill factor~20%)

- n-on-p shallow junction
- 4μm fully depleted region (active volume)
- no protective epoxy (epoxy cracks avoided)

I-V measurements: forward bias

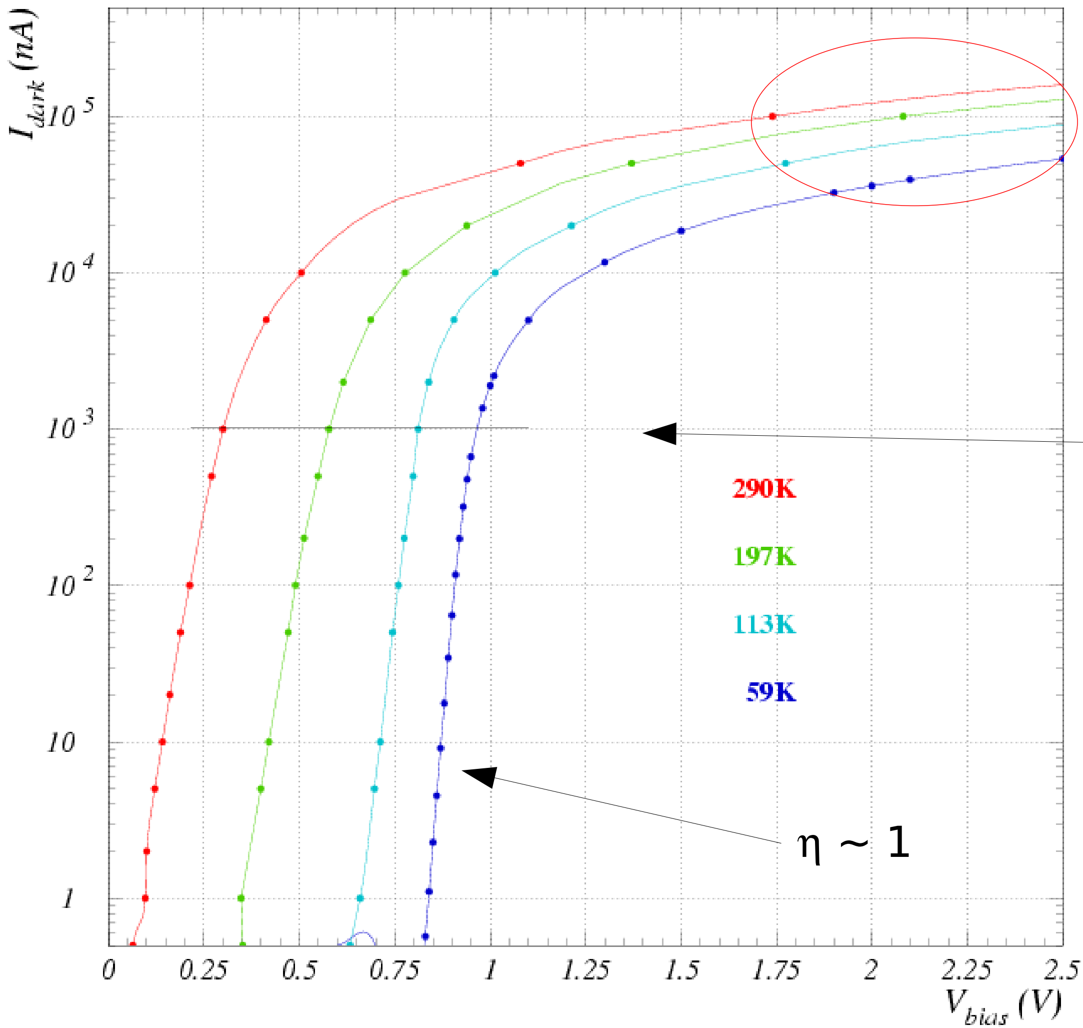

3 **Ohmic** behavior at high current

Linear fit → R_{series} ~ R_q / N_{cells}

2 **Voltage drop** (V_d) decreases linearly with T decreasing (e.g. at 1μA)

1 **Forward current** $J_F \sim \exp(V_d \frac{q}{\eta k T})$

Diffusion dominating: η → 1
Recombination dominating: η → 2

I-V measurements: forward bias

Voltage drop at fixed forward current → precise **measurement of junction T**...
... otherwise not trivially measured !

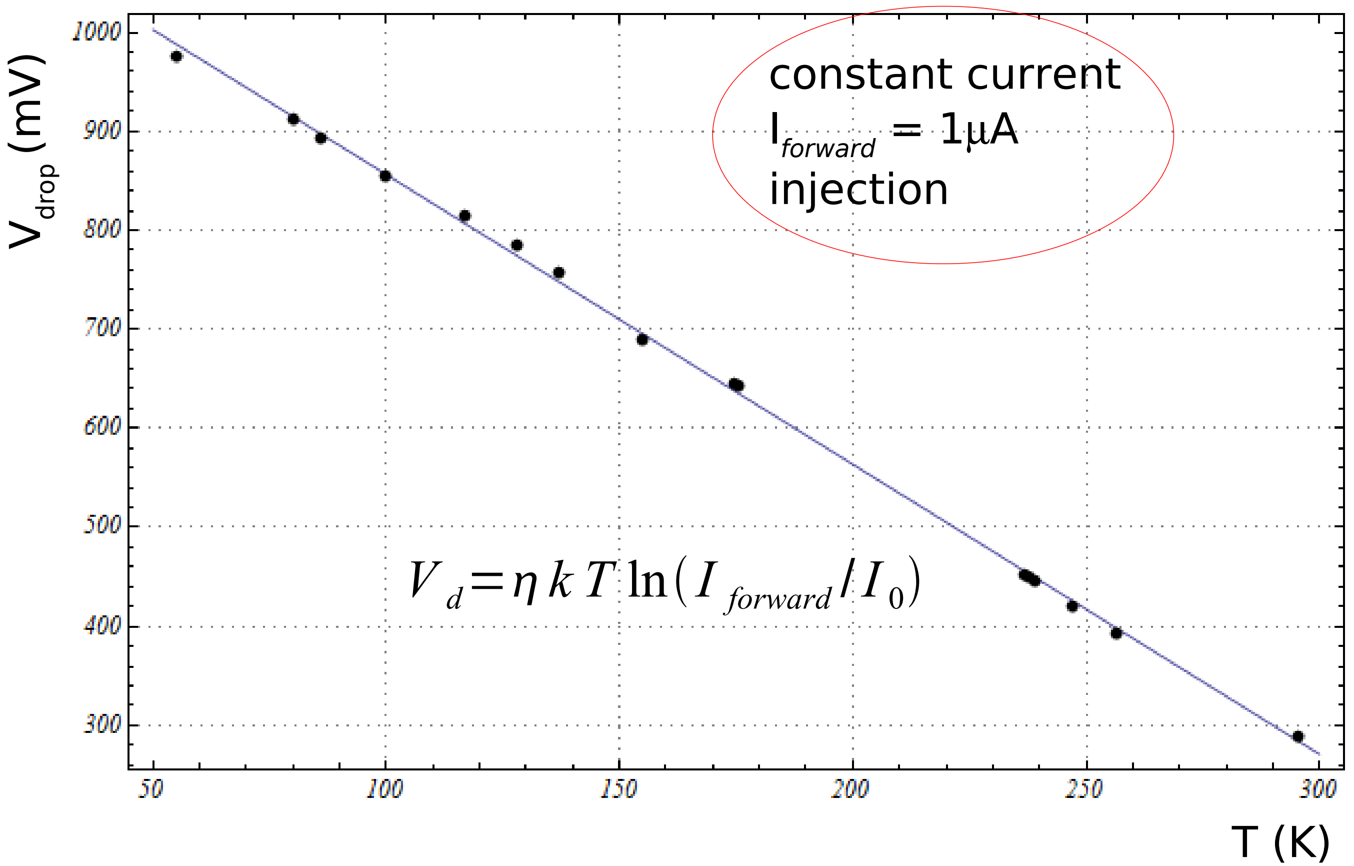

- linear dependence with slope $dV_{drop}/dT|_{1\mu A}$ ~ 3mV/K
- precise **calibration**/probe of junction Temperature

Series Resistance vs T

1) Fit at high V of forward characteristic → **measurement of series resistance R_s**

2) Exponential recovery time (afterpulses envelope) → **measurement of R_s**

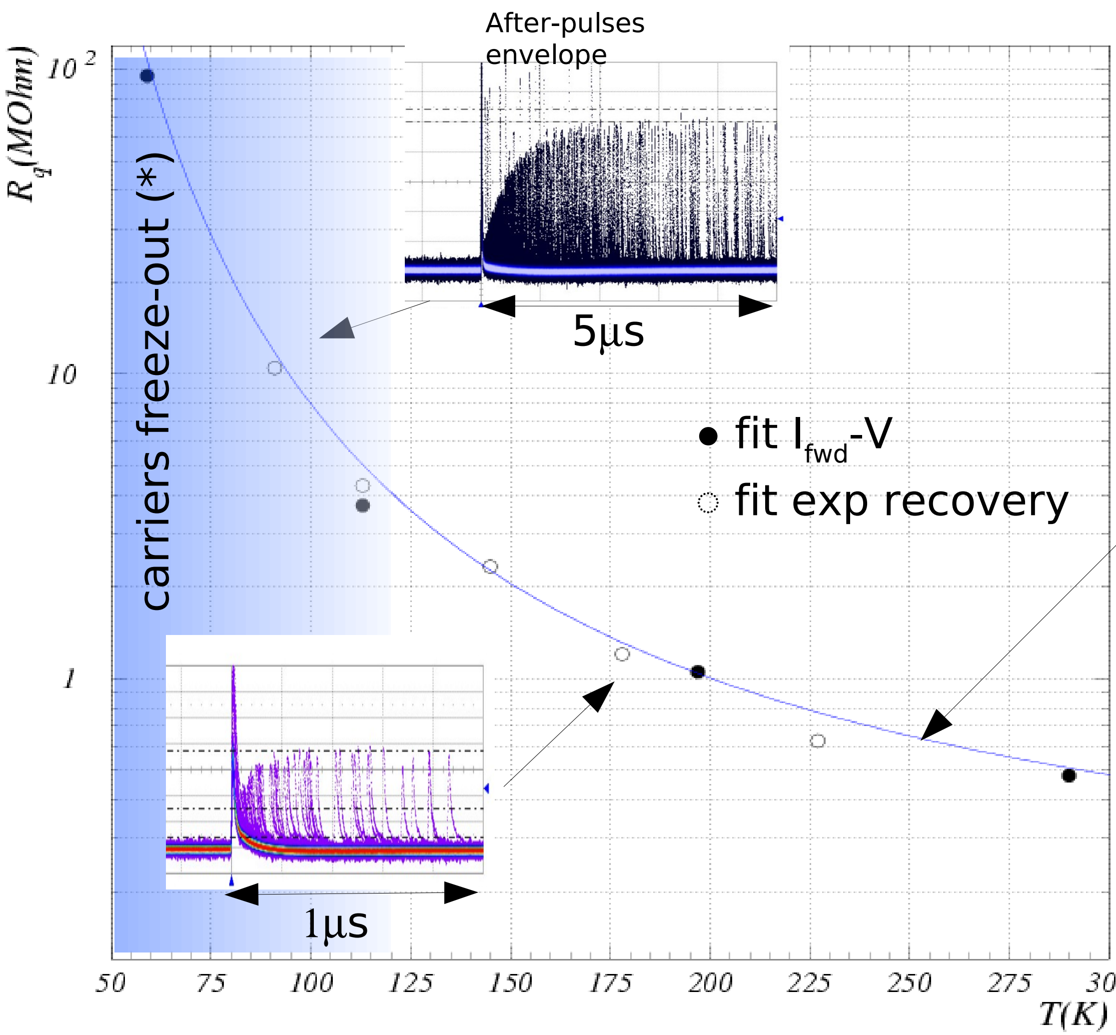

Measurements (1) and (2) consistent
→ **dominant effect from quenching resistor R_q**
(→ R bulk gives smaller effect)

Empirical fit:

$$R_q(T) \sim 0.13\,(1 + 300/T\, e^{300/T})\, M\,\Omega$$

Afterpulses envelope

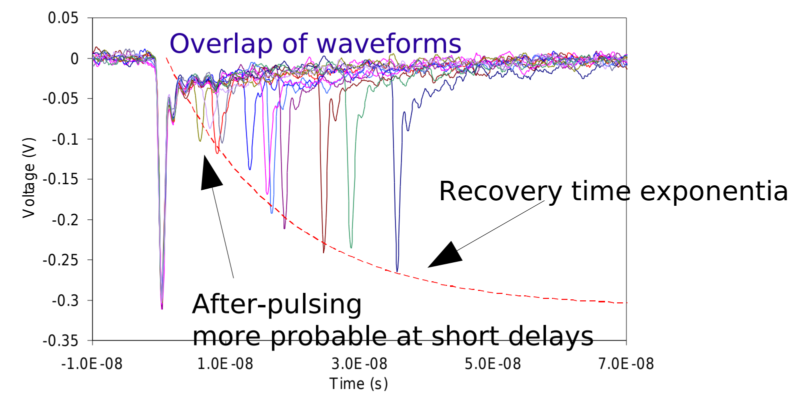

(*) carrier losses at very low T due to ionized impurities acting as shallow traps

I-V measurements: reverse bias

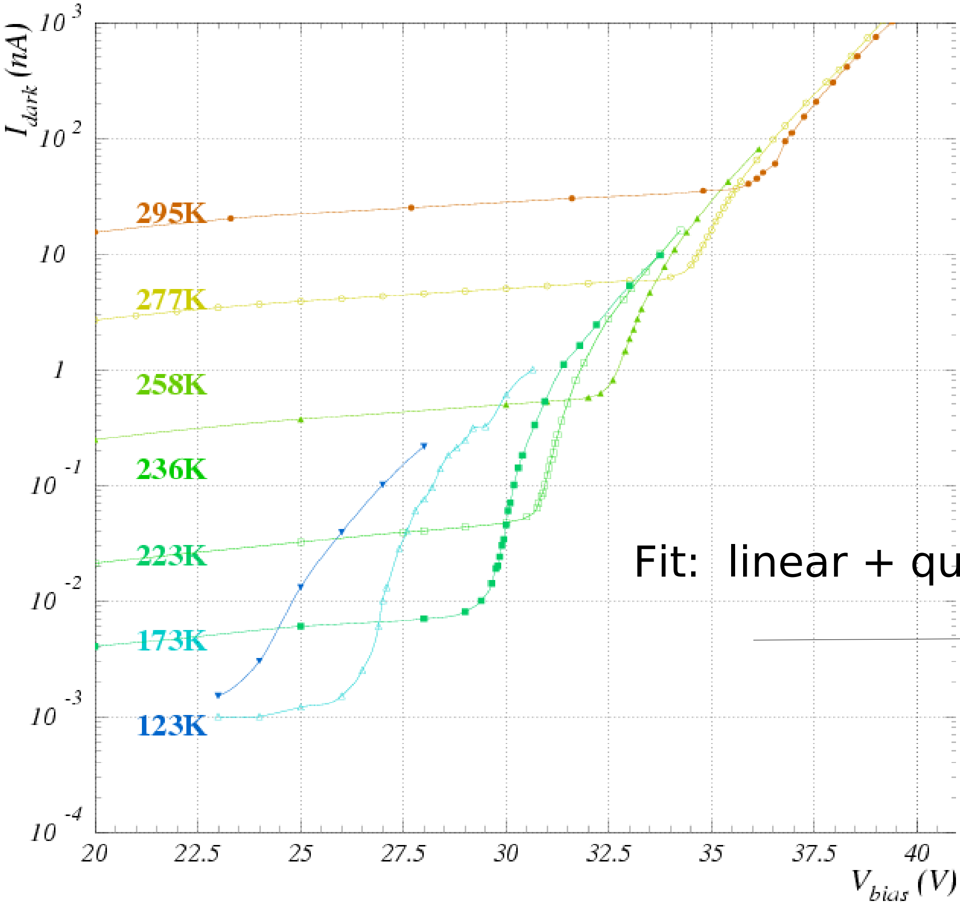

Fit: linear + quadratic (V > $V_{breakdown}$)

$V_{breakdown}$ vs T

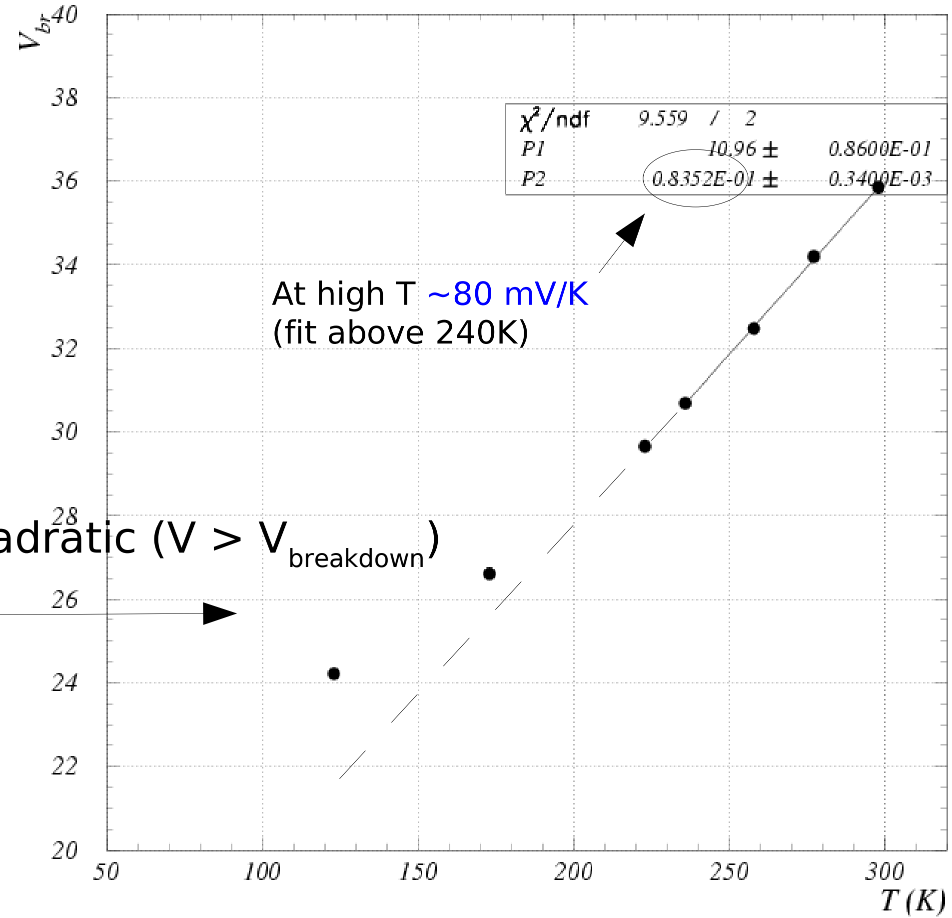

Avalanche breakdown voltage decreases due
to larger carriers mobility at low T → larger ionization rate
(at constant electric E field)

V breakdown vs T

Breakdown Voltage

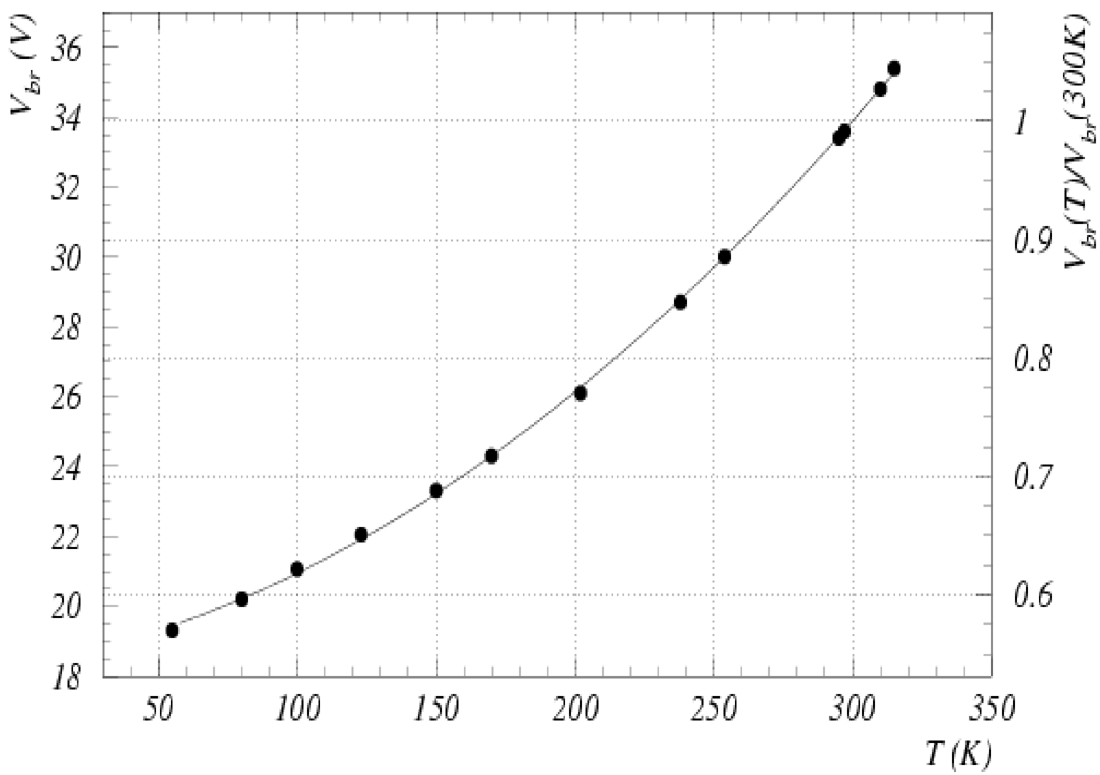

Consistent with Breakdown simulations for abrupt junctions with p-region doping at a level of ~10^{17} cm^{-3}

Temperature coefficient

better stability at low T

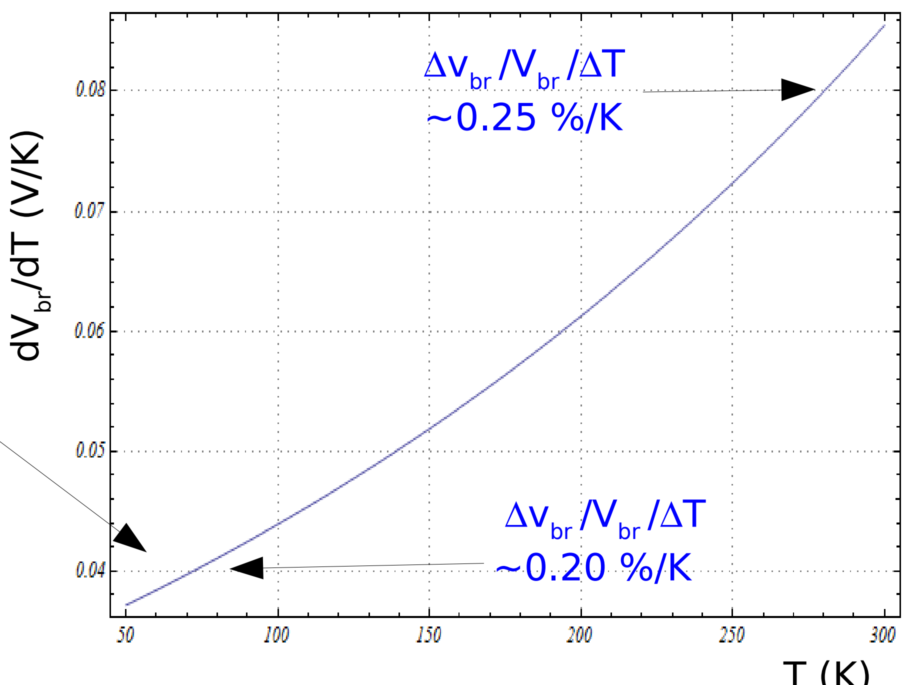

Dark current vs T (constant ΔV)

Thermal noise mainly due to G-R in the High E Field region

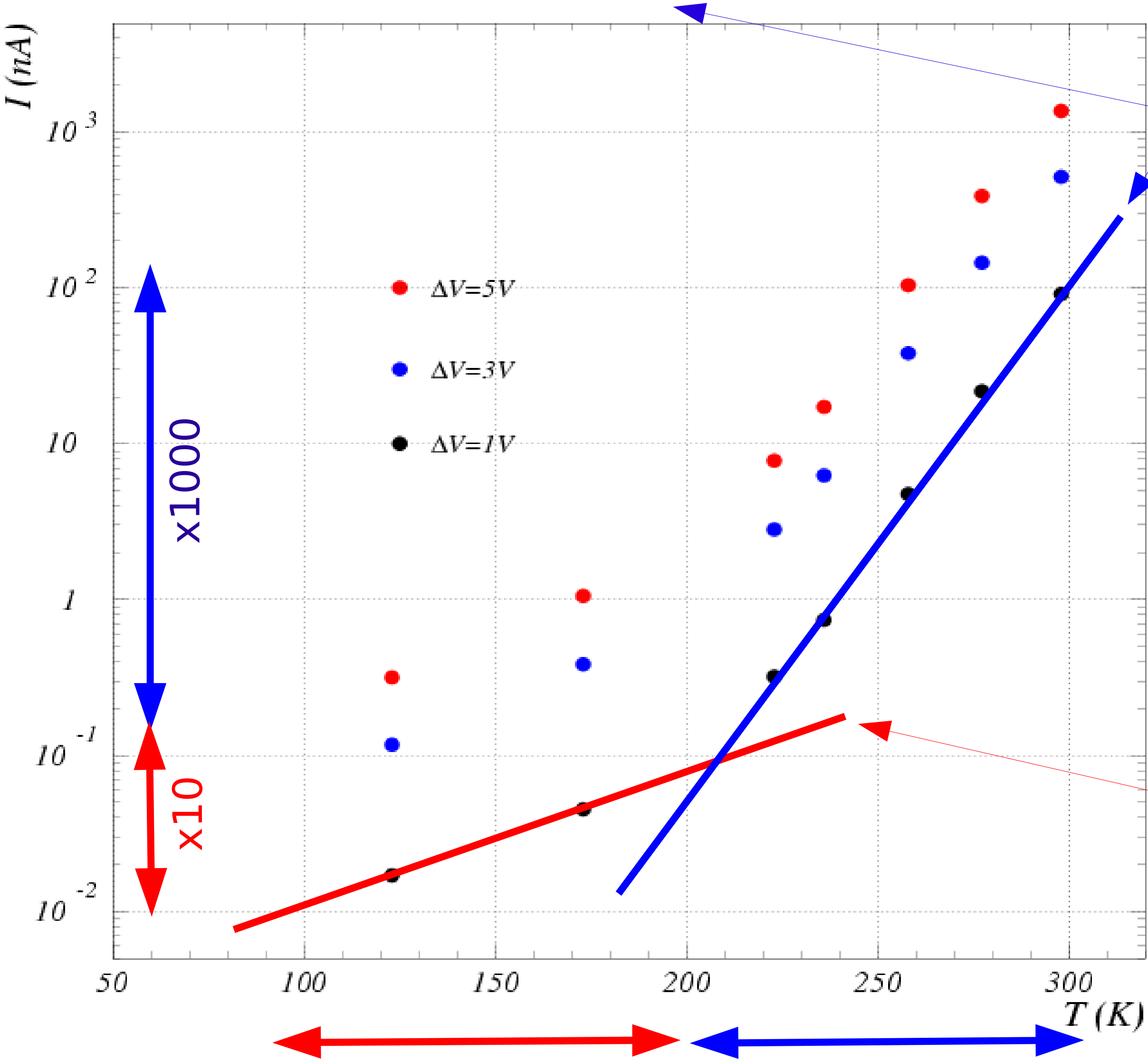

Tunnel noise dominating for T<200K (FBK devices)

Main noise mechanisms

1) Generation/Recombination SRH noise (enhanced by trap assisted tunneling)

$$I_{reverse} \sim T^{1.5} \exp \frac{-E_{act}}{K_B T}$$

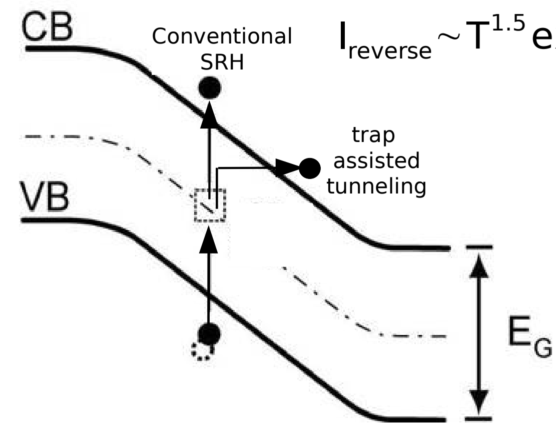

2) Band-to-band Tunneling noise (strong dependence on the Electric field profile)

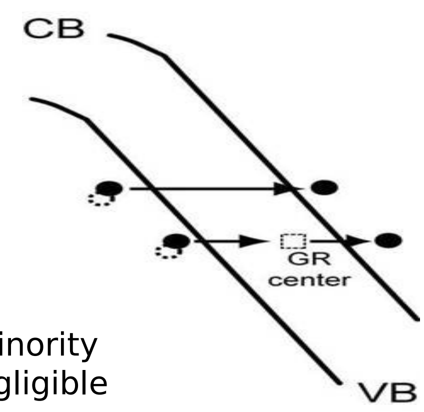

(*) noise due to minority carriers diffusion: negligible

Dark count rate vs T (constant ΔV)

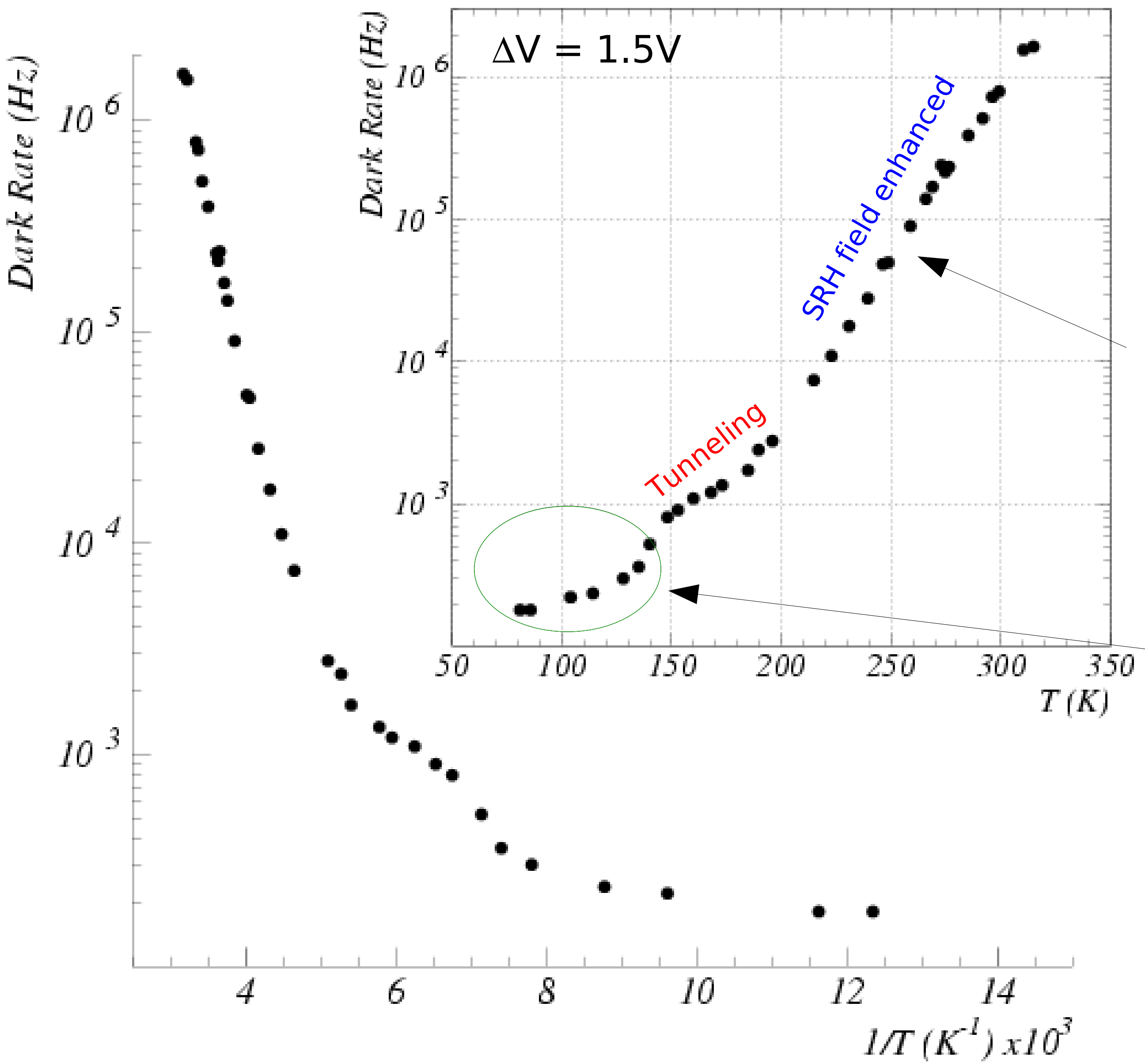

Measurement of
counting rate of ≥1p.e.
at fixed ΔV=1.5V
(→ constant gain)

$$DCR \sim T^{1.5} \exp\frac{-E_{act}}{K_B T}$$

Activation energy E_{act}~0.36eV

Additional structure ???
Under investigation

After-Pulsing (AP)

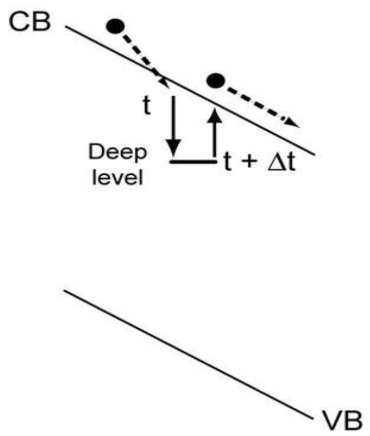

Carrier trapping and delayed release

$$P_{afterpulsing}(t) = P_c \cdot \frac{\exp(-t/\tau)}{\tau} \cdot P_{trigg} \propto \Delta V^2$$

~Few % level at 300K

avalanche triggering probability
$\propto \Delta V(t)$

τ : trap lifetime
depends on trap level position

quadratic dependence on ΔV

P_c : trap capture probability
$\propto$ carrier flux (current) during avalanche $\propto \Delta V$
$\propto$ N traps

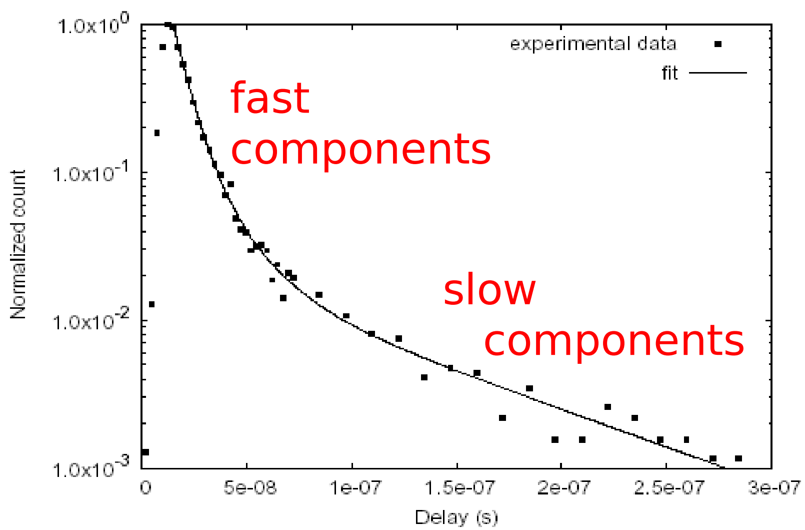

Fig. 10. Spectrum of the delay time from the primary pulse to the after-pulse.

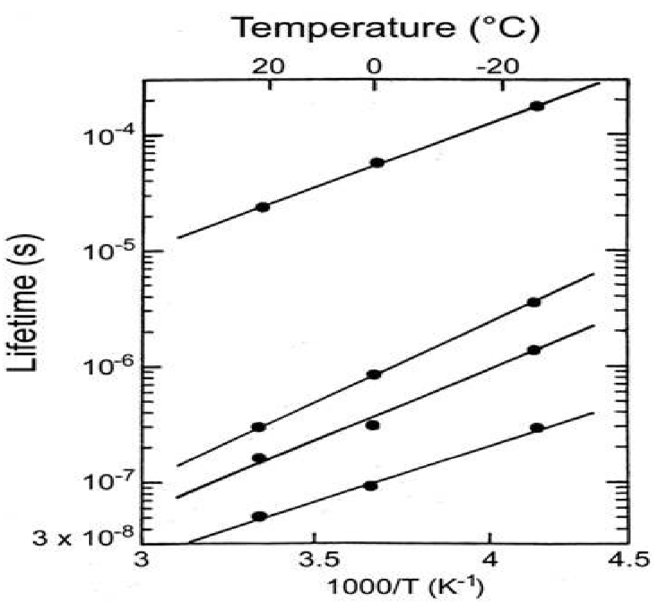

S.Cova, A.Lacaita, G.Ripamonti, IEEE EDL (1991)

After-Pulses vs T (constant ΔV)

Measurement by waveform analysis:
- trigger on single carrier pulses (with no preceding pulses within Δt=5μs), **count subsequent pulses** within Δt=5μs (find the after-pulsing rate r_{AP})
- **Subtract dark count** contribution
- extract **after-pulsing probability P_{AP}** corrected for after-pulsing cascade

$$P_{AP} = \frac{r_{AP}}{1 + r_{AP}}$$

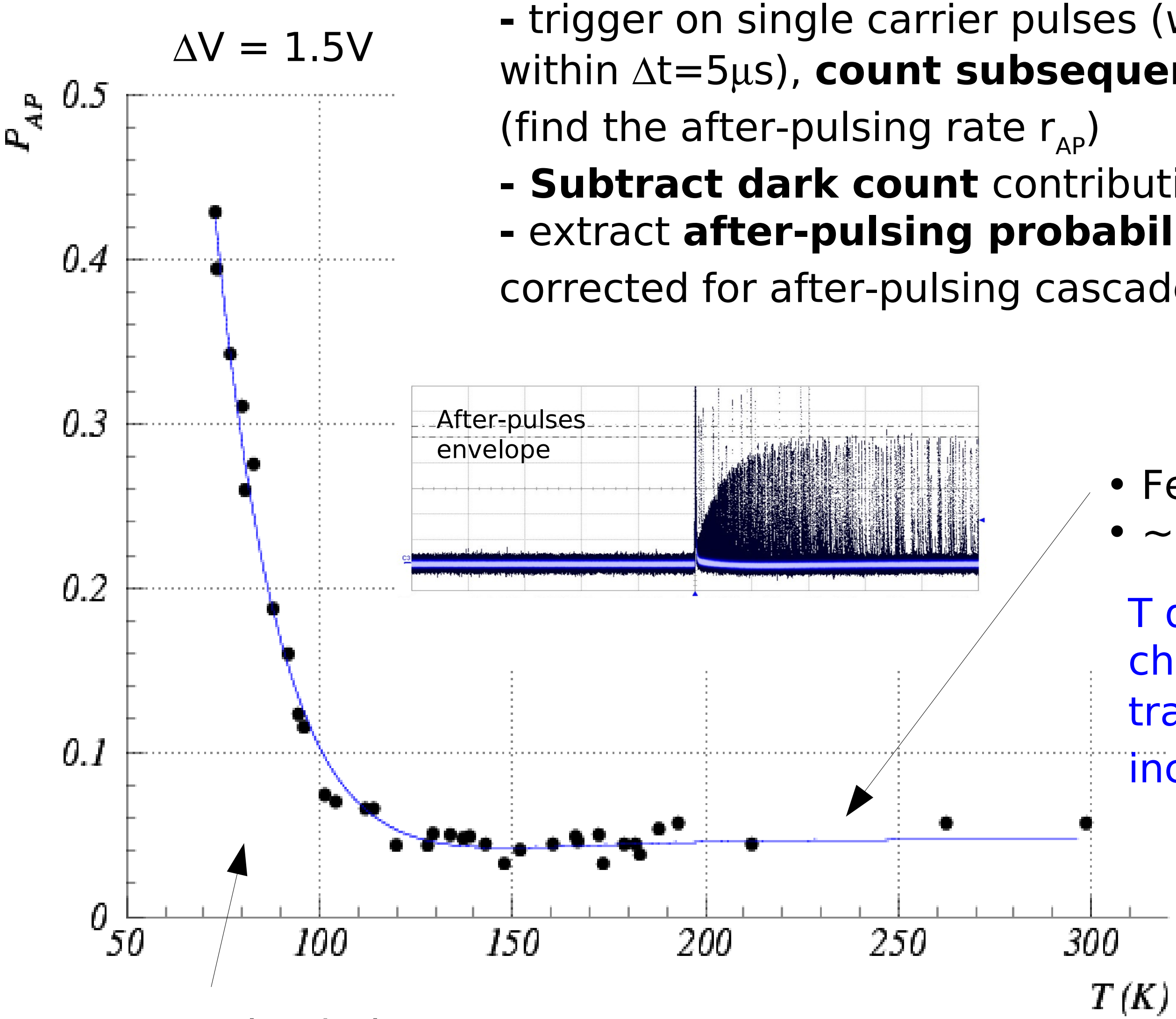

- Few % at room T
- ~constant down to ~120K

T decreasing: increase of characteristic time constants of traps (τ_{traps}) is compensated by increasing cell recovery time (R_q)

- several % below 100K

T<100K: additional trapping centers activated ? possibly related to carrier freeze-out (under investigation)

→ On-going work:
analysis of life-time evolution vs T of the various traps (at least 3 found)

DR, AP, Gain, X-talk vs ΔV (constant T)

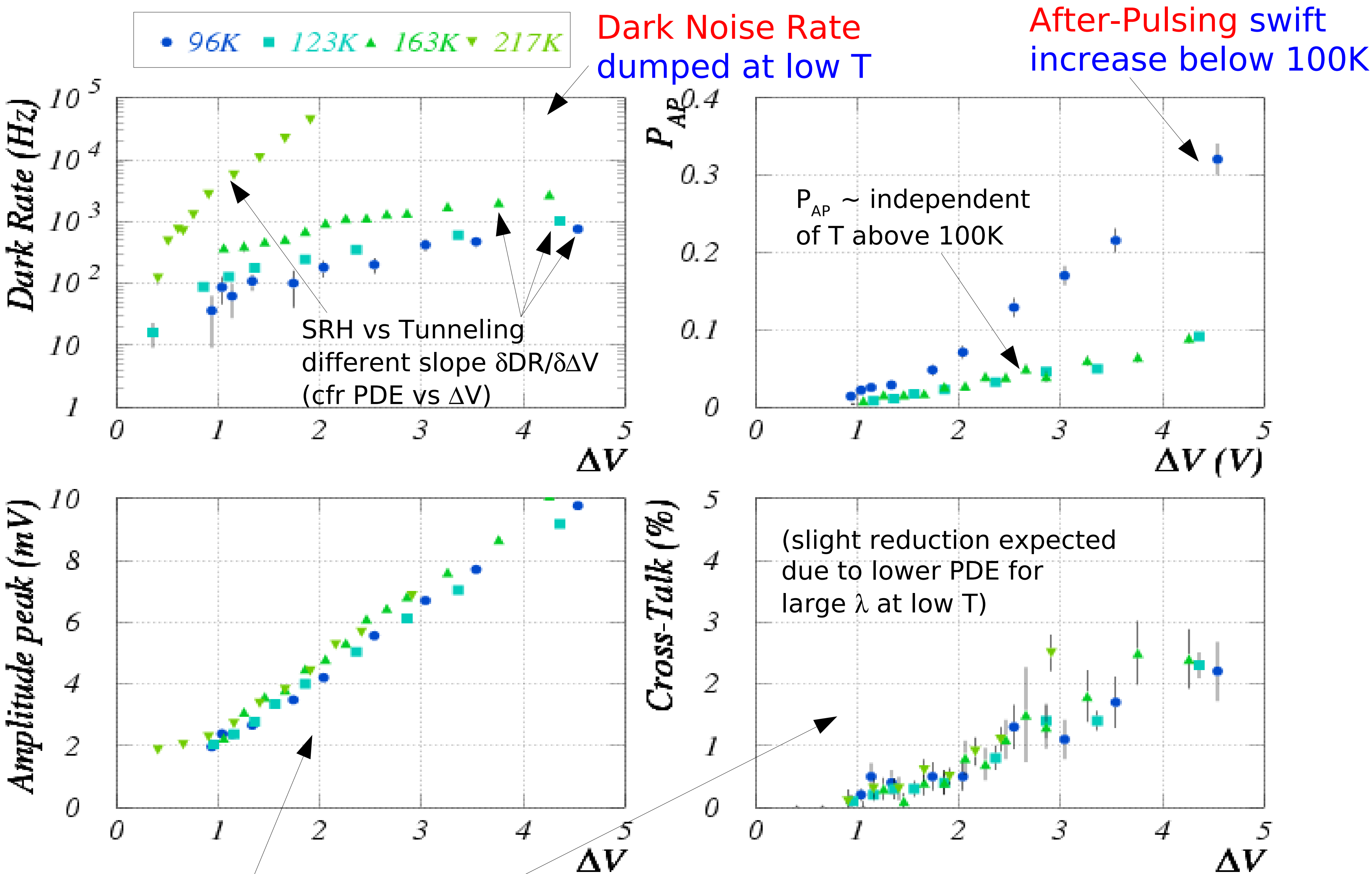

Gain and Cross-Talk are independent of T

Photo-Detection Efficiency (PDE) vs ΔV and λ

SiPM with ε_{geom} ~22%

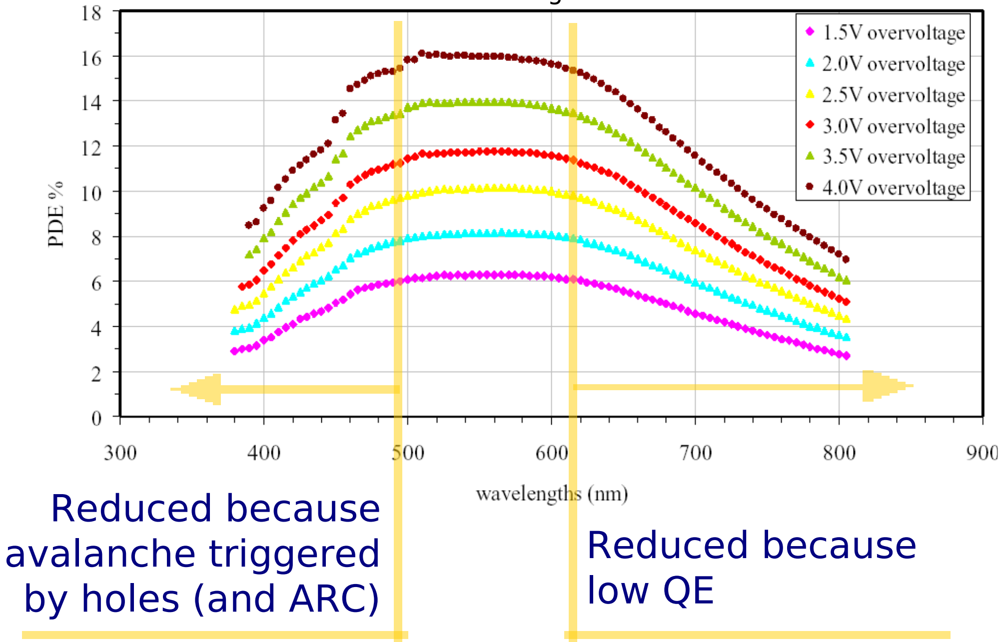

PDE dependence on λ (at different ΔV) – room T

PDE =

ε_{geom} (fraction of active area)

x

QE (efficieny of photo-conversion)

x

P_{trigg} (avalanche triggering probability)

Expected to be T dependent

SiPM with ε_{geom} ~50%

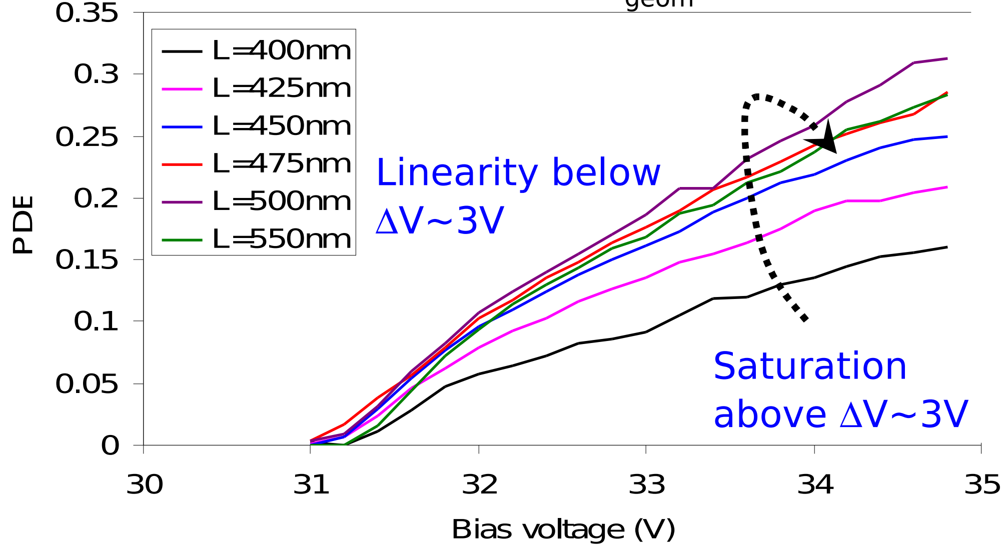

PDE dependence on ΔV (at different λ) – room T

PDE vs λ (constant ΔV=2V) - halogen lamp (CW)

Measure →
- I_{sipm} / G = current drawn by SiPM / SiPM gain
- $I_{photons}$ = rate of photons by calibrated photo-diode

→ Find: $\boldsymbol{PDE = I_{sipm} / G / I_{photons}}$

which differs from absolute PDE but for a common factor due to different photon acceptance of SiPM wrt calibrated diode (different light paths)

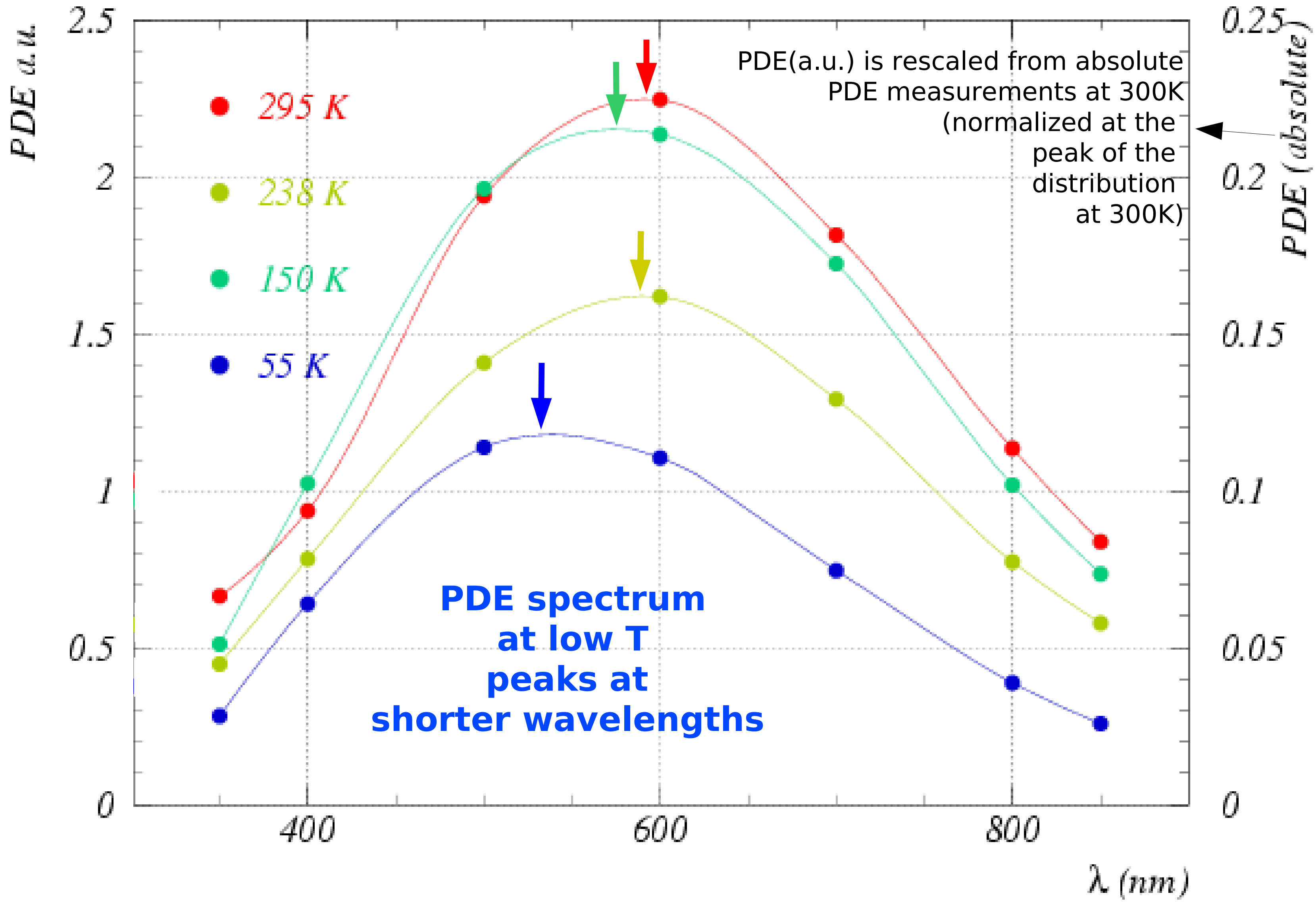

PDE vs T (constant ΔV=2V) - halogen lamp (CW)

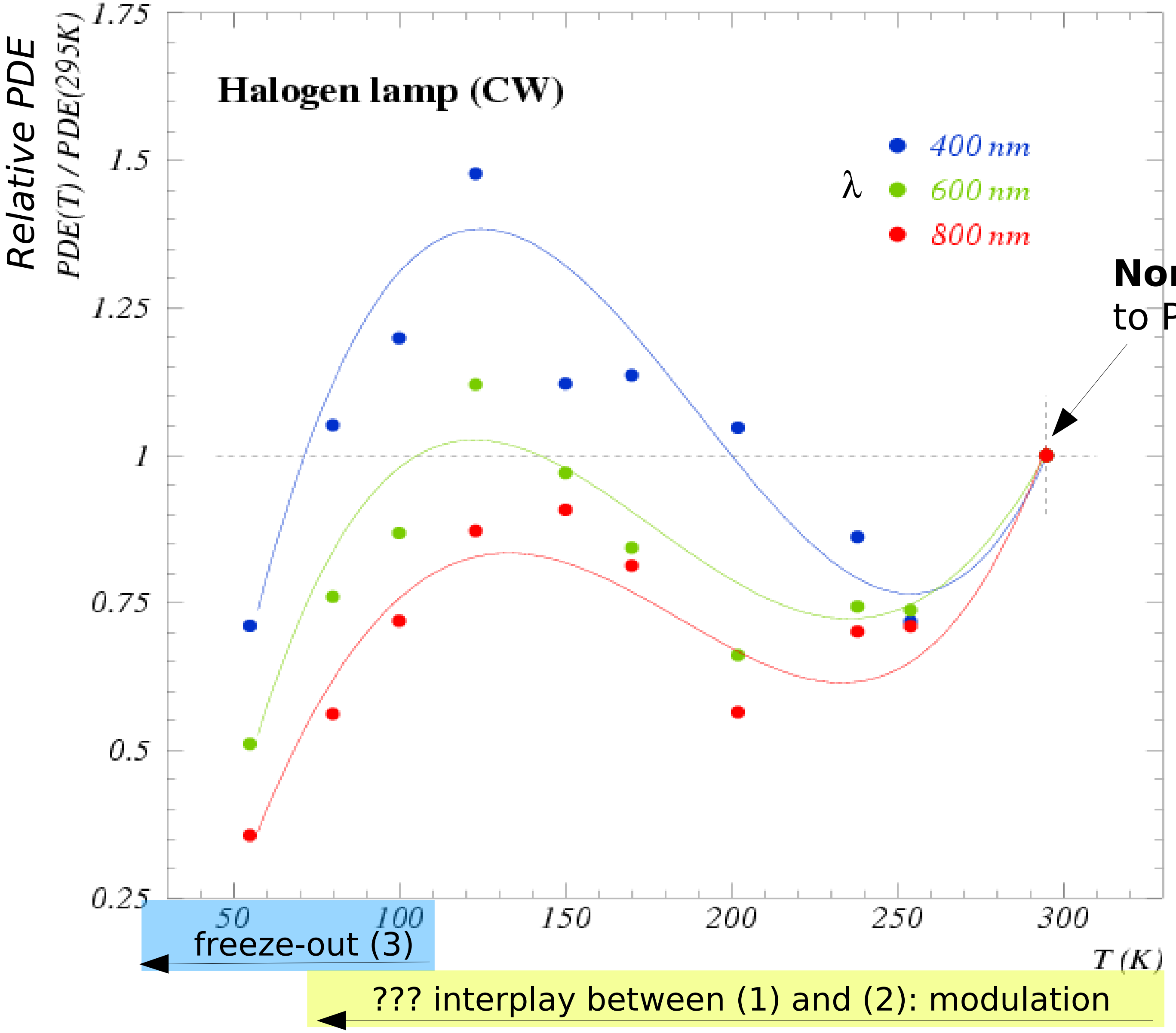

$PDE = I_{sipm} / G / I_{photons}$

When T decreases we expect:

1) silicon E_{gap} increasing
→ larger attenuation length
→ lower QE (for larger λ)

2) mobility increasing
→ larger impact ionization
→ larger trigg. avalanche P_{01}

3) carriers freeze-out
onset below 120K
→ loss of carriers

PDE vs T (ΔV=2V) – LED and Laser

PDE dependence on T at constant gain:
similar results with LED (cont. light - 380nm)
and Laser (pulsed light – 405nm)

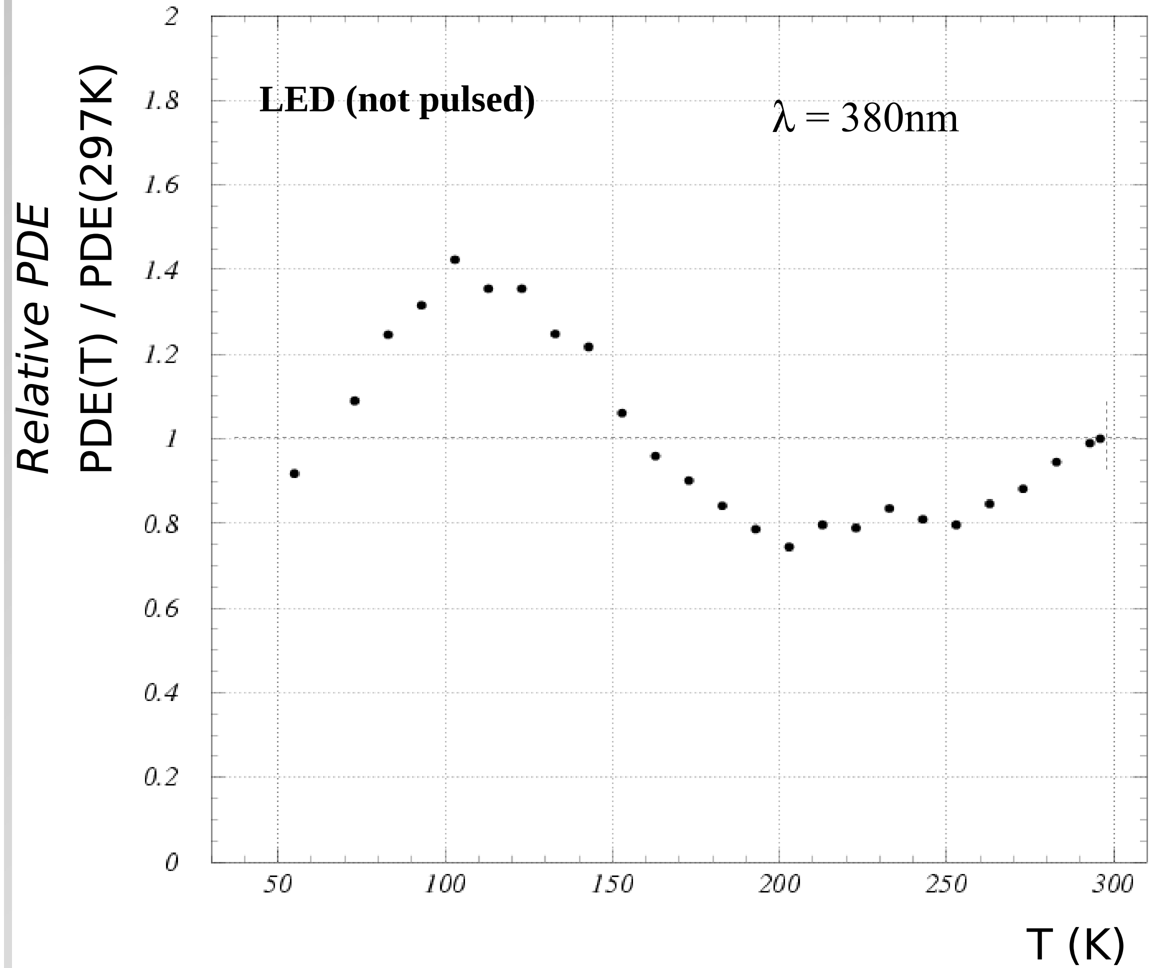

$PDE(T) \equiv I_{SiPM}(T) / I_{LED}$

Normalization with PDE at T=297K

Some common features
with APDs (proportional mode)

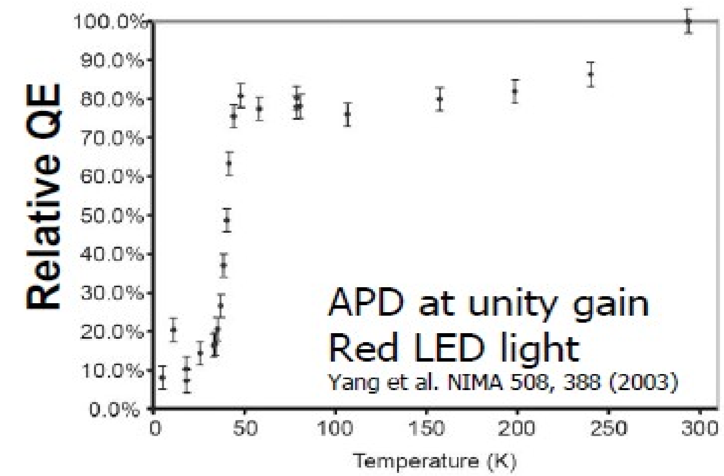

APD at 400nm < λ < 700nm
Johnson et al, IEEE NSS 2009

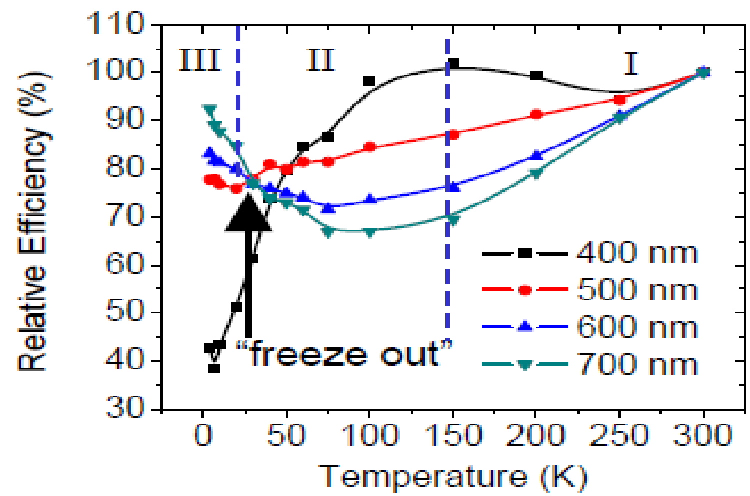

Additional effects in APD
(depletion region depends on T, ...)

PDE vs ΔV (constant T) – pulsed laser (405nm)

Measure →

- I_{pe} = average number of photo-el. in coincidence with laser trigger x trigger rate
- $I_{photons}$ = average rate of photons measured by calibrated photo-diode

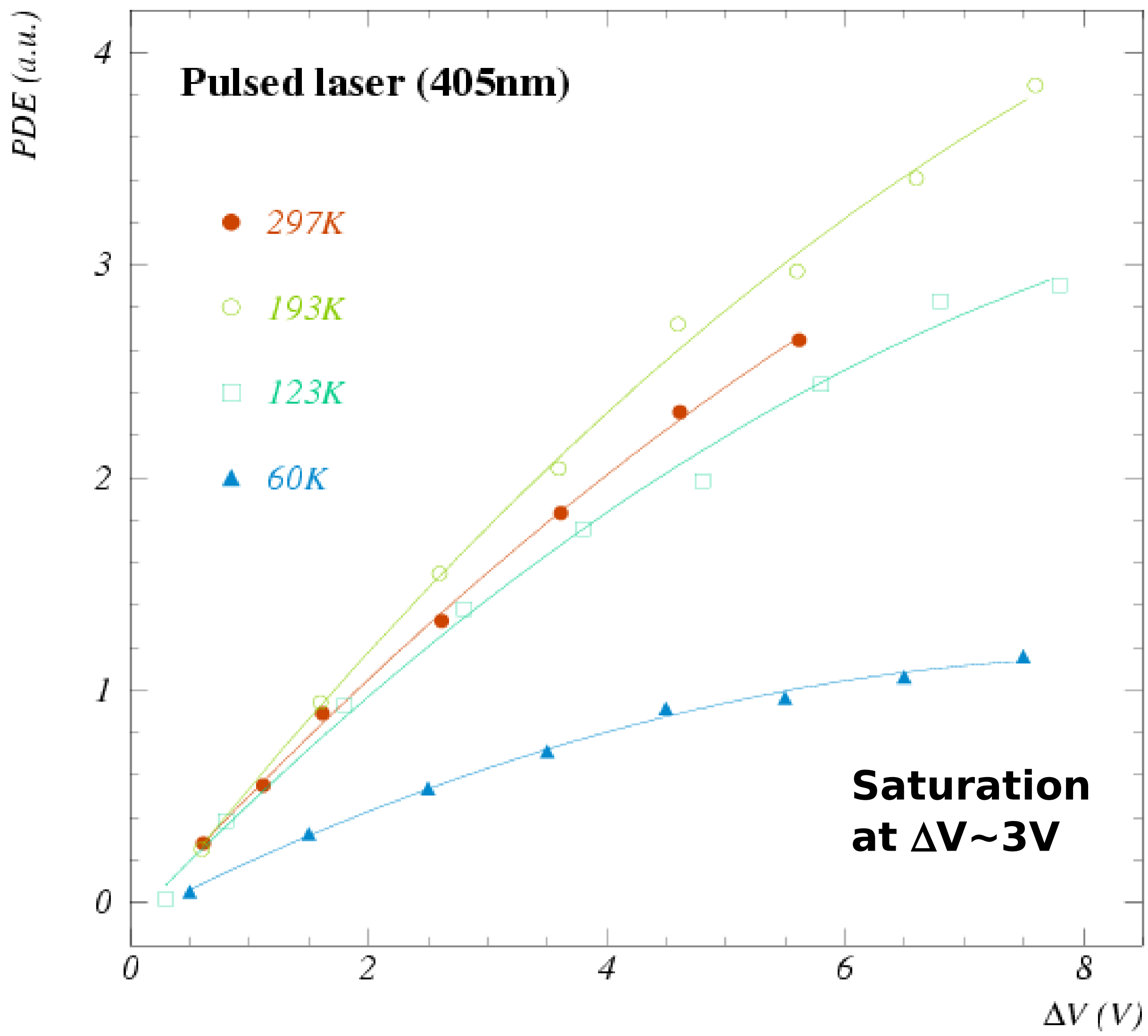

→ Find: $PDE = I_{pe} / I_{photons}$

which differs from absolute PDE but for a common factor due to different photon acceptance of SiPM wrt calibrated diode (different light paths)

Saturation starts earlier at low T

Understanding PDE vs T

Doping and Field profiles (IRST)

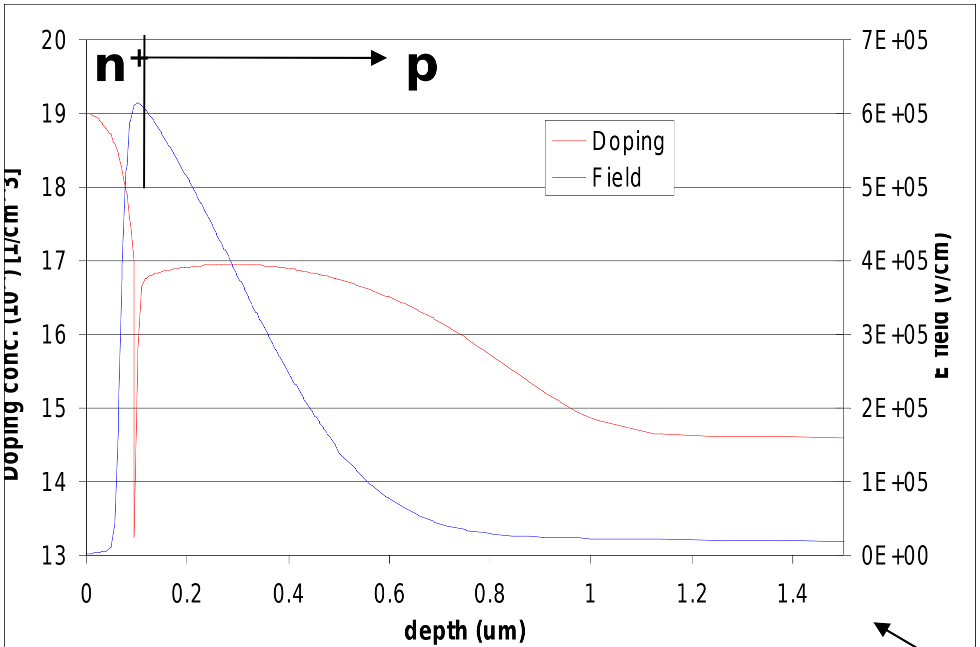

Light absorption in Silicon

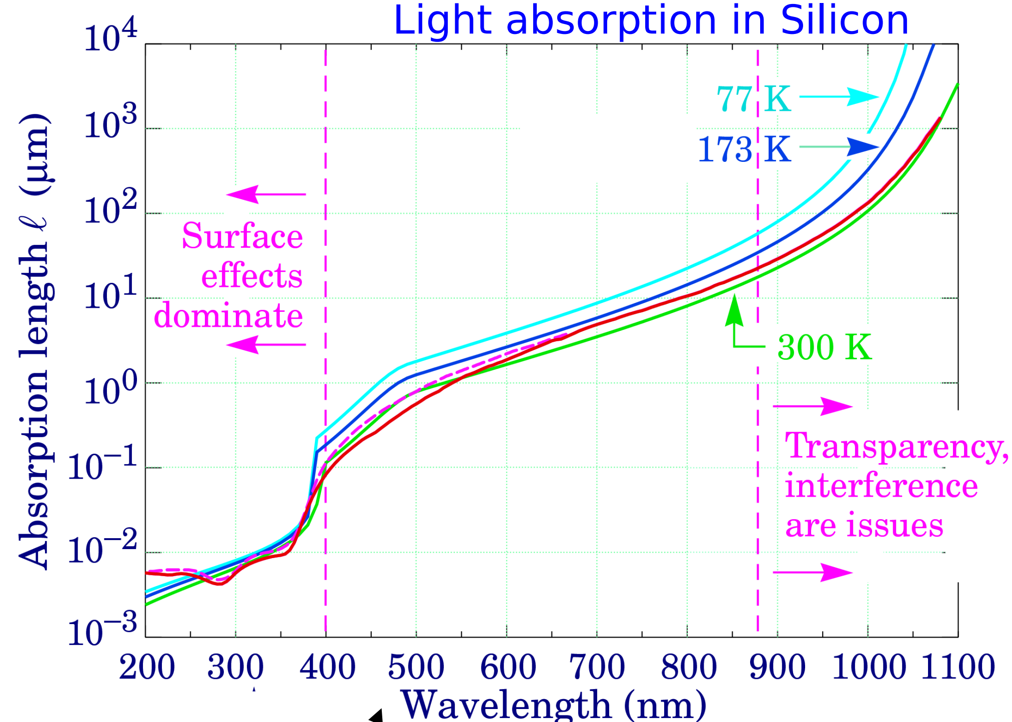

V_{BD} versus doping concentration

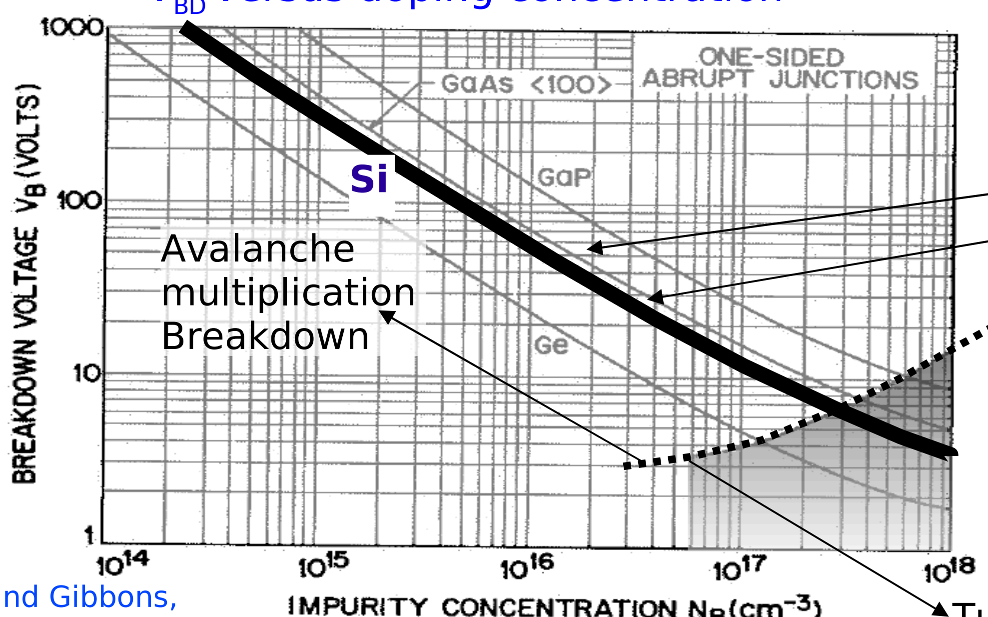

Tunneling effect Breakdown

Sze and Gibbons, Appl. Phys Lett. 8 (1966)

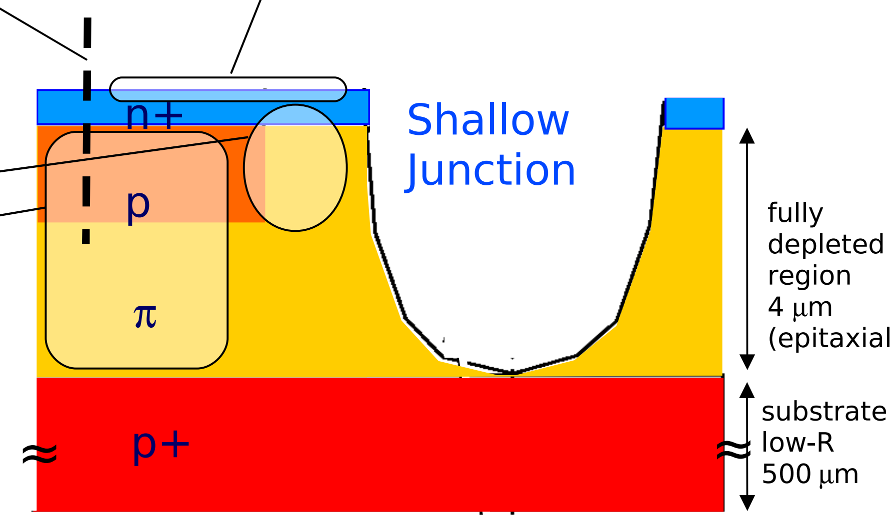

Understanding PDE vs T: 1D model

Preliminary results

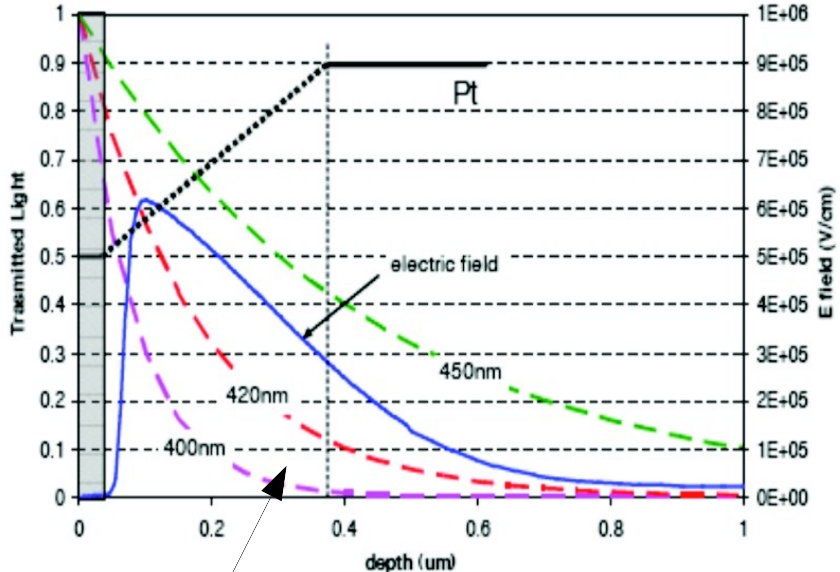

E field profile +

+ impact ionization

calculate

Breakdown voltage vs T

Avalanche triggering probability
for electrons and holes ($P_{trigger}e$, $P_{trigger}h$)
(using differential equations method after Oldham et al, IEEE TNS 19 (1972) 1056)

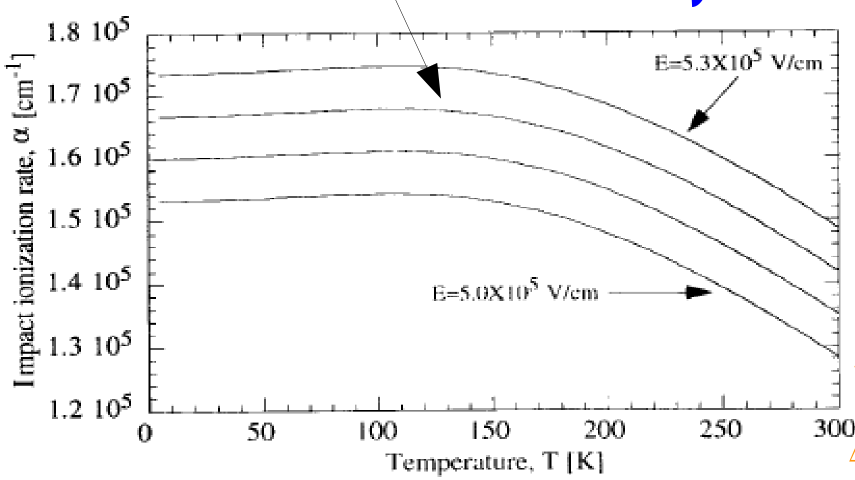

FIGURE 1.43. The impact ionization rate α as a function of temperature T_A with the electric field E as a parameter calculated from Okuto and Crowell's (85) model.

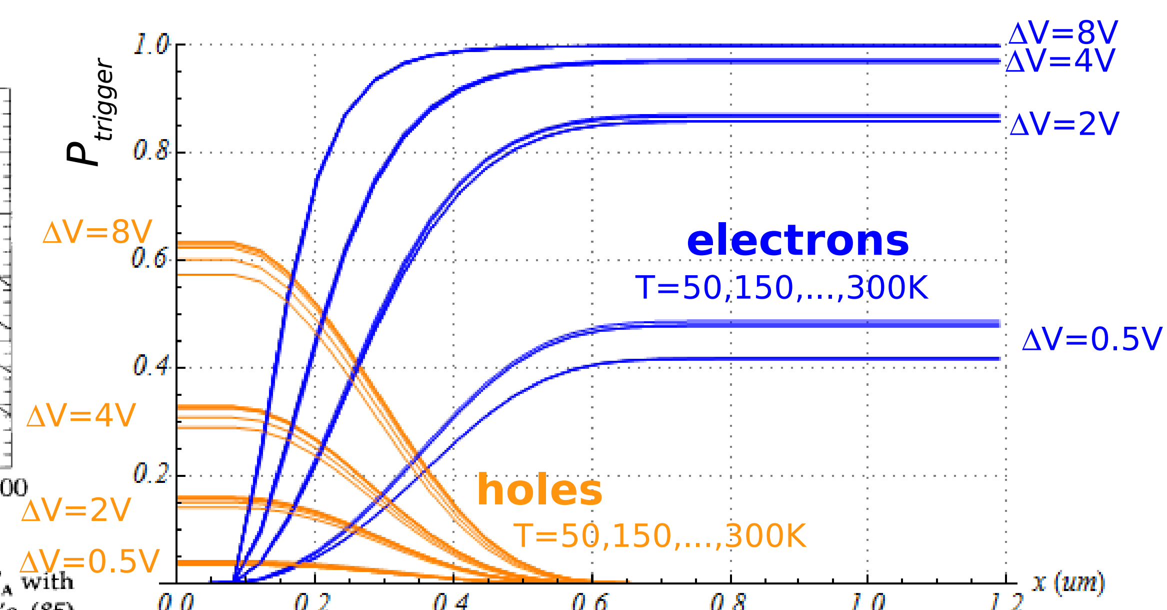

Understanding PDE vs T: 1D model

Preliminary results

avalanche triggering probability +

\+ light **absorption length in Si (1/α)**

calculate →

PDE as a function of (λ ,T,ΔV)
obtained by the convolution of $P_{trigg}(x)$ and $\alpha \exp(-\alpha x)$
(integrated over the depletion layer)

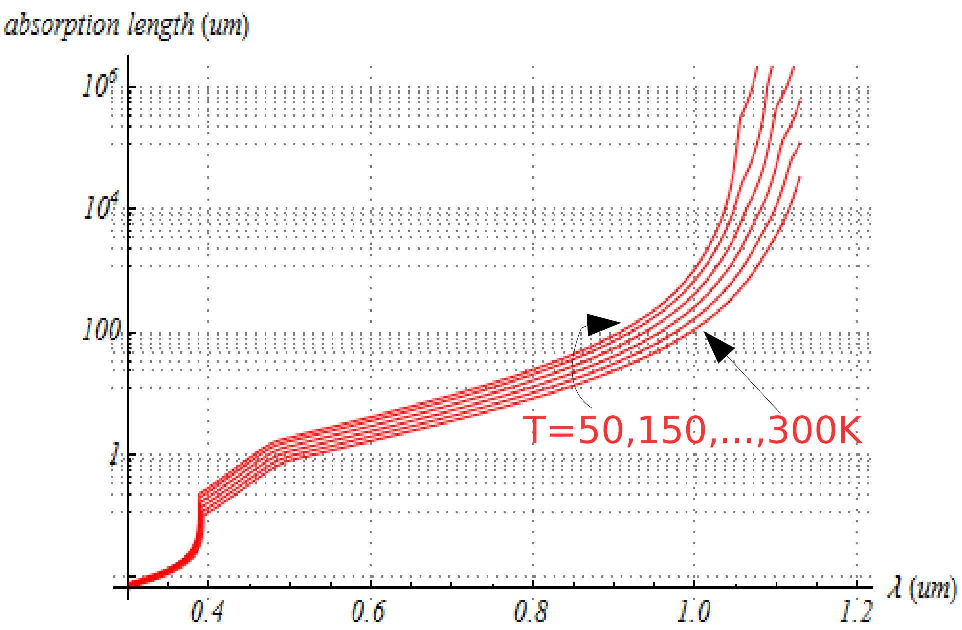

Rajkanan et al, Solid State Ele 22 (1979) 793

Accounting E_{gap} variations with T, etc...

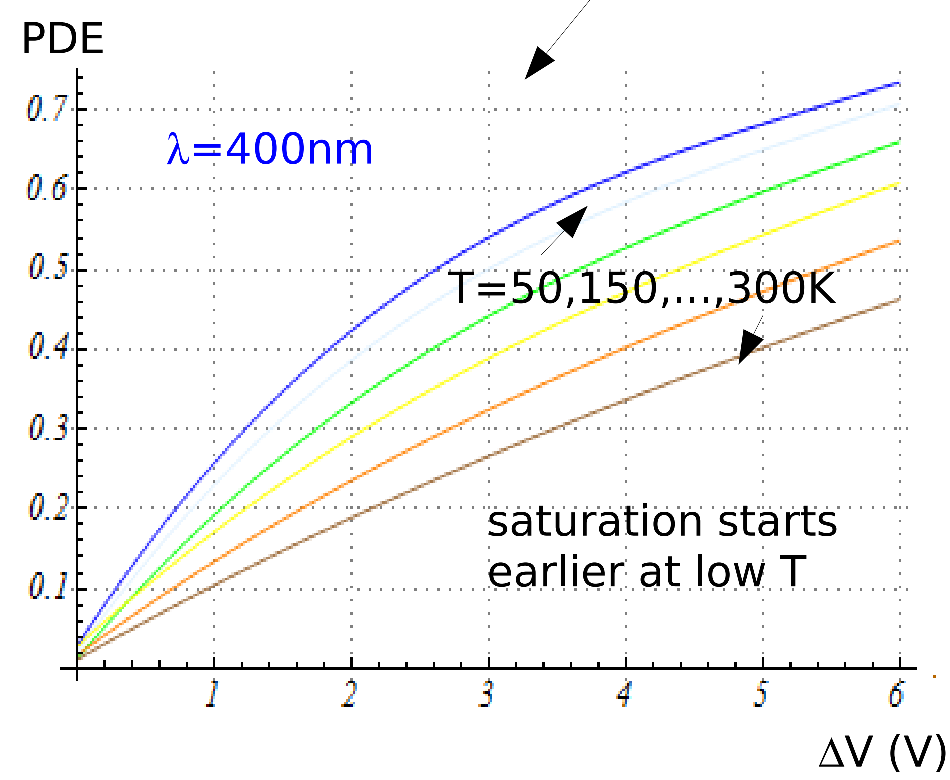

Understanding PDE vs T: 1D model

Preliminary results

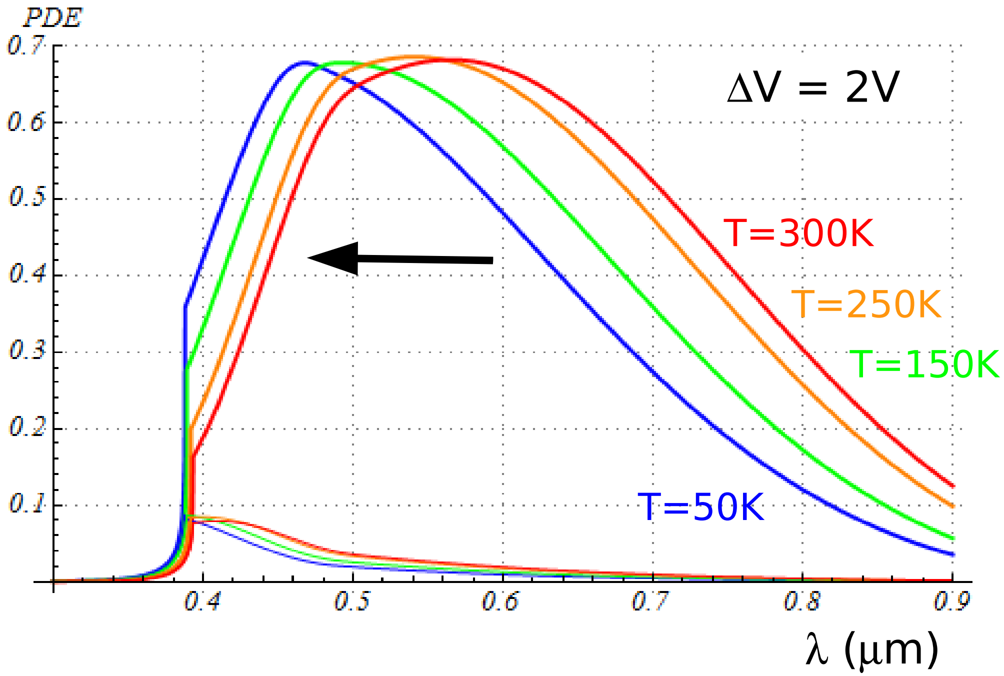

1) main contribution to PDE from electrons → PDE distribution shifted toward short λ at low T because of larger absorption length (photo-generation deeper into depletion layer → gain for shorter λ, loss for longer λ)

(see also PDE vs T)

2) tunneling effects not (yet) included in the model (enhancement of PDE, interplay with band gap variations with T)

3) freeze-out not (yet) included in the model

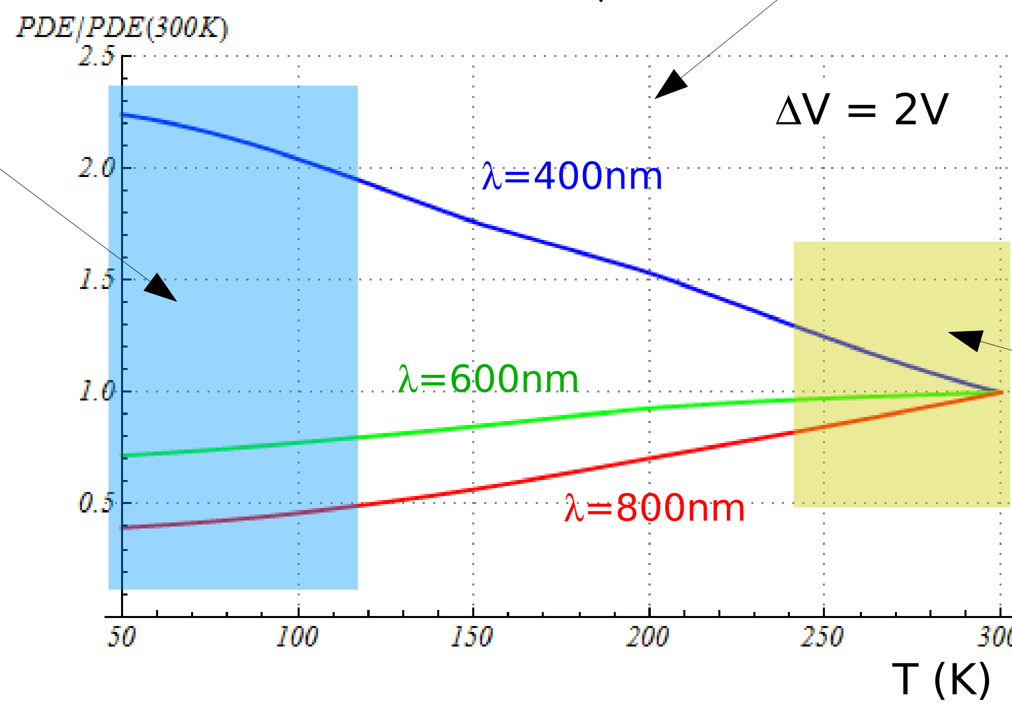

4) something else is missing: need to explain PDE decreasing with T for 250K<t<300K

to be understood !

G.Collazuol - DIRC2011 4/6/2011

Overview – SiPM timing properties

• Intrinsic timing: discussion of intrinsic timing properties based on measurements of single photon timing resolution

G.C. et al NIMA 581 (2007) 461

• A few comments about Signal shape, Front-End and Read-Out Electronics aiming at timing applications in low light intensity conditions

GM-APD timing: avalanche development

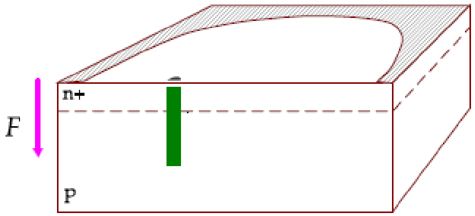

Longitudinal multiplication

Duration ~ few **ps**
Internal current
up to ~ few **μA**

(1) Avalanche "seed": free-carrier concentration rises exponentially by **"longitudinal" multiplication**

(2) E field locally lowered until E_{max} reaches breakdown value

Multiplication is self-sustaining
Avalanche current steady until new multiplication triggered in near region

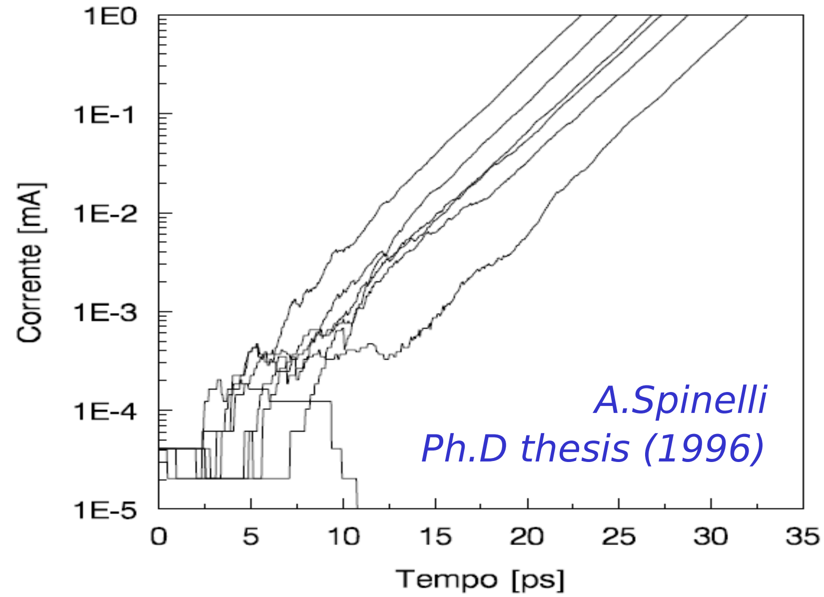

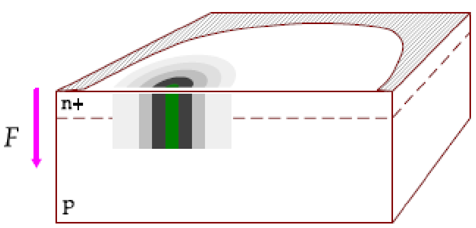

Transverse multiplication

Duration ~ few**100 ps**
Internal current
up to ~ few **10μA**

(3) Avalanche spreads "transversally" over the junction

(**diffusion speed ~some 10μm/ns** enhanced by multiplication)

(4) Passive quenching mechanism effective only after transverse **avalanche size ~10μm**

(Otherwise avalanche spreads over the whole active depletion volume → avalanche current reaches a final saturation steady state value)

Simulation w/o quenching:
→ steady current reached

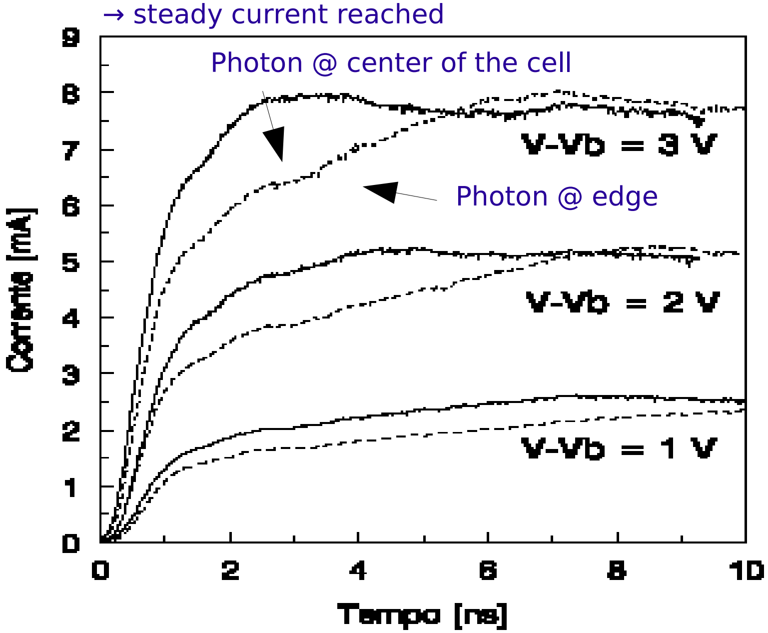

GM-APD timing: fast and slow components

1) Fast component: gaussian with time scale O(100ps)

Statistical fluctuations in the avalanche:

- **Longitudinal** build-up (minor contribution)
- **Transversal** propagation (main contribution):
  - via Multiplication assisted diffusion (dominating in few um thin devices) A.Lacaita et al. APL and El.Lett. 1990
  - via Photon assisted propagation (dominating in thick devices - O(100um)) PP.Webb, R.J. McIntyre RCA Eng. 1982 A.Lacaita et al. APL 1992

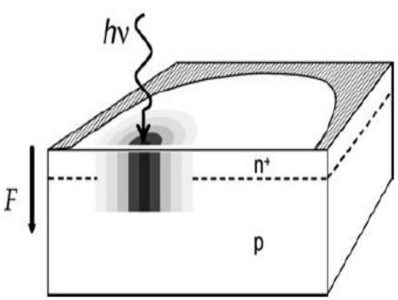

Multiplication assisted diffusion

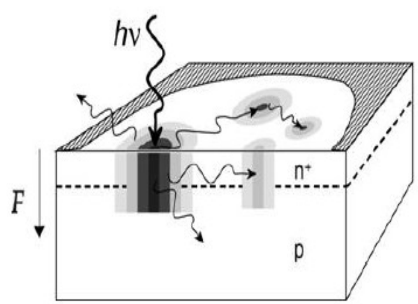

Photon assisted propagation

- **Fluctuations** due to impact ionization statistics
- Jitter at minimum → O(10ps) (very low threshold → not easy)
- additional **Fluctuations** due to longitudinal position of photo-generation due to finite drift time in low E field region (even at saturated velocity)

- **Fluctuations** due to large variance of the transverse diffusion speed
- Jitter → O(100ps) (usually threshold set high)
- dependence of avalanche build-up rate on transverse impact position (→ cell size)

Higher over-voltage → improved time resolution

GM-APD timing: fast and slow components

2) Slow component: minor non-gaussian tails with time scale O(ns)

Carriers photo-generated in the neutral regions beneath the junction and reaching the electric field region by diffusion

G.Ripamonti, S.Cova Sol.State Electronics (1985)

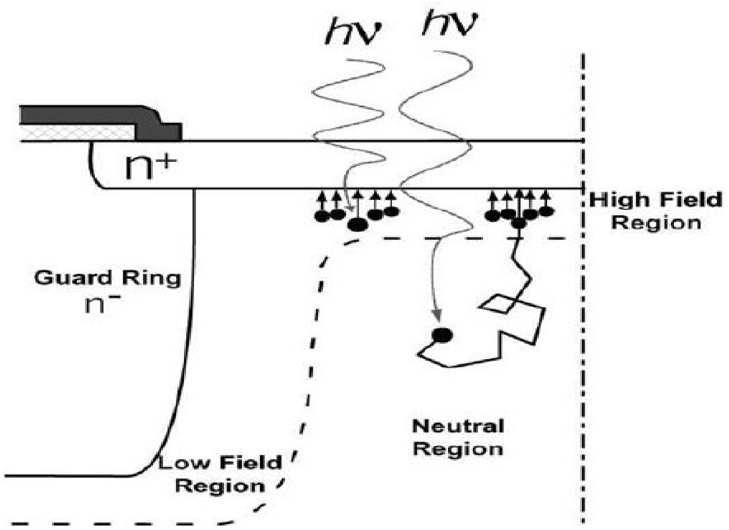

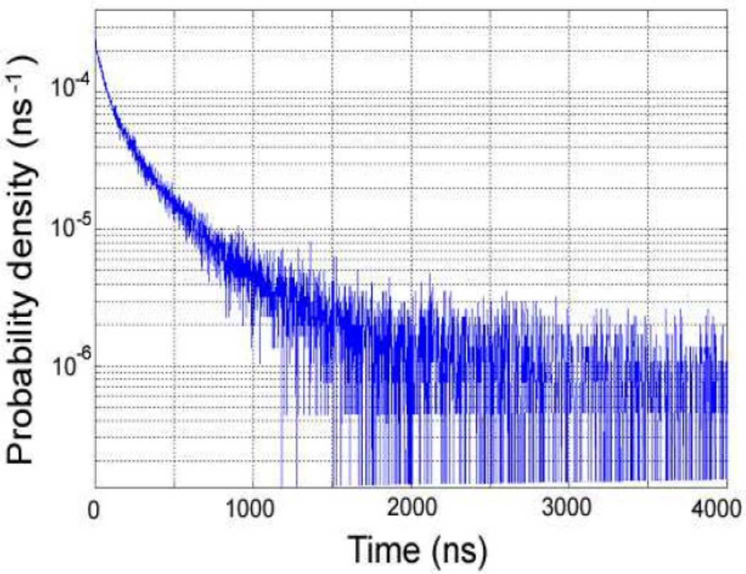

tail lifetime: $\tau \sim L^2 / \pi^2 D$
L = effective neutral layer thickness
D = diffusion coefficient

S.Cova et al. NIST Workshop on SPD (2003)

Shorter wavelengths → higher resolution (reduced tails)

Experimental Setup

Pump Laser
Millenia V (Spectra-physics)
solid state CW visible laser

Crystal for Second Harmonic Generation (SHG)
conversion 800 nm → 400 nm
efficiency at % level

Low noise LV suppliers

Dark box

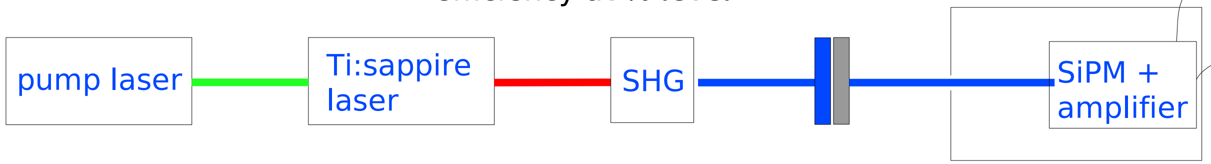

LeCroy SDA 6020
Analog bandwidth: 6GHz
Sampling rate: 20GS/s
Vertical resolution: 8 bits

(Aknowledments: E.Marcon, LeCroy)

External trigger from Ti:sappire laser signal

Filters
blue + neutral
for rejecting IR light and tune intensity

Mode-locked Ti:sapphire Laser
Tsunami (Spectra-physics)
femtosecond pulsed laser

wavelength: tuned at 800±15 nm
pulse width: ~ 60 fs FWHM
pulse period: ~ 12 ns
pulse timing jitter < 100 fs

Electronics
I → V conversion via R_L (500Ω)
Two stage voltage amplification (= x50) based on high-bandwidth low-noise RF amplifier: gali-5 (MiniCircuit)
Z_{in}= 50Ω

(Aknowledments: F.Morsani and L.Zaccarelli, INFN-Pisa)

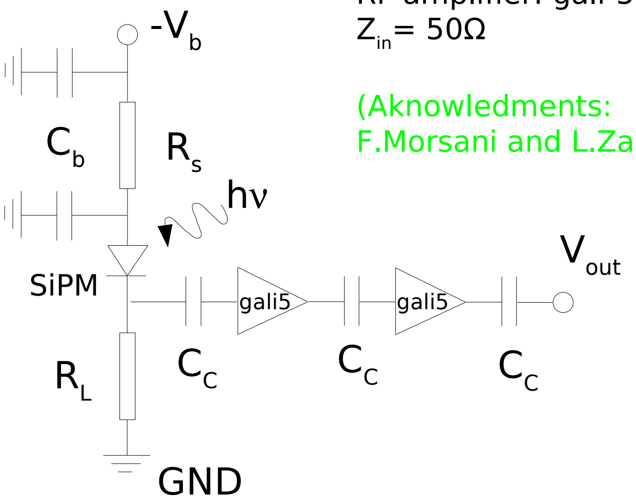

Data taking conditions:

- different V_{bias}
- both at 800 nm and 400 nm
- with different light intensities (counting rates in the range 10÷20 Mhz ie 15÷30 KHz per single cell)

Waveform analysis: method

(1) Selection of candidate peaks:

- single photon peaks
- proper signal shape
- low instantaneous intensity (no activity before/after within 50ns)
- low noise during the previous 10 ns (typical noise ~ 1mV rms)

(2) Peak reconstruction

- optimum time reconstruction
- amplitude and width (baseline shift correction)

(3) Time difference Δt between consecutive peaks

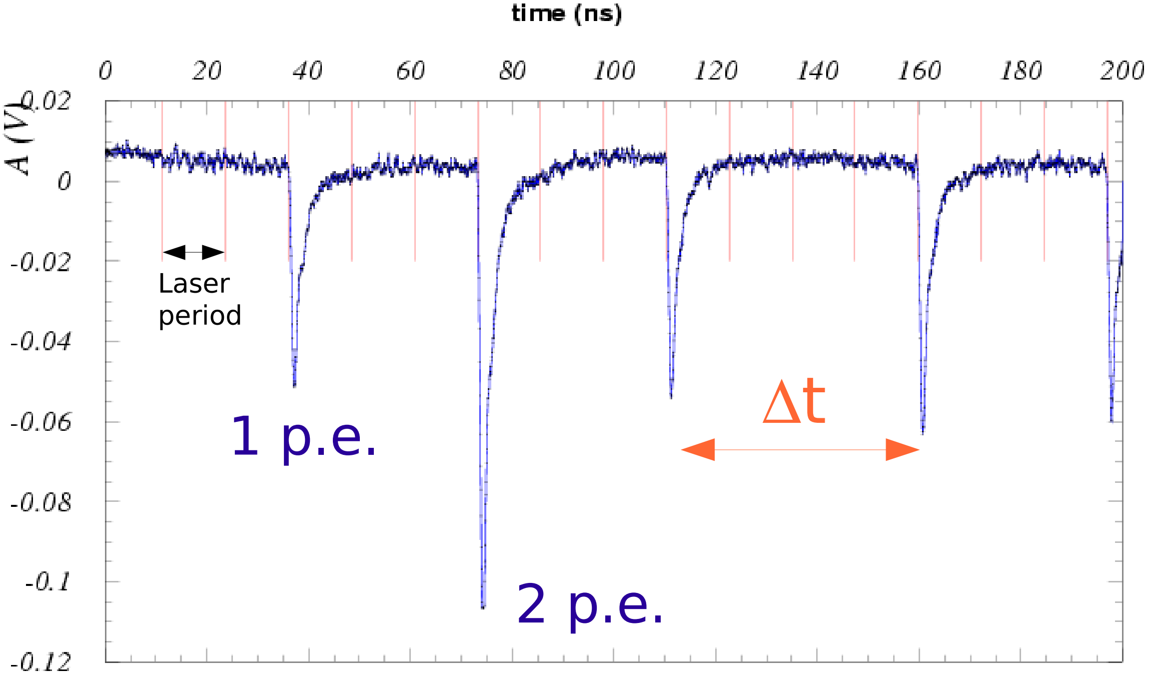

NOTE: good timing properties even up to $10 MHz/mm^2$ photon rates

Waveform analysis: optimum timing filter

Different methods to reconstruct the time of a peak:

✗ parabolic fit to find the peak maximum
✗ average of time samples weighted by the waveform derivative
✔ digital filter: weighting by the derivative of a reference signal
→ best against noise (signal shape known)

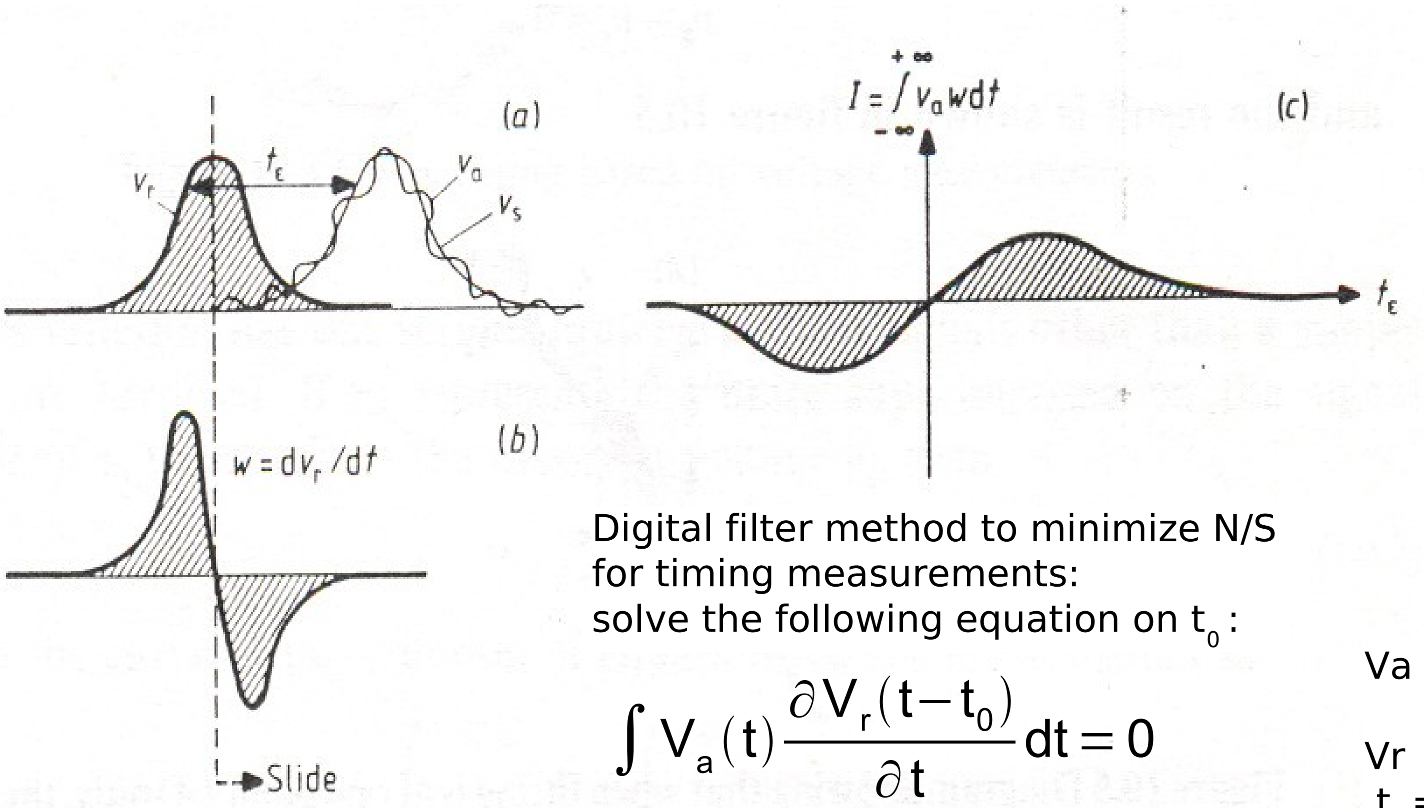

Digital filter method to minimize N/S
for timing measurements:
solve the following equation on t_0 :

$$\int V_a(t) \frac{\partial V_r(t-t_0)}{\partial t} dt = 0$$

Va = measured signal
(includes noise)
Vr = reference signal
t_0 = reference time

Single Photon Timing Resolution (SPTR)

Analysis of the distributions of the t difference between successive peaks (modulo the laser period T_{laser}=12.367ns)

Gaussian + Tails (long λ)

rms~50-100 ps

~ exp (-t / O(ns))
contrib. several %
for long wavelengths

Data at λ=400nm
fit gives reasonable χ^2
with gaussian (σ_t^{fit}) +
constant term (dark noise contribution)

The detector resolution is obtained by
$\sigma_t^{fit}/\sqrt{2}$

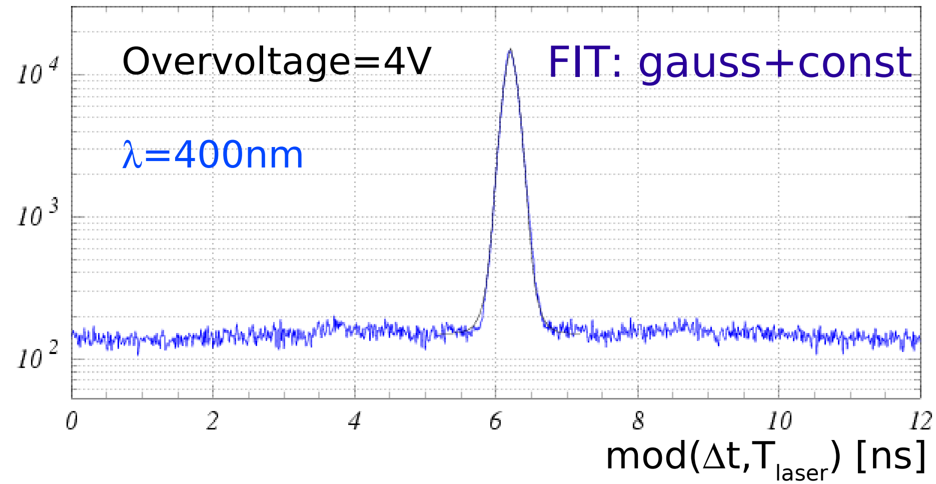

Data at λ=800nm
fit gives reasonable χ^2 with an additional exponential term $\exp(-\Delta t/\tau)$

- $\tau \sim 0.2 \div 0.8$ns in rough agreement with diffusion tail lifetime: $\tau \sim L^2 / \pi^2 D$ if L is taken to be the diffusion length
- Contribution from the tails ~ 10÷30% of the resolution function area

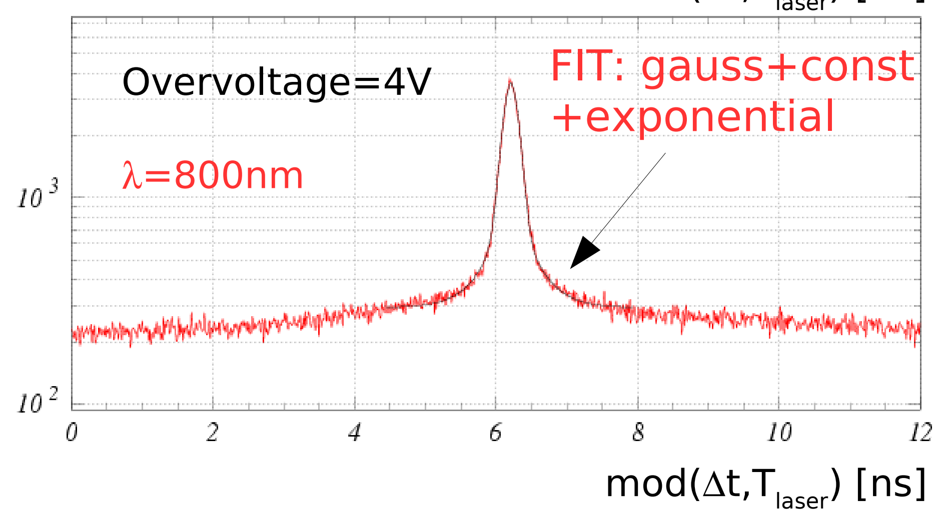

Distributions of the difference in time between successive peaks (modulo the measured laser period T_{laser}=12.367ns)

IRST – single photon timing res. (SPTR)

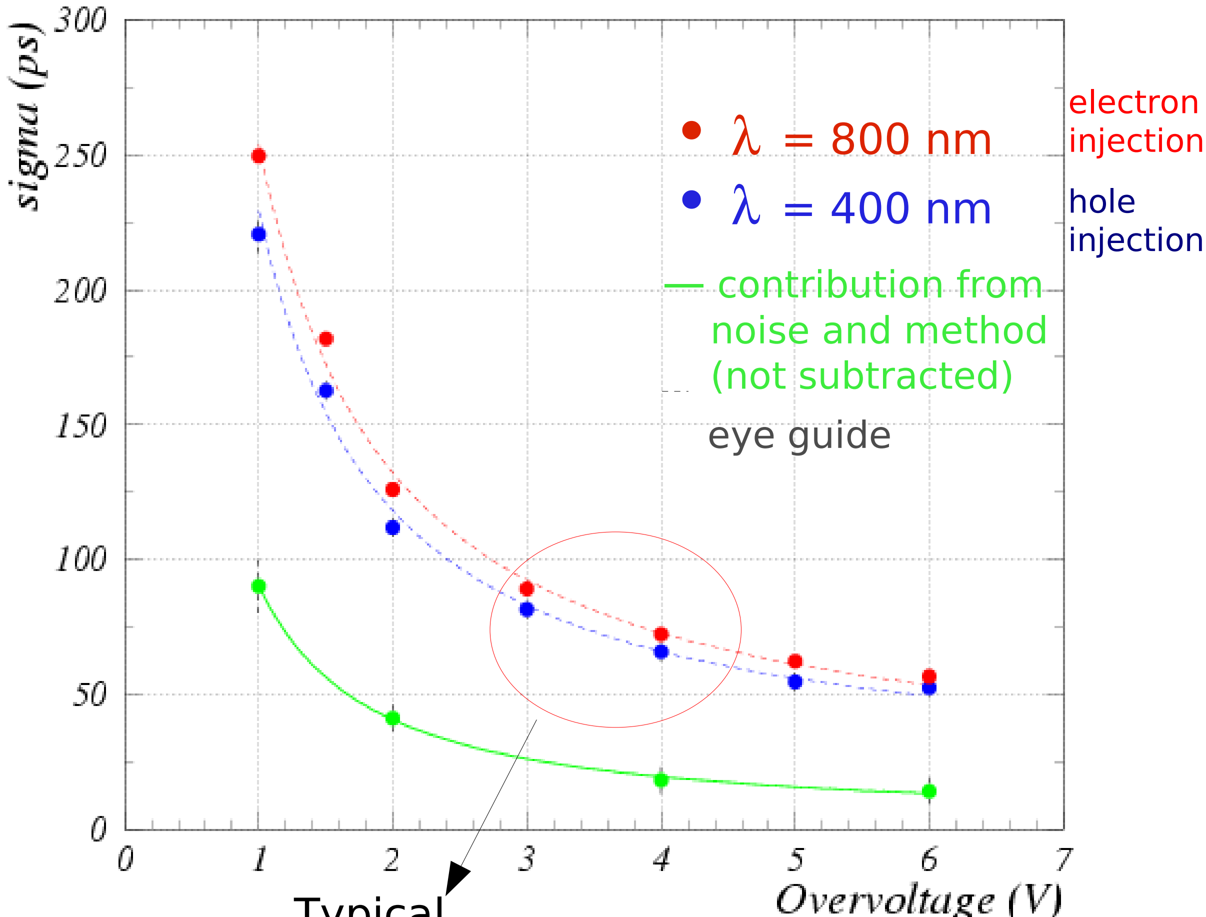

Typical working region

Better resolution for short wavelengths: carriers generated next to the high E field region

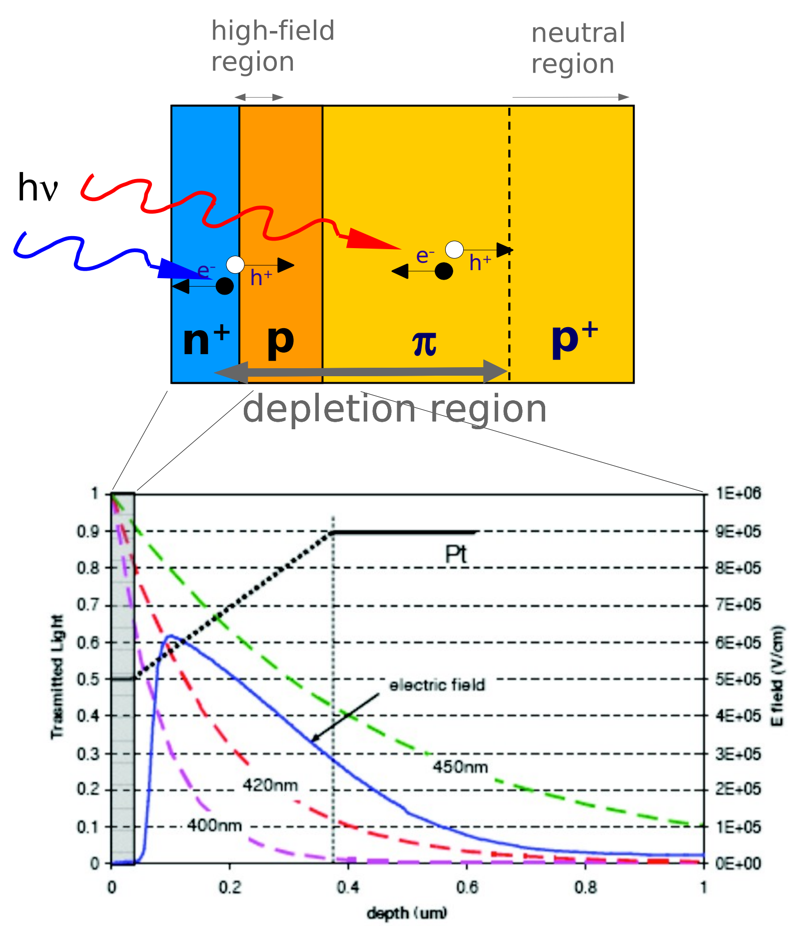

G.Collazuol et al NIMA 581 (2007) 461

IRST devices - shallow junction

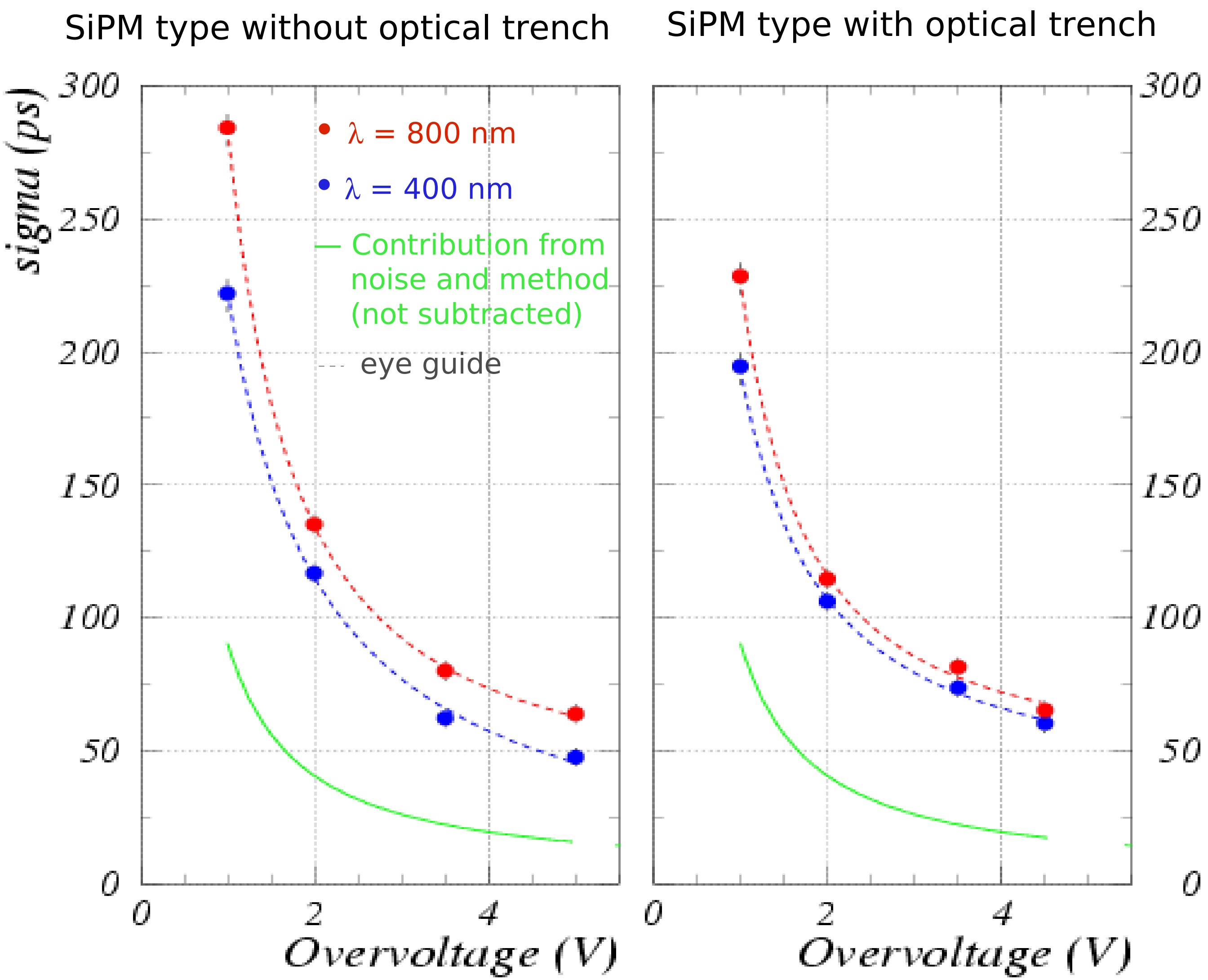

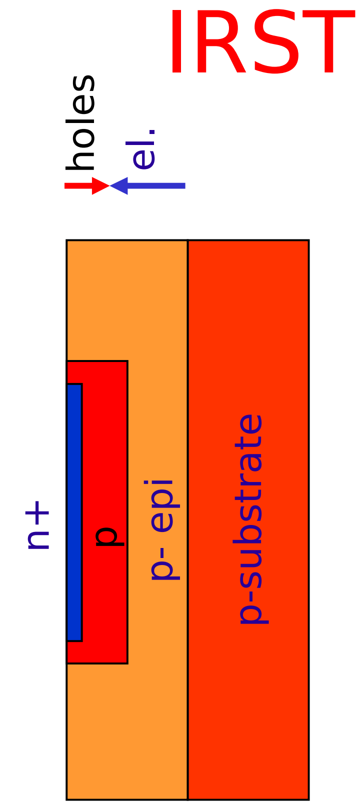

Results in fair agreement for devices with the same structure

Hamamatsu - shallow junction

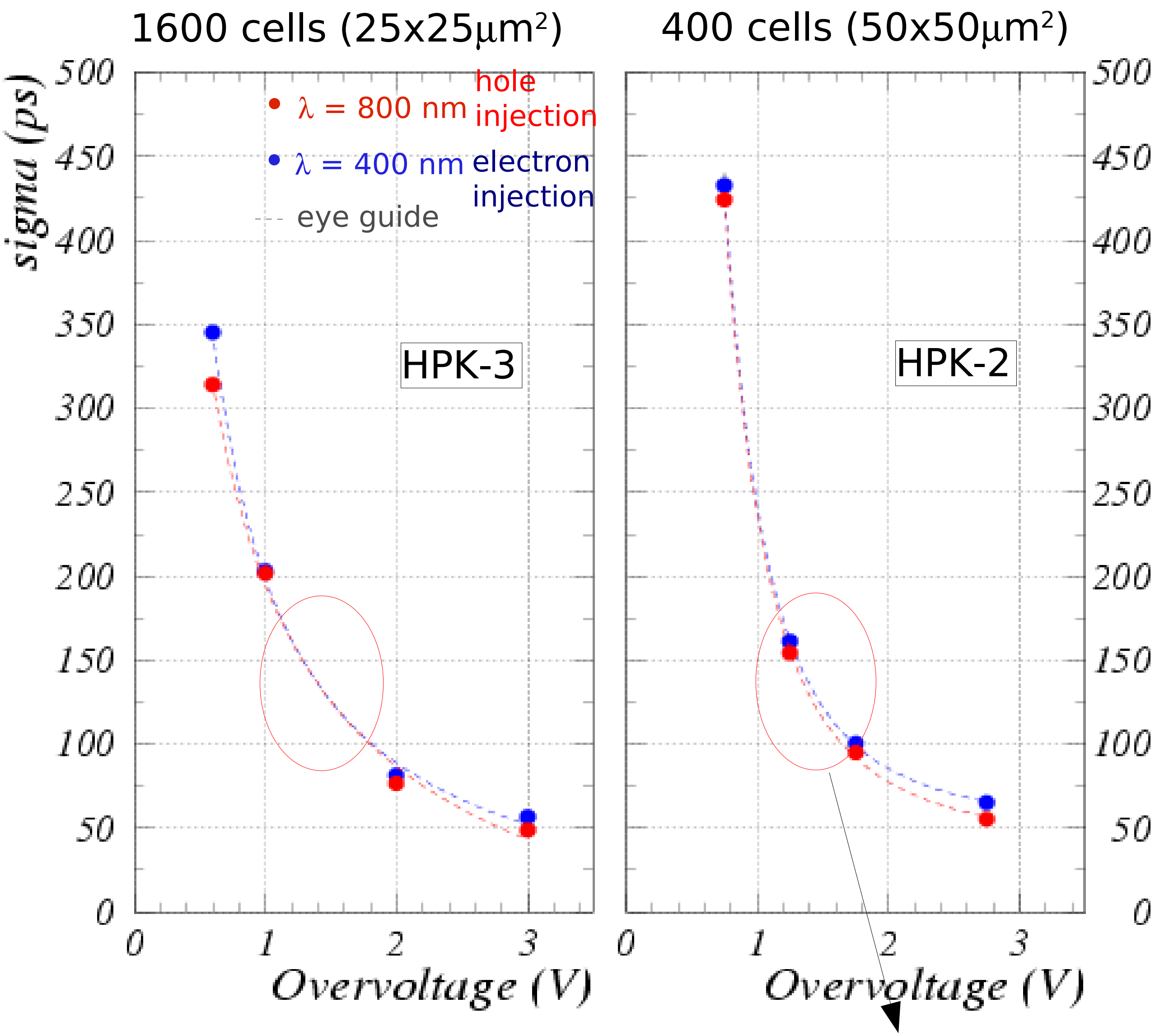

Suggested
Operating range

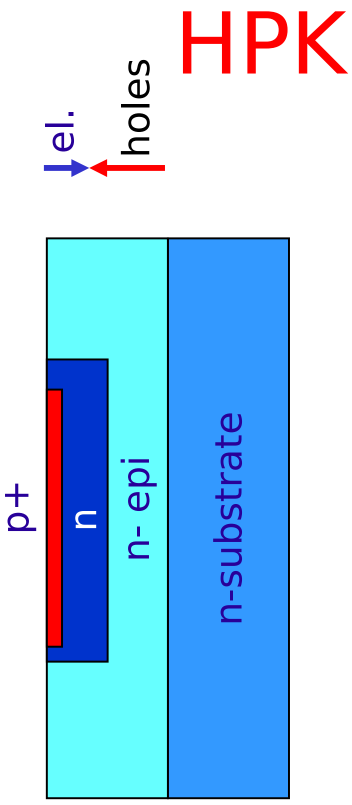

G.Collazuol et al (unpublished)

CPTA/Photonique - deeper structures

a) Green-Red sensitive
SSPM 050701GR_TO18

b) Blue sensitive
SSPM 050901B_TO18

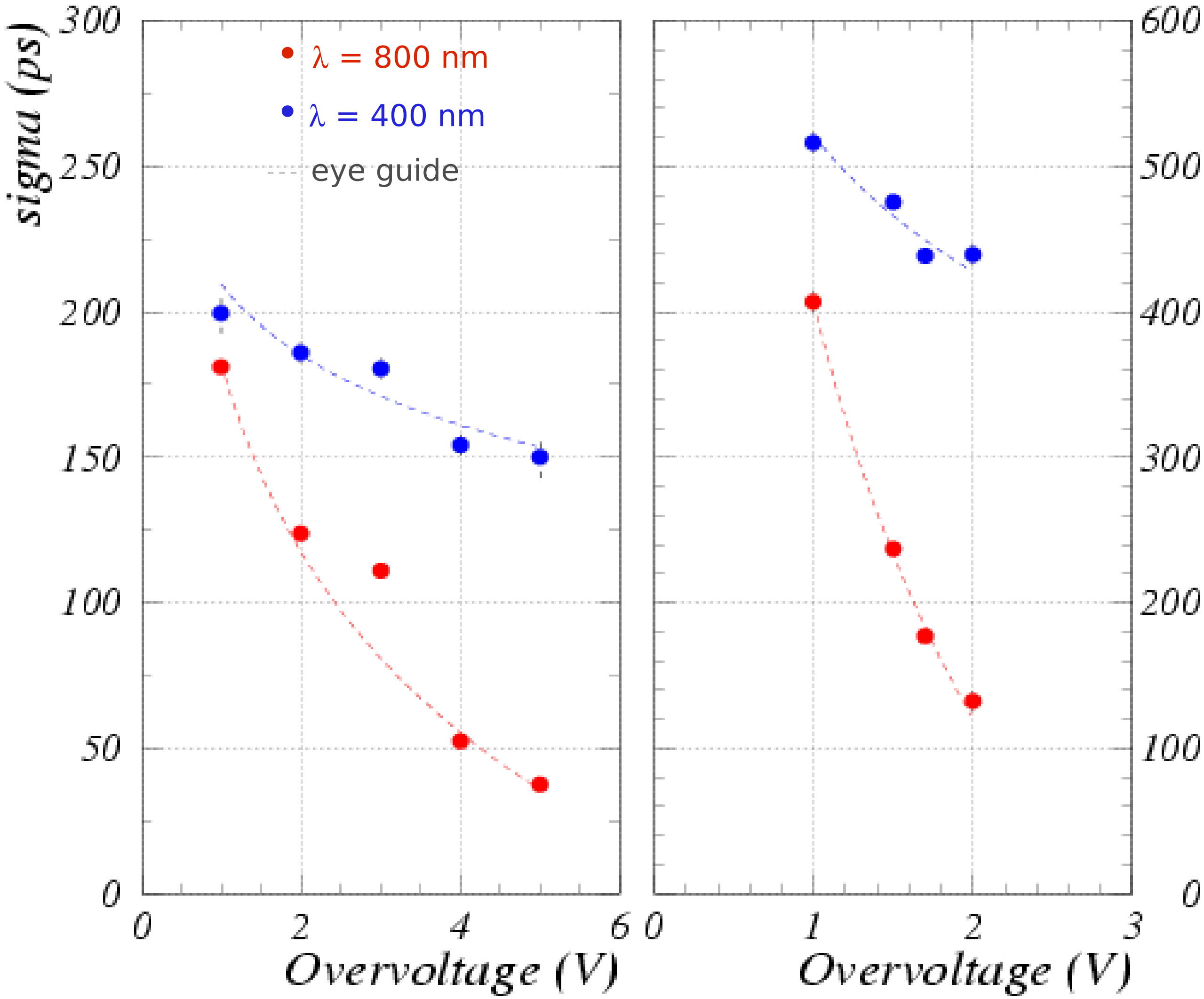

Two different structures:
a) thick n^+/p
b) p^+/n deep junction

G.Collazuol et al (unpublished)

SPTR: position dependence

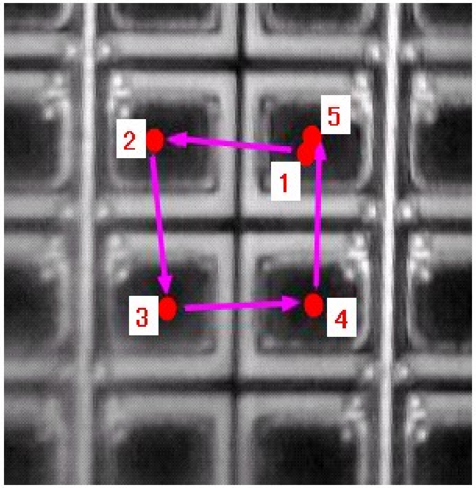

	FWHM (ps)	FWTM (ps)
1	199	393
2	197	389
3	209	409
4	201	393
5	195	383

K.Yamamoto PD07

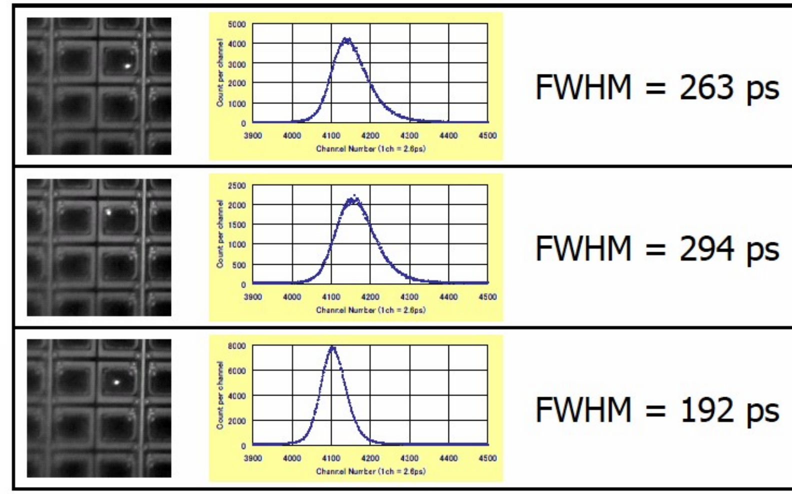

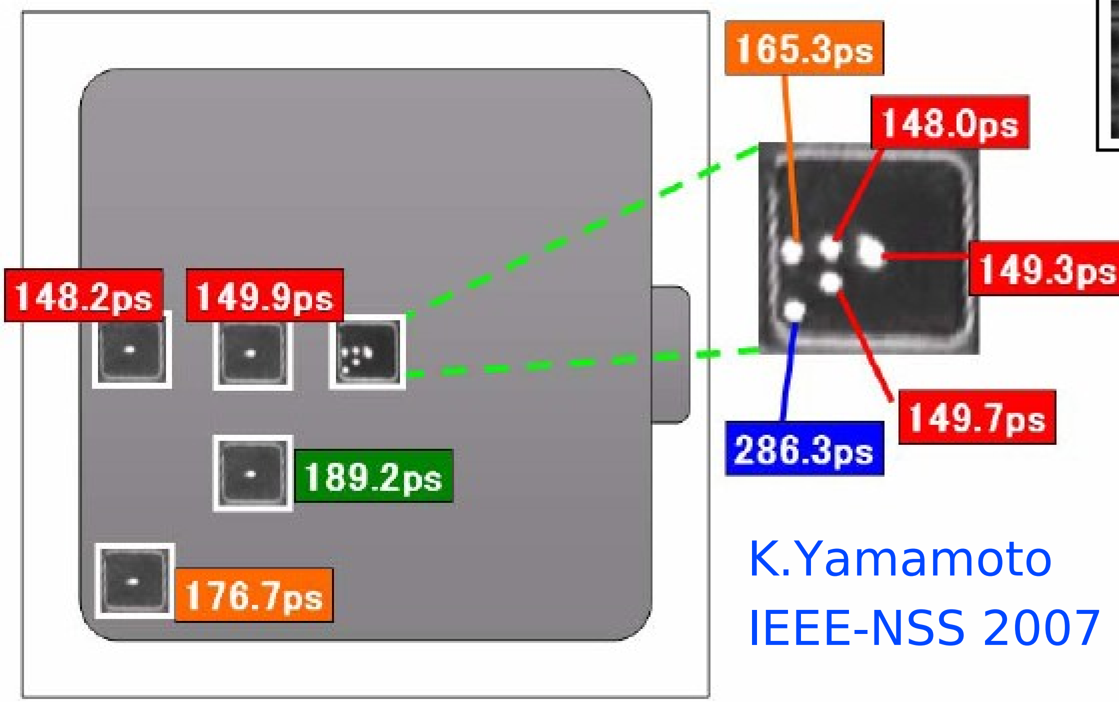

K.Yamamoto
IEEE-NSS 2007

Lower jitter if photo-conversion at the center of the cell

Due to higher V_{bd} at edges
→ cfr PDE vs position

Data include the system jitter
(common offset, not subtracted)

SPTR: timing at low T

Timing: better at low T

Lower jitter at low T due to higher mobility

(Over-voltage fixed)

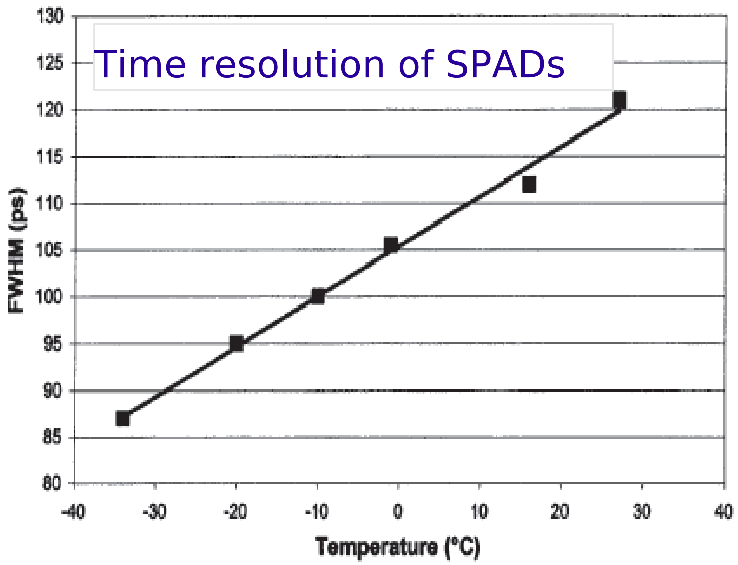

Fig. 11. FWHM of the SPAD response as a function of the temperature for a 20 μm diameter SPAD at 10 V overvoltage.

S.Cova el al, IEEE TED (2003)

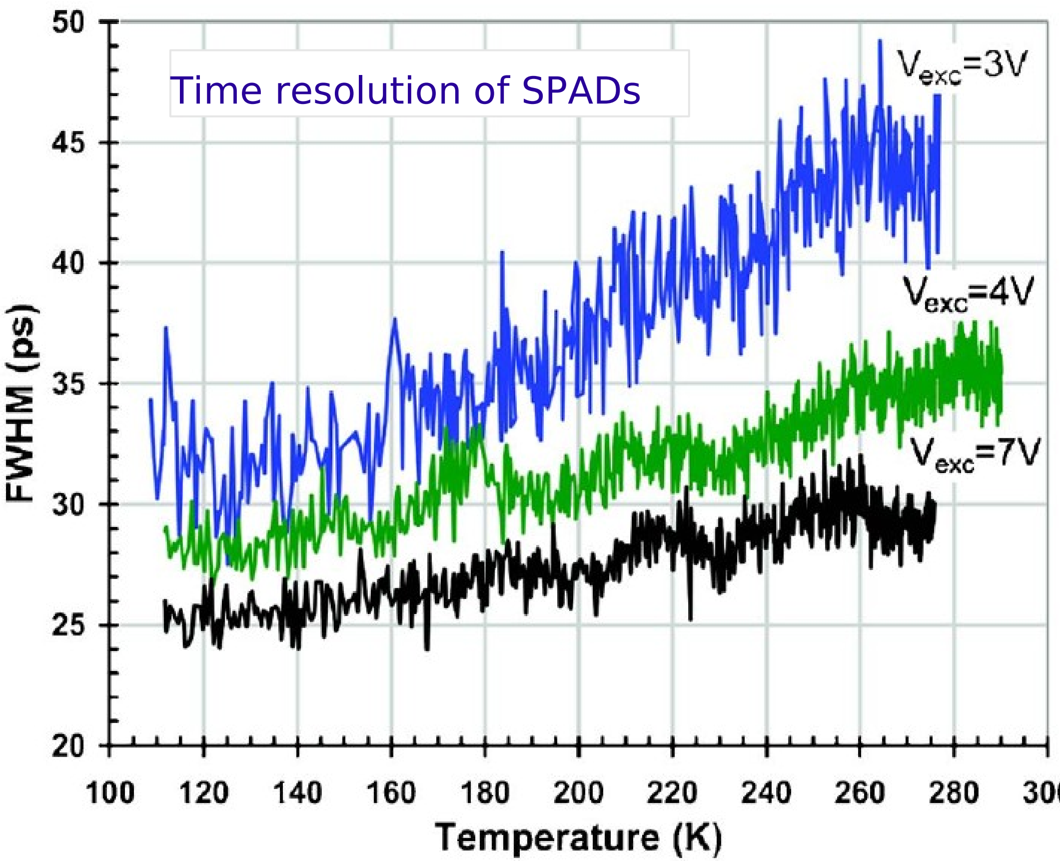

I.Rech el al, Rev.Sci.Instr. 78 (2007)

Timing properties → fast timing devices

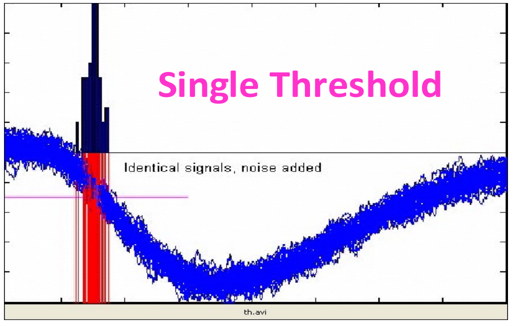

Timing by (single) threshold:

→ time spread proportional to 1/rise-time and noise

$$\sigma_{time} = \frac{\sigma_{amplitude}}{\frac{df(t)}{dt}}$$

Timing with optimum filtering:

→ best resolution with f'(t) weighting function

$$\sigma^2_{time} = \frac{\sigma^2_{amplitude}}{\int dt \left[\frac{df(t)}{dt}\right]^2}$$

Pulse sampling and Waveform analysis:

Sample, digitize, fit the (known) waveform
→ get time and amplitude

$$\sigma^2_{time} = \frac{\sigma^2_{amplitude}}{N_{samples} \int dt \left[\frac{df(t)}{dt}\right]^2}$$

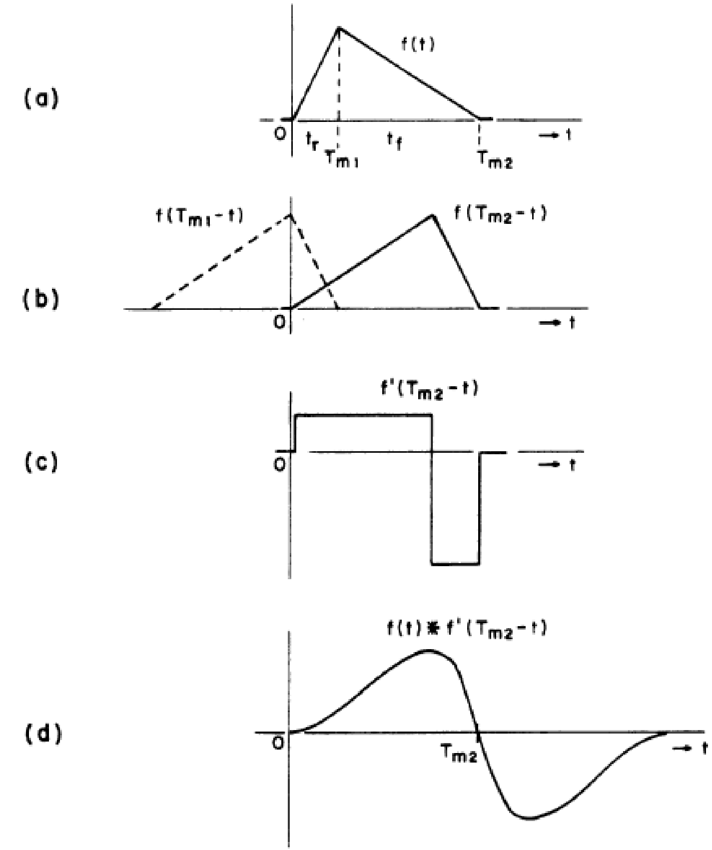

Fig. 7. Optimum filter for timing in presence of white noise (method of derivation).
(a) signal waveform
(b) optimum filter for amplitude measurements.
(c) optimum filter for timing - derivative of (b).
(d) output waveform.

V.Radeka IEEE TNS 21 (1974)

SiPM equivalent circuit (detailed model)

Single cell model → $(R_d||C_d)+(R_q||C_q)$
SiPM + load → $(||Z_{cell})||C_{grid} + Z_{load}$

Signal = slow pulse ($\tau_{d\ (rise)}, \tau_{q\text{-}slow\ (fall)}$) +
+ fast pulse ($\tau_{d\ (rise)}, \tau_{q\text{-}fast\ (fall)}$)

- $\tau_{d\ (rise)} \sim R_d(C_q+C_d)$
- $\tau_{q\text{-}fast\ (fall)} = R_{load}\ C_{tot}$ (fast; parasitic spike)
- $\tau_{q\text{-}slow\ (fall)} = R_q\ (C_q+C_d)$ (slow; cell recovery)

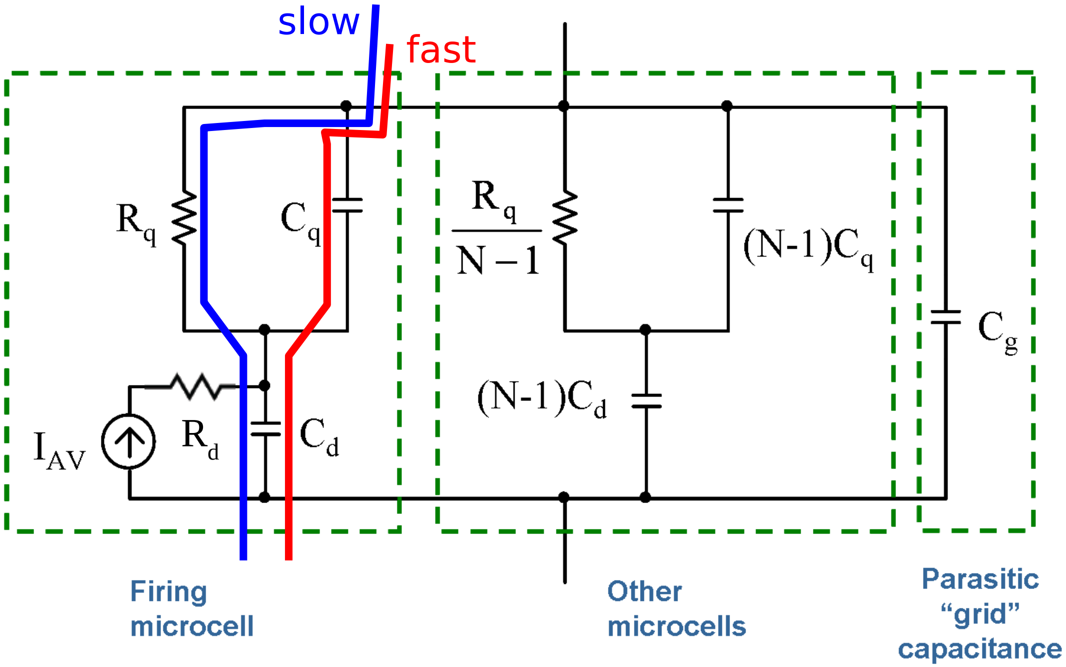

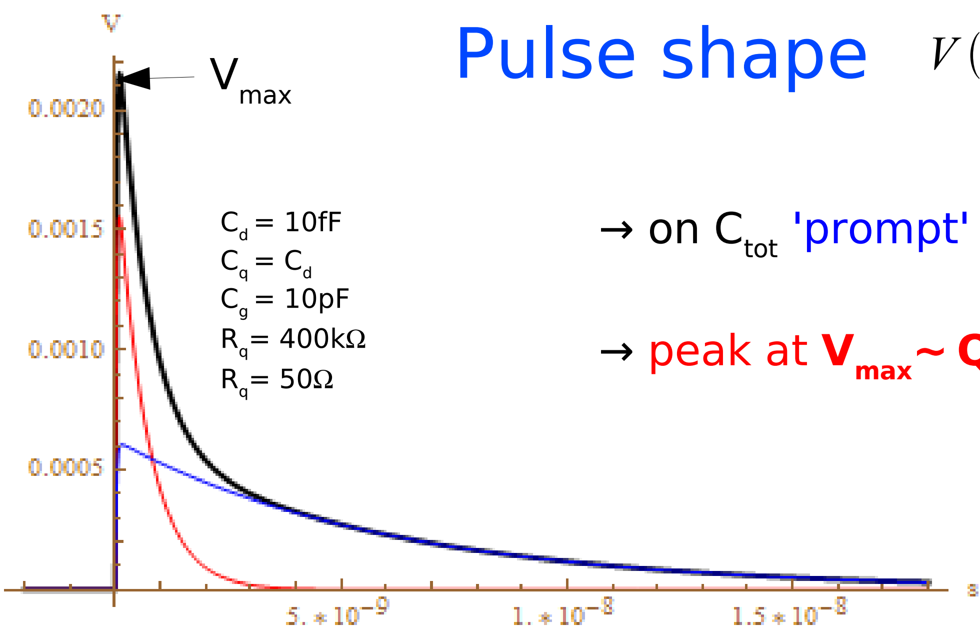

Pulse shape

$$V(t) \simeq \frac{Q}{C_q+C_d}\left(\frac{C_q}{C_{tot}} e^{\frac{-t}{\tau_{FAST}}} + \frac{R_{load}}{R_q}\frac{C_d}{C_q+C_d} e^{\frac{-t}{\tau_{SLOW}}}\right)$$

→ on C_{tot} 'prompt' charge $\mathbf{Q_{fast} = Q\ C_q/(C_q+C_d)}$

→ peak at $\mathbf{V_{max} \sim Q_{fast}/C_{tot}}$ **is independent of $\mathbf{R_{load}}$**

Optimizing signal shape for timing

Single cell model → $(R_d||C_d)+(R_q||C_q)$
SiPM + load → $(||Z_{cell})||C_{grid} + Z_{load}$

Signal = slow pulse ($\tau_{d\ (rise)}, \tau_{q\text{-}slow\ (fall)}$) +
+ fast pulse ($\tau_{d\ (rise)}, \tau_{q\text{-}fast\ (fall)}$)

- $\tau_{d\ (rise)} \sim R_d(C_q+C_d)$
- $\tau_{q\text{-}fast\ (fall)} = R_{load}\ C_{tot}$ (fast; parasitic spike)
- $\tau_{q\text{-}slow\ (fall)} = R_q\ (C_q+C_d)$ (slow; cell recovery)

High C_q improves timing performances

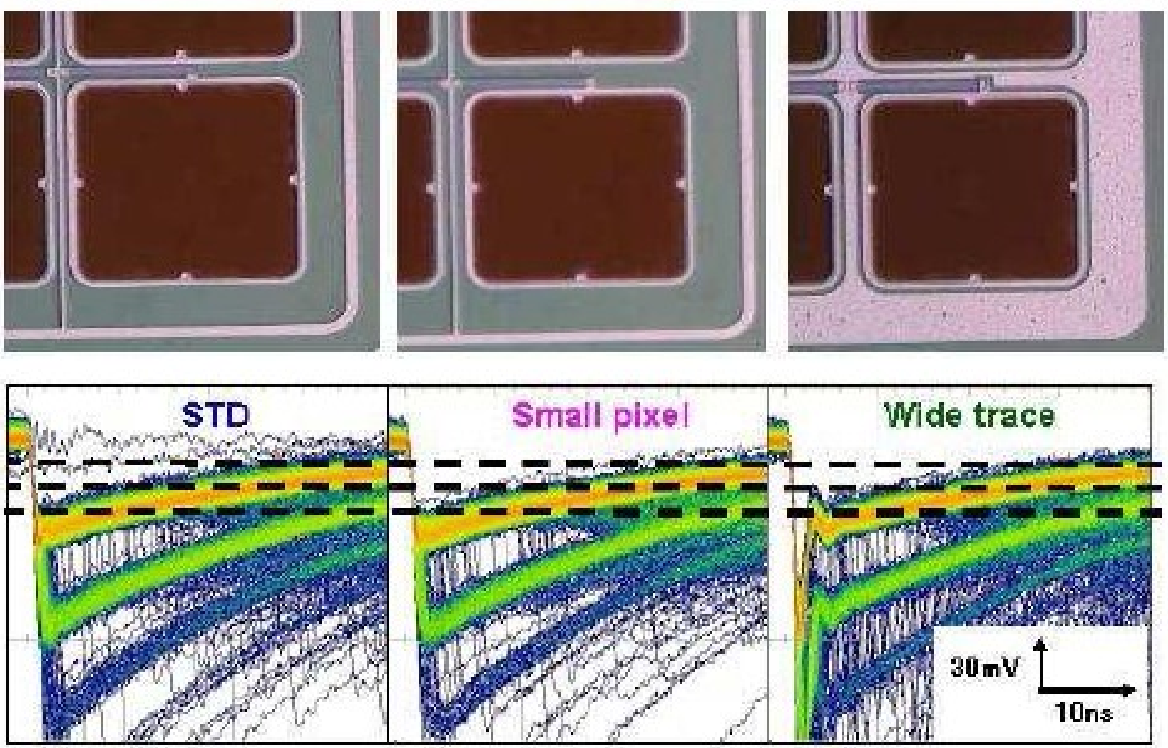

Yamamura et.al. at PD09

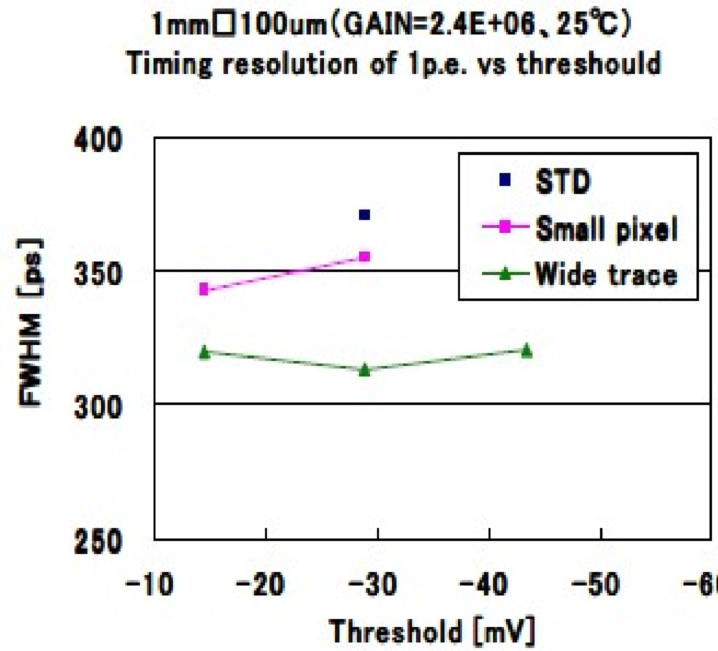

ASICs for SiPM signal readout (QDC/TDC)

W.Kucewicz "Review of ASIC developments for SiPM signal readout" - talk at CERN 11-2-2011

Chip Name	Measured quantity	Application	Input configuration	Technology
FLC_SiPM	Pulse charge	ILC Analog HCAL	Current input	CMOS 0,8 μm
MAROC	Pulse charge, trigger	ATLAS luminometer	Current input	SiGe 0,35 μm
SPIROC	Pulse charge, trigger, time	ILC HCAL	Current input	SiGe 0,35 μm
NINO	Trigger, pulse width	ALICE TOF	Differential input	CMOS 0,25 μm
PETA	Pulse charge, trigger,time	PET	Differential input	CMOS 0,18 μm
BASIC	Pulse height, trigger	PET	Current input	CMOS 0,35 μm
SPIDER (VATA64-HDR16)	Pulse height, trigger, time	SPIDER RICH	Current input	
RAPSODI	Pulse height, trigger	SNOOPER	Current input	CMOS 0,35 μm

ASICs for SiPM signal readout (QDC/TDC)

W.Kucewicz - CERN 11-2-2011

Chip Name	# of channels	Digital output	Power supply	Area [sqr mm]	Dynamic range	Input resistance	Timing jitter	Year
FLC_SiPM	18	n	5V (0,2W)	10			-	2004
MAROC2	64	y	5 V	16	80 pC	50 Ω		2006
SPIROC	36	y	5 V	32				2007
NINO	8	n	(0,24W)	8	2000 pe	20 Ω	260 ps	2004
PETA	40	y	(1,2W)	25	8 bit		50 ps	2008
BASIC	32	y	3,3 V	7	70 pC	17 Ω	~120 ps	2009
SPIDER (VATA64-HDR16)	64	n		15	12 pC			2009
RAPSODI	2	y	3,3 V (0,2W)	9	100 pC	20 Ω	-	2008

- Only a few of the suitable for low light intensity
- None is optimized for timing performances

ASICs for waveform sampling

Best performances for timing with Waveform Sampling
→ allowing proper processing of the peculiar SiPM signal
(handling fast/slow trailing front, after-pulses, cross-talk, ...)

	Hawaii	Varner		Saclay/Orsay	Delagnes/	Breton		PSI	S.Ritt	This proposal
	Blab1	Lab1-2	Lab 3	Hamac	Matacq	Sam	Planned	DRS3	DRS4	
Sampling	100 MHz-6 GHz		20 MHz-3.7GHz	40 MHz	0.7-2.5 GHz	0.7-2.5 GHz	10 GHz	10 MHz-5 GHz	5 GHz	10-20 GHz
Bandwidth (3db)	300 MHz		900 MHz	50 MHz	200-300 MHz	300 MHz	650 MHz	450 MHz	950MHz	> 1.5 GHz
Channels	1	8	9	8	1	2		12 6 2 1	8 4 2 1	4 16
Triggered mode	Yes		Common stop		Yes			Common stop	Common stop	Channel trigger
Resolution	10 bit			13.3 bit	13.4 bit	11.6 bit		11.6 bit	11.5 bit	8-10-bit
Samples	128 rows of 512	256	256	144	2520	256	2048	1024-12288	1024-8192	256
Clock			33 MHz	40 MHz	100 MHz				fsamp/2048	20-40 MHz
Max latency	560 us	2.2ms	50us							
Input Buffers	Yes			Yes	Yes	Yes	No	No	No	No
Differential inputs	No	No	No	Yes	Yes	Yes		Yes	Yes	Yes
Input impedance	50 Ohms	50 Ohms	50 Ohms Ext	10 MOhm/3pF	50 Ohms				11pF	50 Ohms
Readout clock	500 MHz			5 MHz	5 MHz	16 MHz		33 MHz	33MHz	500 MHz
Locked delays	Ext DAC	Ext DAC	Ext DAC			Yes		Ext PLL	Int PLL	Int PLL
On-chip ADC	12-b +500MHz TDC			No		No		No	No	Yes
R/W simultaneous	Yes			Yes		No		No	Yes	No
Power/ch	15mW/1.6W			36 mW	250-500 mW	150 mW		2-8mW	7.2mW at 2GS/s	
Dynamic range	1mV/1V			0.26mV/2.75V	175 uV-2V	0.65mV-2 V		0.35mV/1.1V	.35mV/1V	1V
Xtalk	Inter-rows 0.1%		10%			0.30%		< 0.5%		
Sampling jitter			4.5ps			25ps			6ps	?
Power supplies	-tbd/+2.5	-tbd/2.5V	-tbd/2.5V	-1.7/3.3V				2.5V	2.5V	1.2V
Process	TSMC .25	TSMC .25	TSMC .25	HP/DMILL .8	AMS .8	AMS .35	AMS .18	UMC .25	UMC .25	IBM .13
Chip area	5.25 mm2	10 mm2	2.5mm2	19.8mm2	30mm2			25mm2		1mm2/ch
Temp coeff	0.2%/°C		0.2%/°C					5e-5/°C	25ppm/°C	
Cost/channel	500$/40 10$/2k								10-15$	

Table by J.F.Genat “A 20 GS/s sampling ASIC in 130nm CMOS technology” - TWEPP 2010

Conclusions

Properties at low T

- Breakdown V decreases non linearly with T, as expected
  → better stablility against T variations than at T room
- Dark rate reduced by several orders of magnitude
  → tunneling mechanism(s) below ~200K
- After-pulsing at % level down to 100K; blow up below 100K
- PDE vs T: modulation up to ±50% wrt T room
  → PDE decr. as T 300K → 250K, incr. as T 250K → 120K, then freeze-out
- PDE vs λ: PDE peaks at lower λ as T decreases
- Cross-talk and Gain (detector capacity) are independent of T (at fixed ΔV)
- Timing resolution improves at low T

SiPMs behave very well at low T, even better than at room T
In the range **100K<T<200K SiPM perform optimally**;
→ excellent alternatives to PMTs in cryogenic applications (eg Noble liquids)
→ Optimization for low T (quenching R, …)

Timing Properties

- Intrinsically ultra-fast devices:
  time to breakdown and jitter < 100ps
- Not negligible non-gaussian tails (ns) for longer wavelengths
- Smaller jitter for blue light than red (depends on the struture)
- Peculiar signal shape
  → device optimization for timing
  → waveform sampling superior to CFT/ADC/TDC readout

Additional material

Zoom of the cell: SiPM technology at IRST

Shallow-Junction

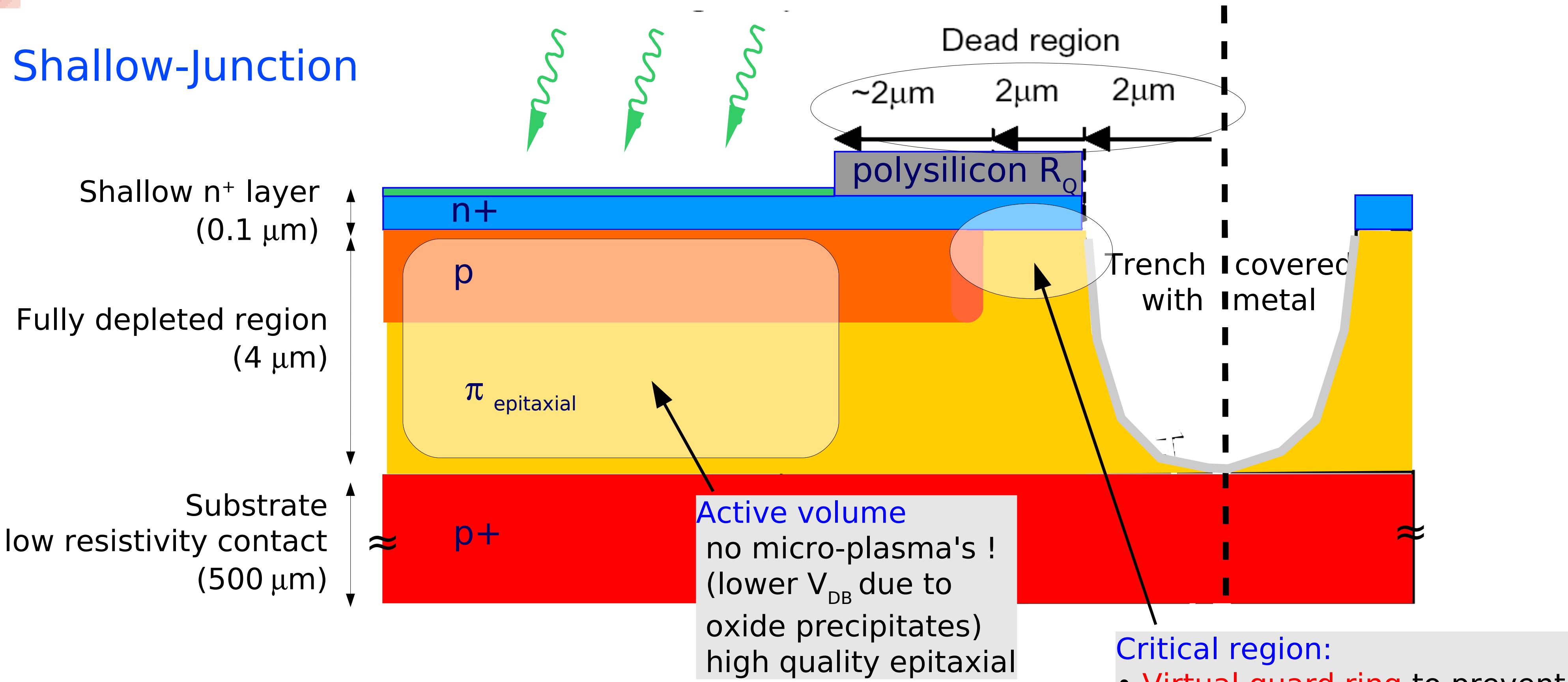

Optimization for the blue light (420nm)

- n^+ on p abrupt junction structure
- Anti-reflective coating (ARC) optimized for λ~420nm
- Very thin (100nm) n^+ layer: "low" doping n^+ layer
  → minimize Auger and SHR recombination
- Thin high-field region: "high" doping p layer (limited by tunneling breakdown)
  → fixes V_{BD} junction well below V_{BD} at edge
- R_Q by doped polysilicon
- Trenches for optical insulation (low cross-talk)
- Fill factor: 20% - 80%

C.Piemonte NIM A 568 (2006) 224

Low T

Applications w/ SiPM in cryogenic environments

Secondary scintillation from noble liquids generated by thick GEM (THGEM) for applications in neutrino physics, dark matter searches and PET

ArDM: Two-phase Ar detector using THGEM for DM search [A.Rubbia et al., J. Phys. Conf. Ser. 39(2006)129]

!!! Need recording both ionization and scintillation with a threshold of ≤10keV (200 electrons)

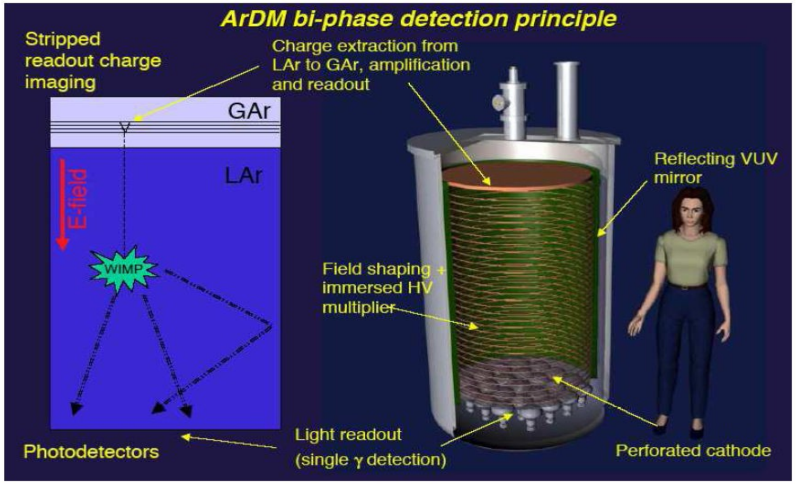

A.Buzulutskov et al.
Vienna Conference VCI 2010 and
arXiv:1005.5216v1

NIR emission spectrum of pure Ar (due to Ar I atomic lines) from avalanche scintillations at 750 Torr, gain~30, yield ~1ph/e. [M.M.Fraga et al. IEEE Trans.Nucl.Sci. 47(2000)933]

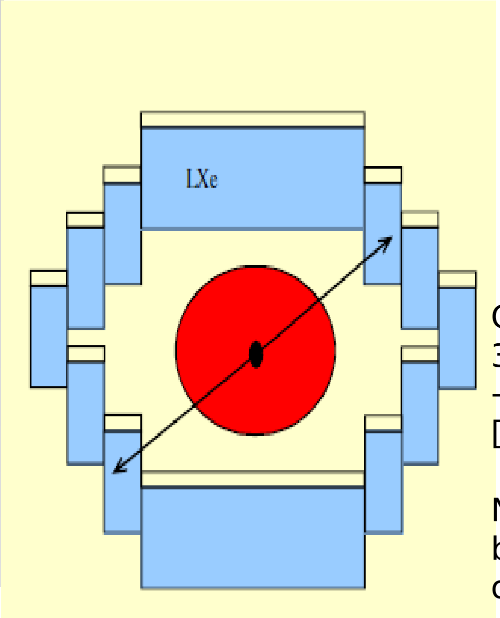

Two-phase Ar and Xe detectors using GEM/THGEM for coherent neutrino-nucleus scattering
[ITEP & Budker INP: Akimov et al. JINST 4 (2009) P06010]

!!! Need single electron counting

GEM-based two-phase Xe avalanche detector for PET:
3D liquid TPC recording 511 keV γ-rays
→ obtain superior (~1mm) spatial resolution.
[Budker INP: CRDF grant RP1-2550 (2003)]

Need for Xe detector with 3D readout of both ionization and scintillation with a threshold of > 100 keV (2000 electrons)

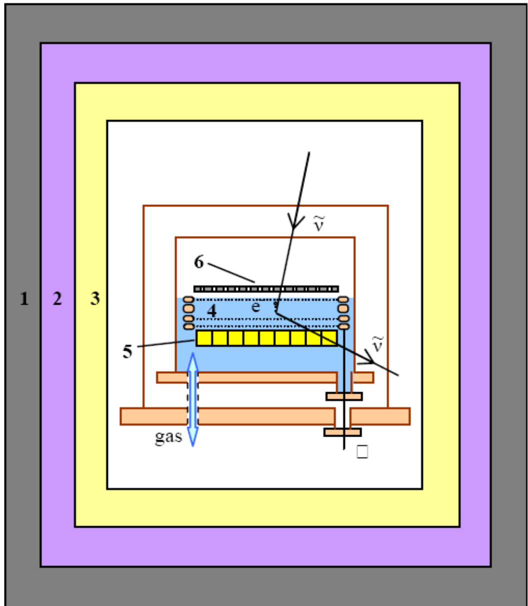

Applications w/ SiPM in cryogenic environments

P.K.Lightfoot, et al.
J. Phys.: Conf. Ser. 179 (2009) 012014

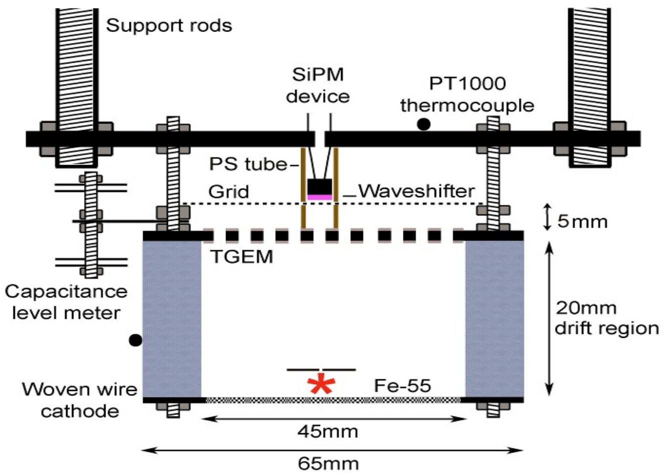

Electroluminescence from the cold gas phase of a double phase Ar system

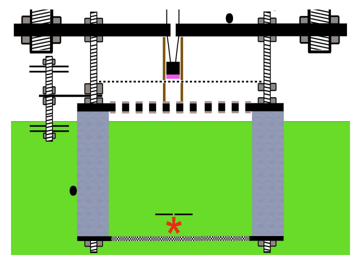

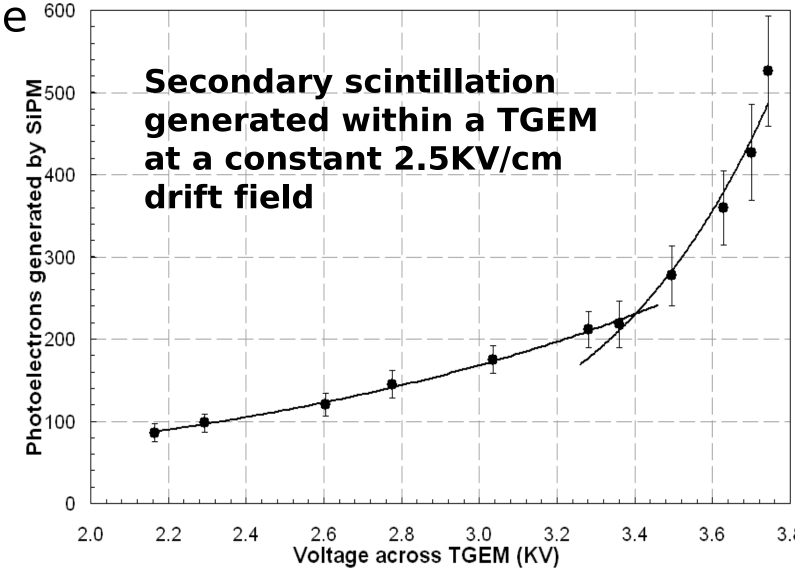

see talk by N.McConkey at this conference !!!

Electroluminescence from LAr

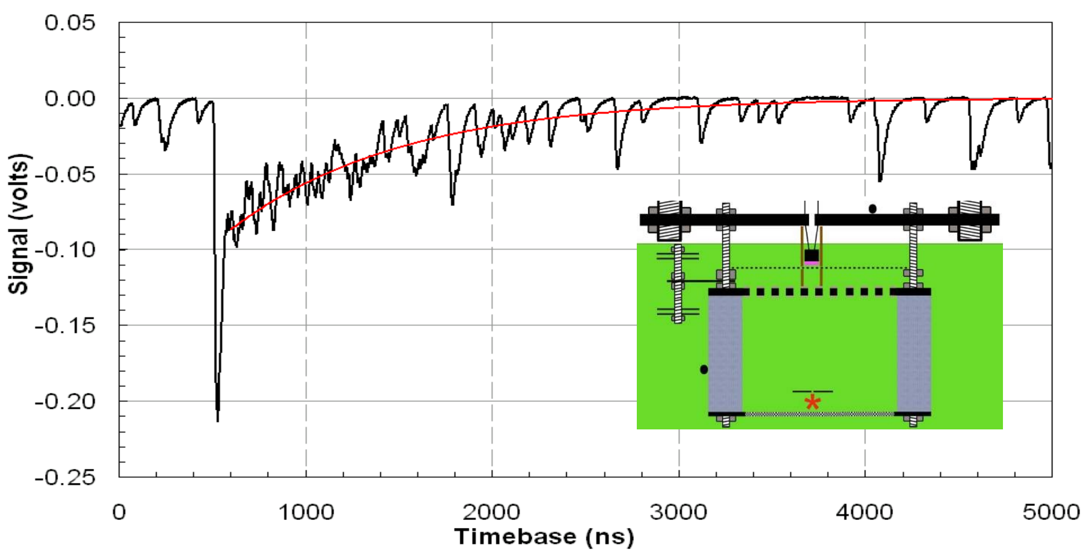

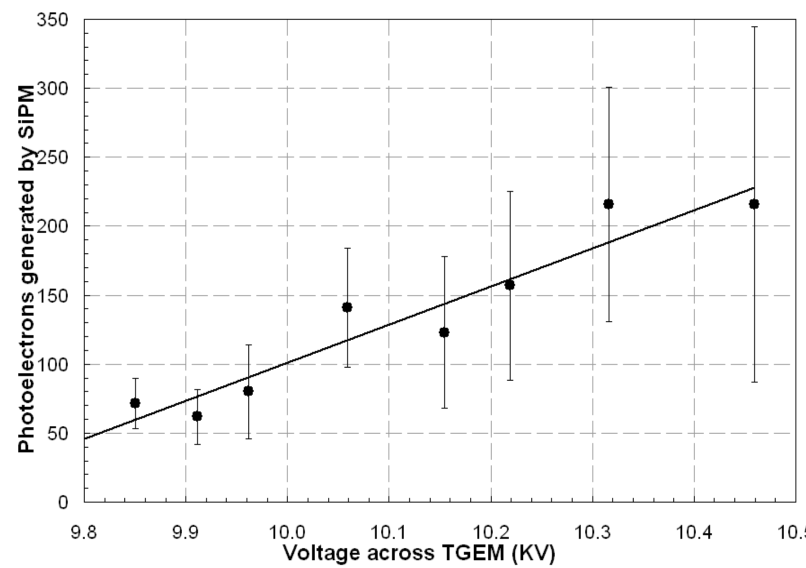

128nm VUV light produced within the TGEM holes was then incident on an immersed SiPM device coated in the waveshifter tetraphenyl butadiene (TPB), the emission spectrum peaked at 460nm in the high quantum efficiency region of the device

Silicon properties at low T: higher mobility

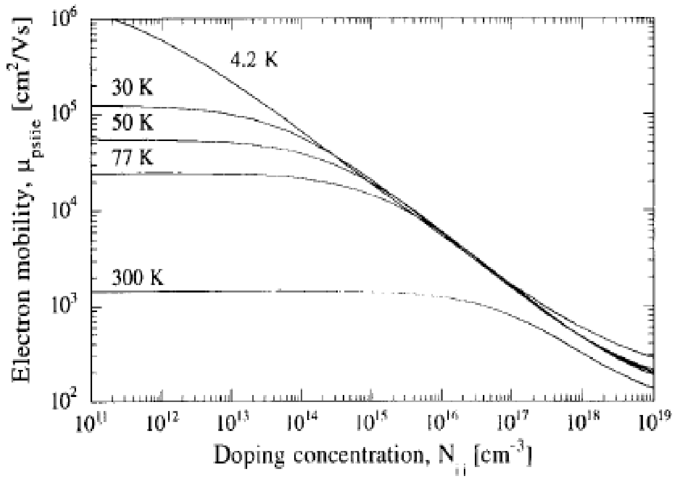

FIGURE 1.16. Calculated electron mobility due to phonon and ionized impurity scattering mechanisms. The five plots correspond to $T = 300, 77, 50, 30$, and 4.2 K.

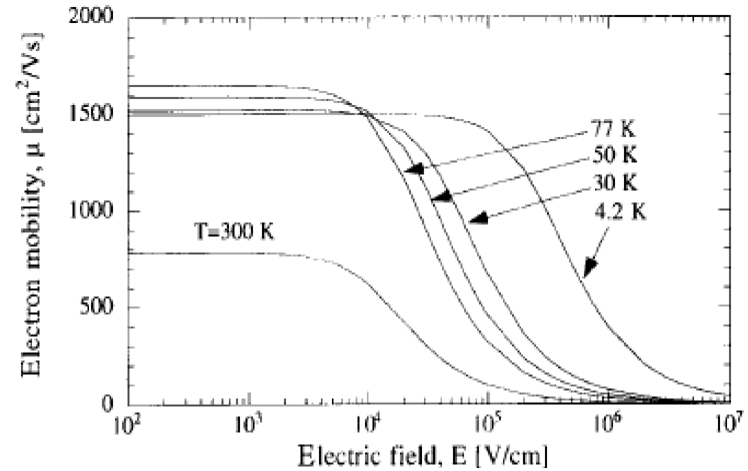

FIGURE 1.17. Calculated electron mobility, due to phonon, ionized impurities, and velocity saturation effects, as a function of the electric field for five temperatures; $N_{ii} = 10^{17}\,cm^{-3}$.

Silicon propt's at low T: carriers freeze-out

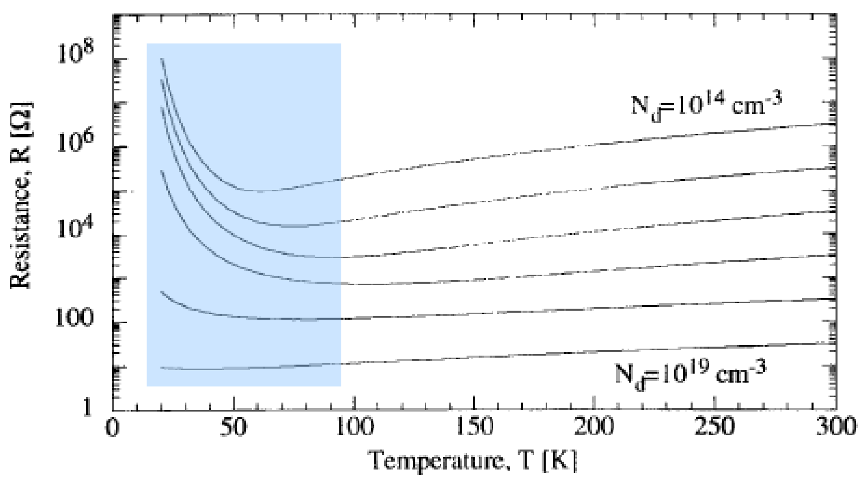

FIGURE 1.14. Calculated electrical resistance of a silicon slab of $(W/L) = 20/50\,\mu m$ and depth of 1 μm for different doping concentration levels.

For T<100 K, the ionized impurities act as shallow traps (provided the impurity doping concentration below of 10^{18} atoms/cm^2) and carriers begin to occupy these shallow levels.

For T<30 K, practically no carriers remain in the bands

Plots from Guiterrez, Dean, Claeys - "Low Temperature Electronics: Physics, Devices, Circuits and Applications", Academic Press 2001

Silicon propt's at low T: impact ionization

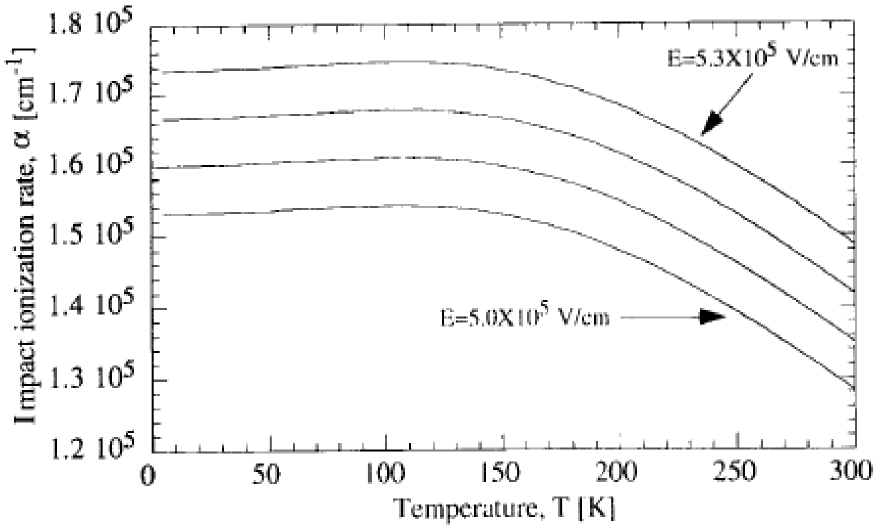

FIGURE 1.43. The impact ionization rate α as a function of temperature T_A with the electric field E as a parameter calculated from Okuto and Crowell's *(85)* model.

For T<77K no data are available → modeling is quite difficult...

Silicon propt's at low T: absorption length

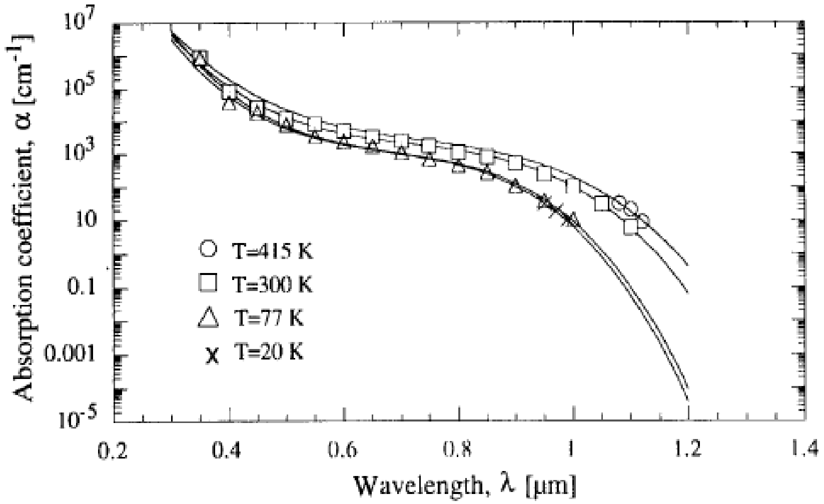

FIGURE 1.53. Experimental (symbols) and fitted (lines) absorption coefficient α of silicon at T = 415, 300, 77, and 20 K [replotted from Rajkanan *et al. (109)*].

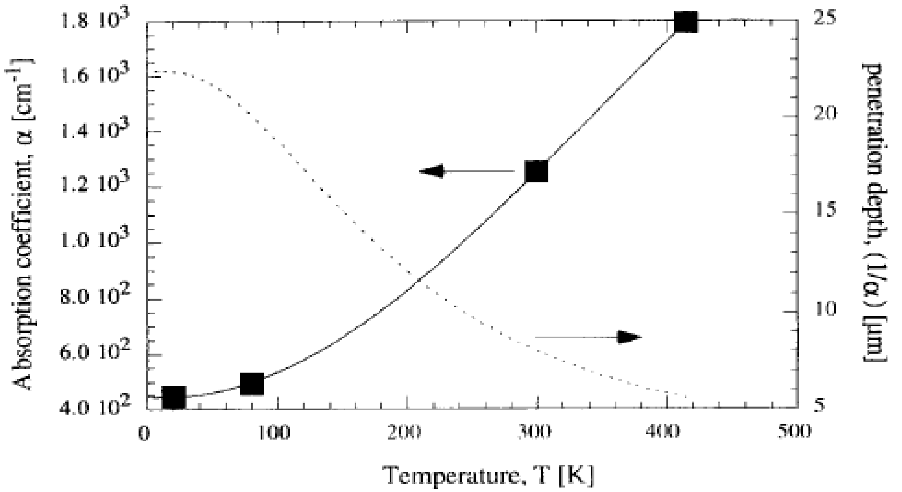

FIGURE 1.54. Measured absorption coefficient α (■) *(101)* and fitted α (solid line) versus temperature *T*. On the right axis the fitted penetration depth (1/α) is also shown.

Avalanche breakdown vs T

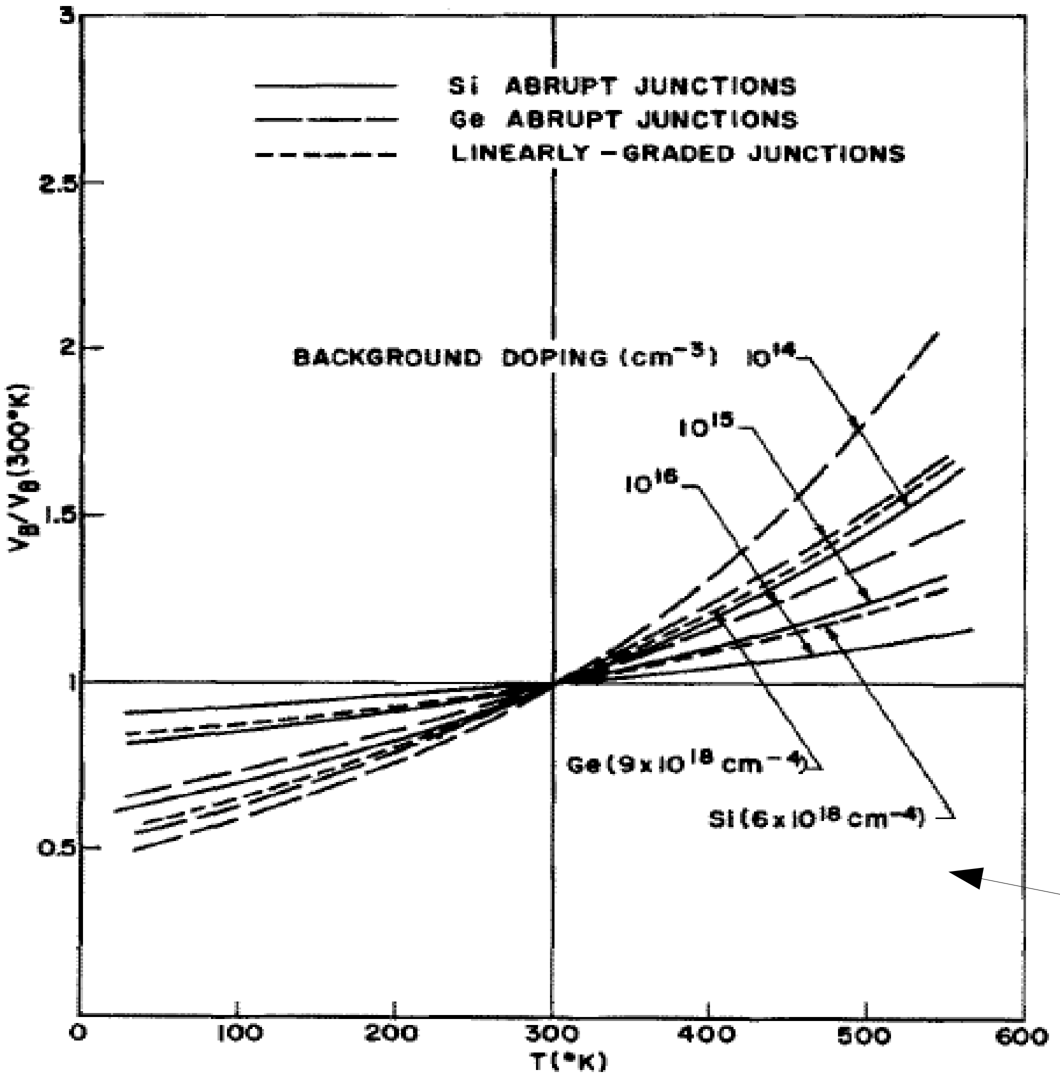

Fig. 4. Breakdown voltage vs temperature for Si and Ge *p-n* junctions. V_B(300°K) is 2000, 330, and 60 V for Si and 950, 150, and 25 V for Ge for dopings of 10^{14}, 10^{15}, and 10^{16} cm^{-3} respectively. The linear-graded junctions have V_B(300°K) the same as those for doping of 10^{15} cm^{-3}.

Avalanche breakdown V is expected to show a **non linear dependence on T** (depending of the junction type and doping concentration)

Breakdown V decreasing with T due to increasing mobility

NOTE: in freeze-out regime Zener (tunnel) breakdown could be relevant.
→ negative Temperature coefficient (increasing with decreasing T)

Crowell and Sze

More recent model by Crowell and Okuto after Shockley, Wolff, Baraff, Sze and Ridley.

p-n junction characteristics: forward bias

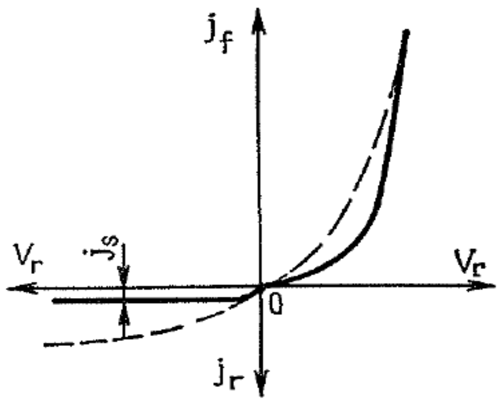

Fig. 8.16. The current-voltage characteristic of a *pn* junction

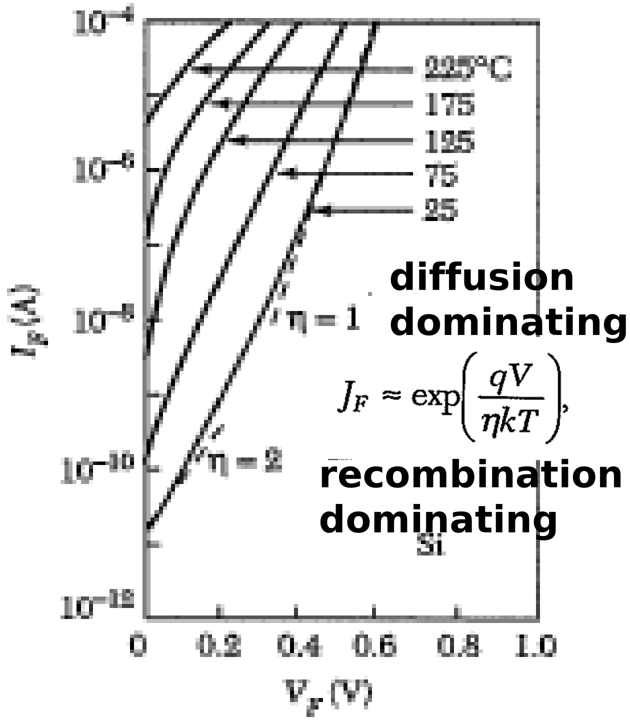

Sze - "Semiconductor devices"

E.Johnson (RMD) at IEEE 2009
"Characterization of CMOS APD at cryogenic T"

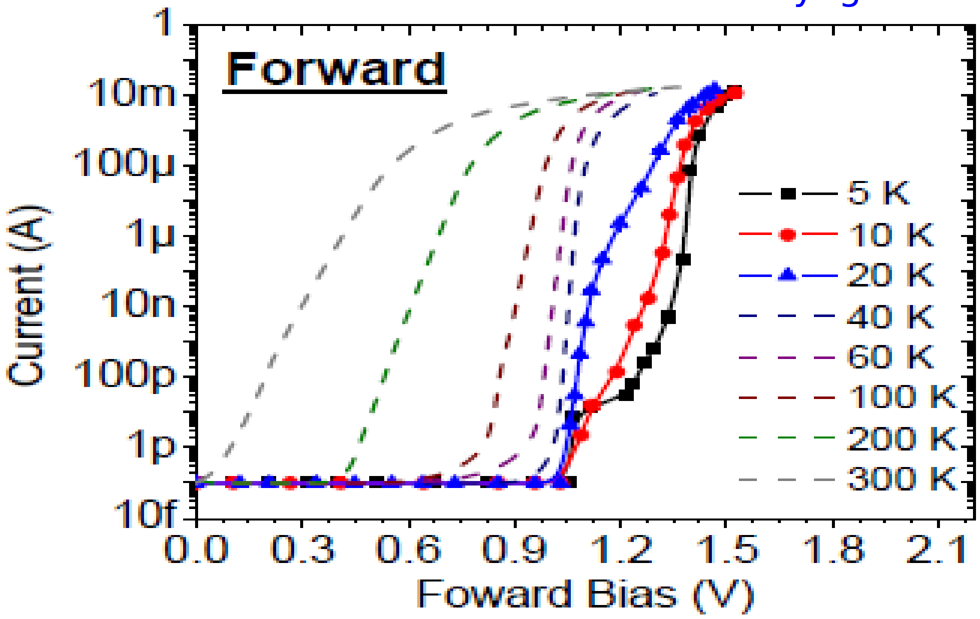

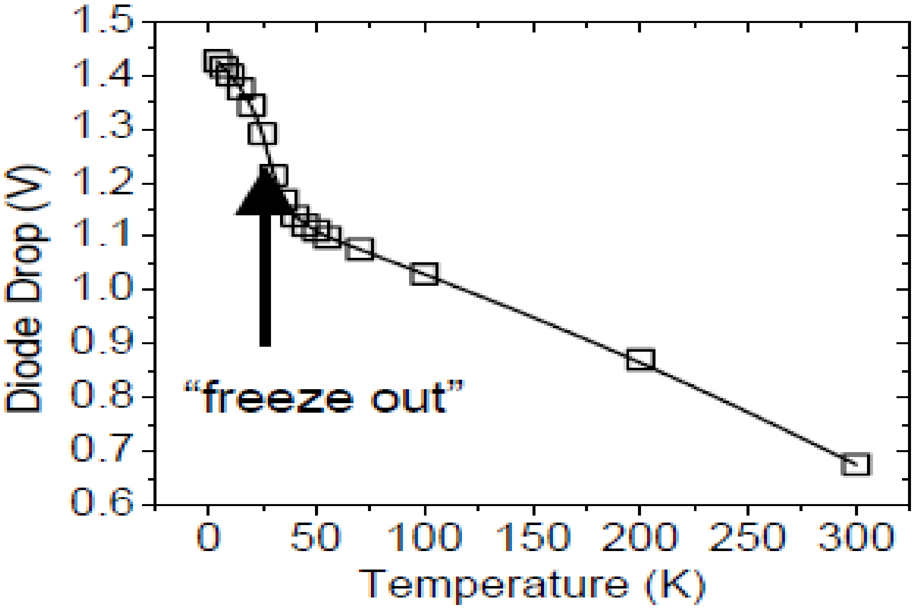

Dark Rate

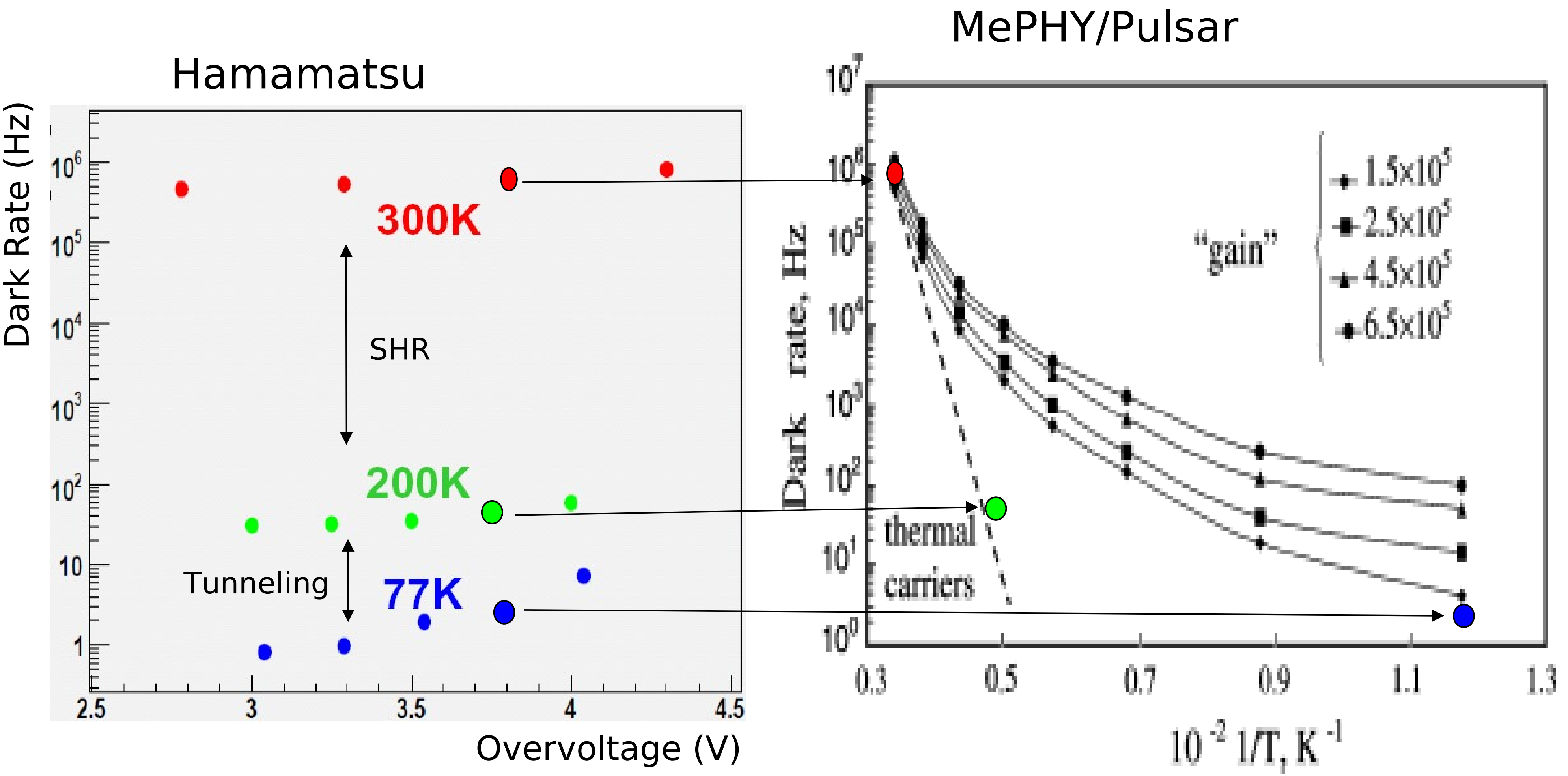

H.Otono – PD07

Dolgoshein et al, NIM A 442 (2000)

Electric field engineering and silicon quality make huge differences in dark noise as a function of T

T dependence: after-pulse, cross-talk

After-pulses: increases at low T

Trap lifetime decreases as T increases

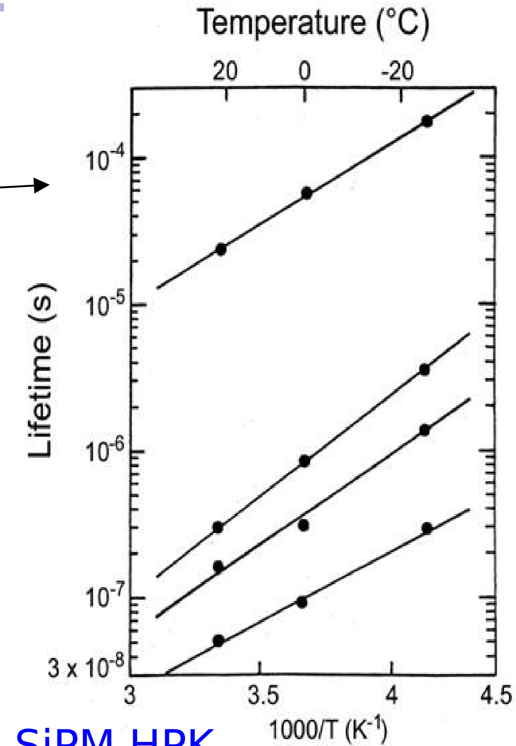

S.Cova, A.Lacaita, G.Ripamonti, IEEE EDL (1991)

Afterpulses - SiPM HPK

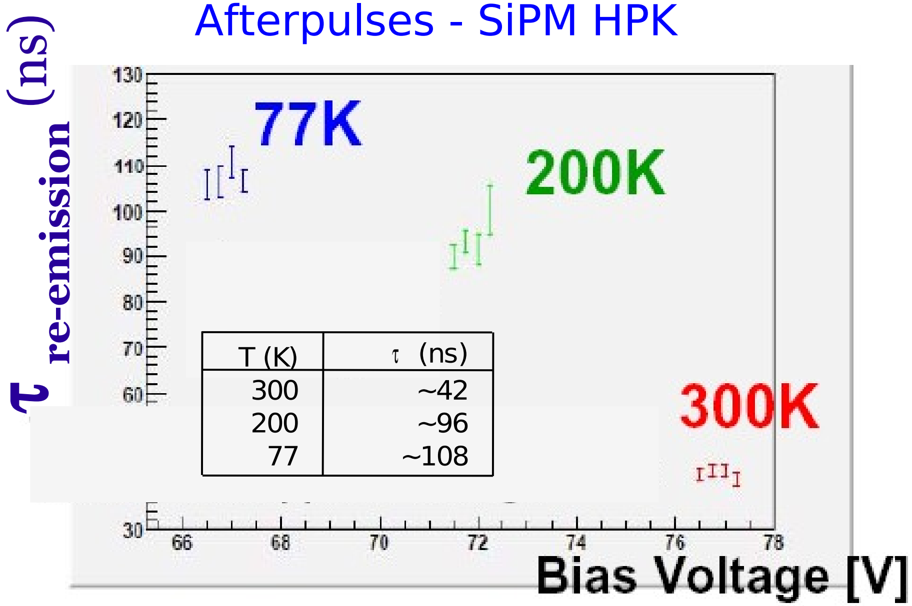

T (K)	τ (ns)
300	~42
200	~96
77	~108

Cross-talk: decreases at low T

Observed slight reduction at low T

(I guess: due to lower PDE for long wavelength photons which dominate the carrier luminescence spectrum)

H.Otono – PD07

Crosstalk - SiPM HPK

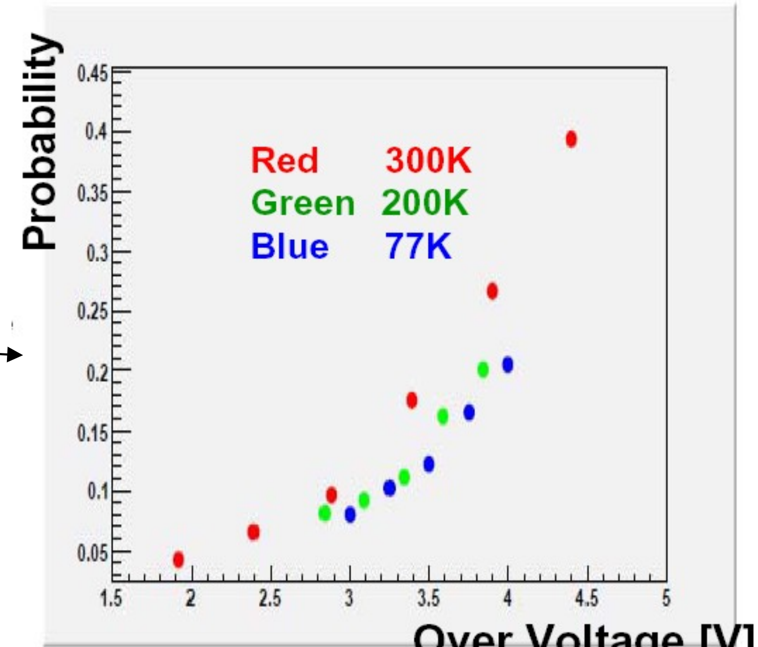

PDE at various λ – T scan (ΔV =2V)

PDE dependence on T at fixed gain. Normalization with calibrated photo-diode current and with PDE at T=300K (double ratio)

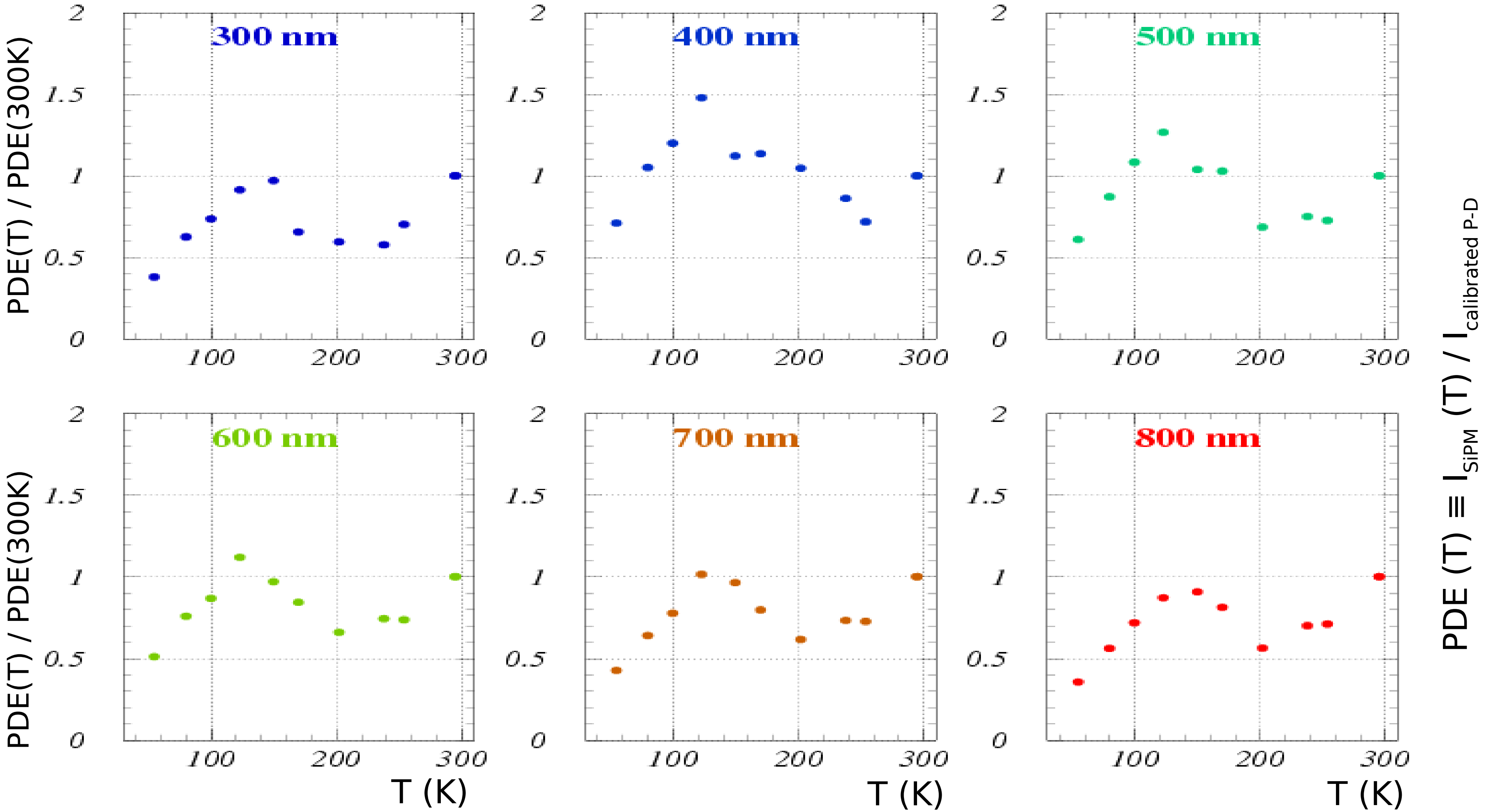

- shape similar at different λ → related to properties of multiplication /recombination
- lower efficiency at low T for longer λ → due to absorption length ~ 1/T (with constant depletion width)

PDE (SPAD/APD devices)

PDE dependence on T
(Over-voltage fixed)

Combination of various effects:

- P_{01} increases at low T because of increased impact ionizazion
- Optical attenuation length increased (Energy gap increases) at low T
- Depletion region widening in APDs, but not in SiPM which are fully depleted

Similar effect expected also for SiPM

SPAD: Cova el al, Rev.Sci.Instr. 7 (2007)

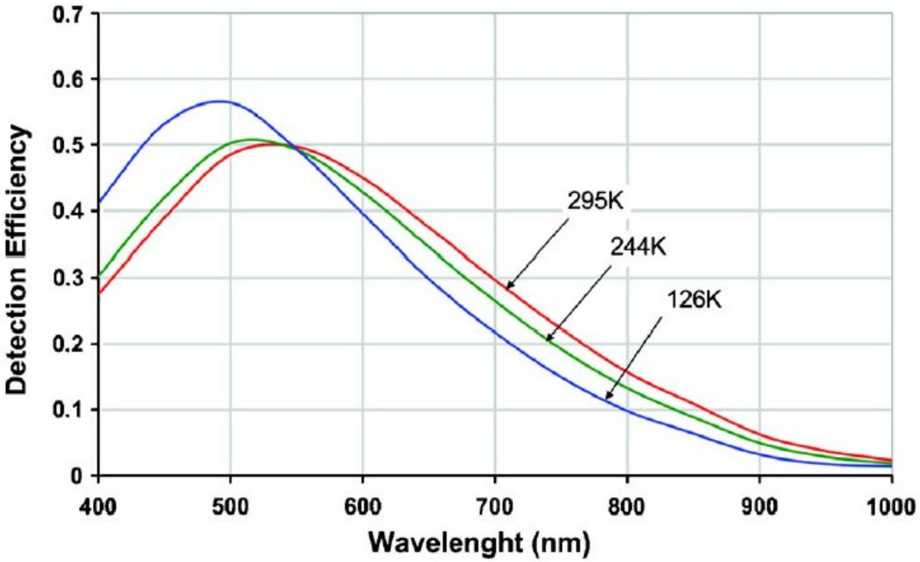

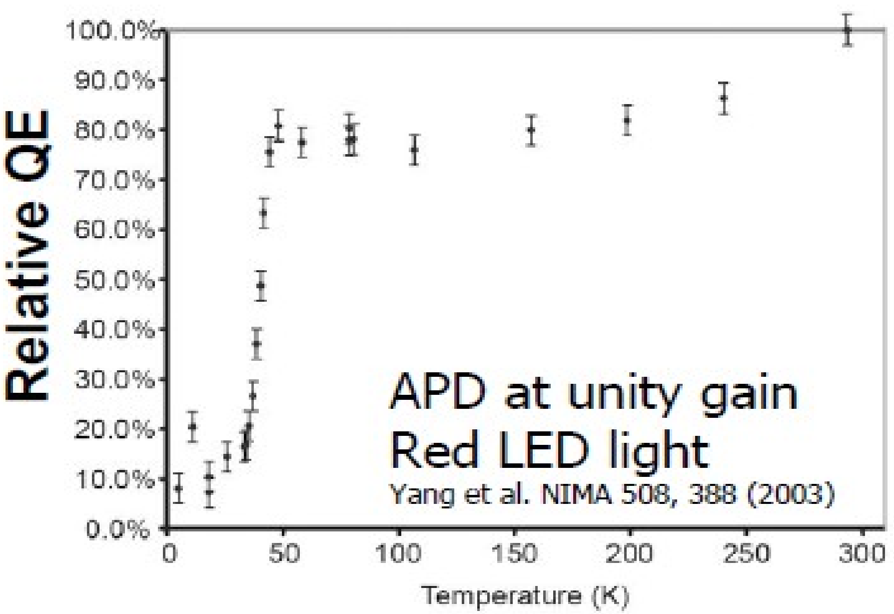

APD: Johnson et al (RMD) IEEE 2009

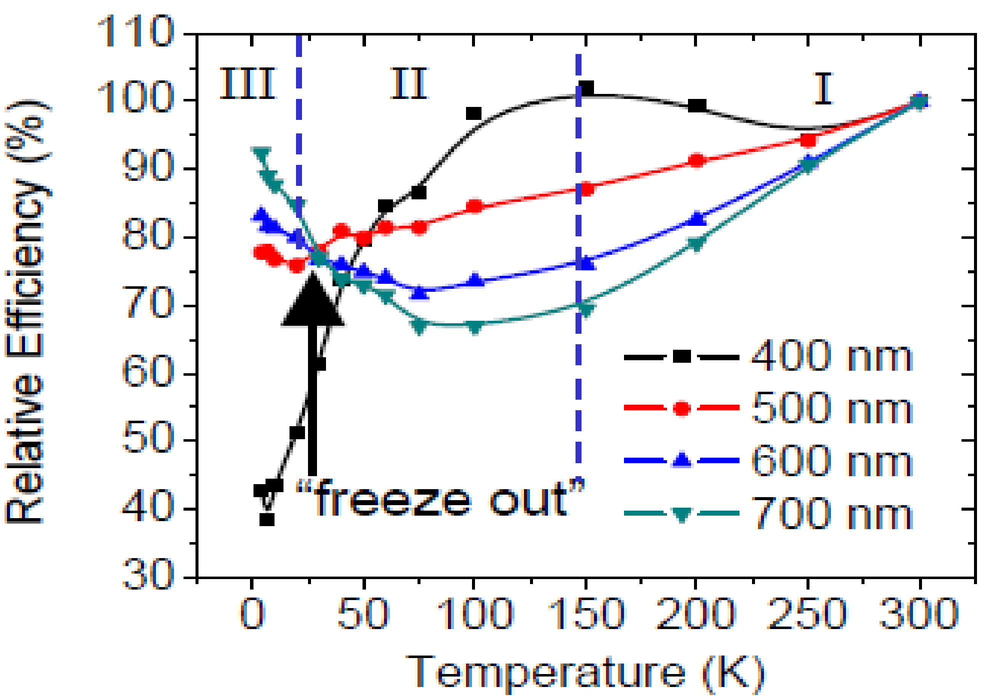

Timing

Many photons (simultaneous)

Dependence of SiPM timing on the number of simultaneous photons

Poisson statistics: $\sigma_t \propto 1/\sqrt{N_{pe}}$

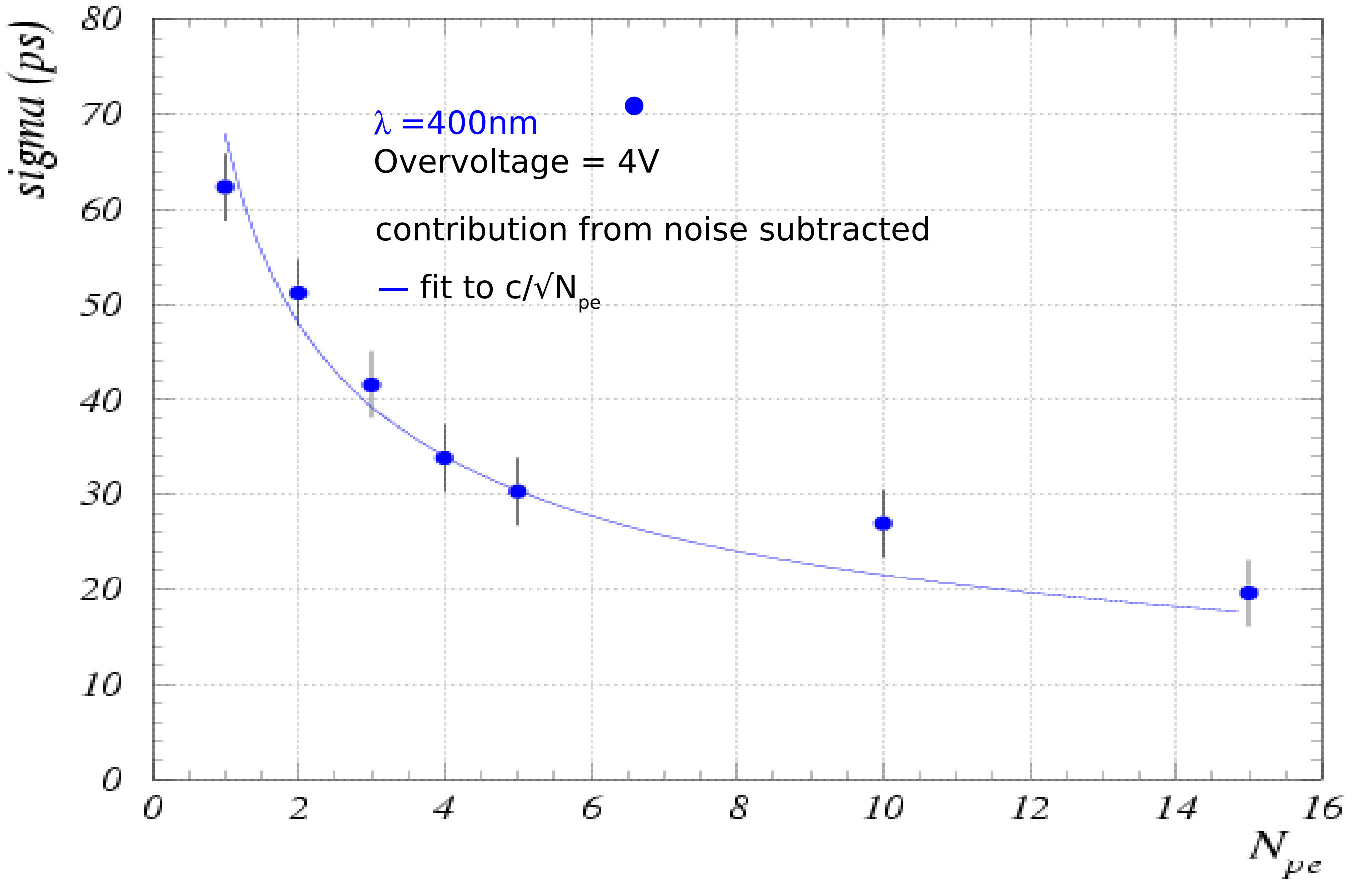

N of simultaneous photo-electrons

SPTR: HPK/CPTA comparison

T.Iijima – PD07
Nagoya and Lubiana groups

SiPM - HPK
(MPPC)

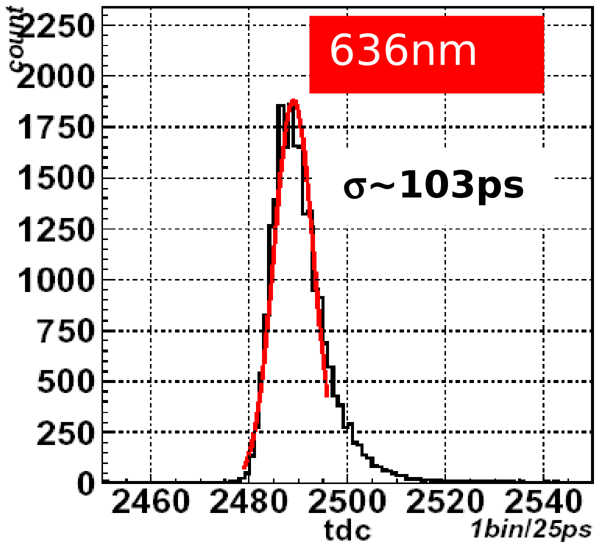

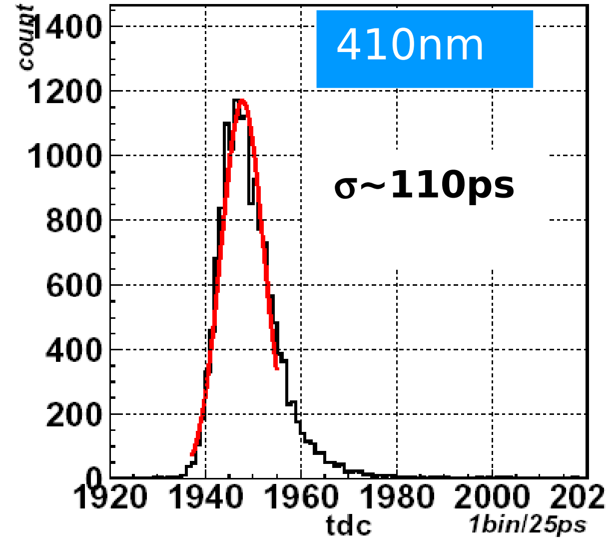

SIPM - CPTA
(MRS-APD)

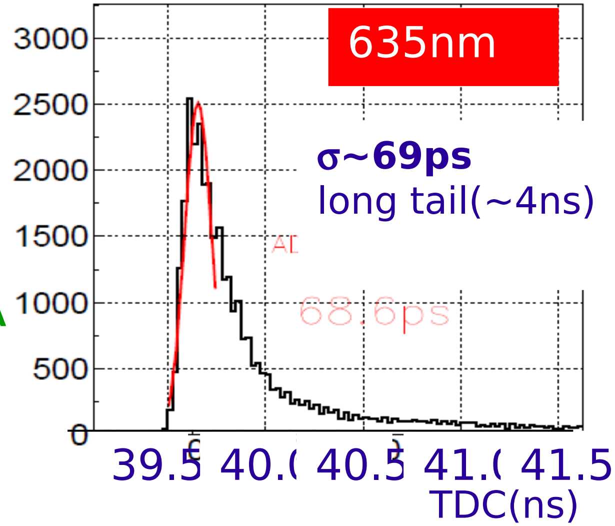

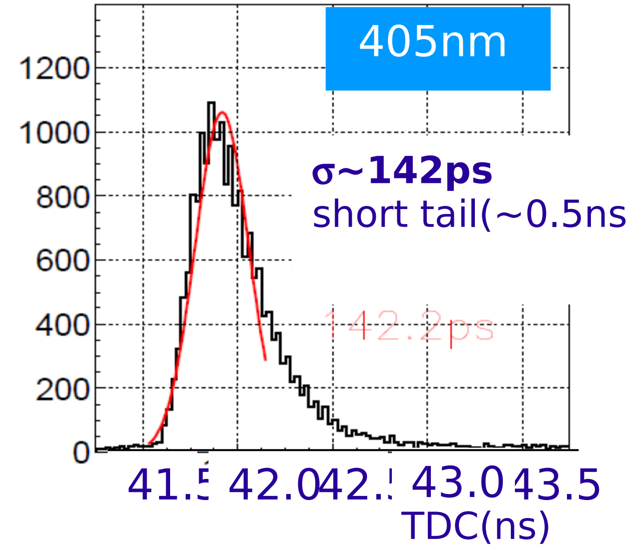

Method: CFD + TDC + Time walk corrections

Compatible with DASIPM measurements

SPTR: cell and sipm size dependence

B.Dolgoshein – LIGHT07

SiPM – MePhI/Pulsar:
576 cells (25x25μm^2)
Area = 1x1 mm^2

SiPM – MePhI/Pulsar:
1600 cells (100x100μm^2)
Area = 5x5 mm^2

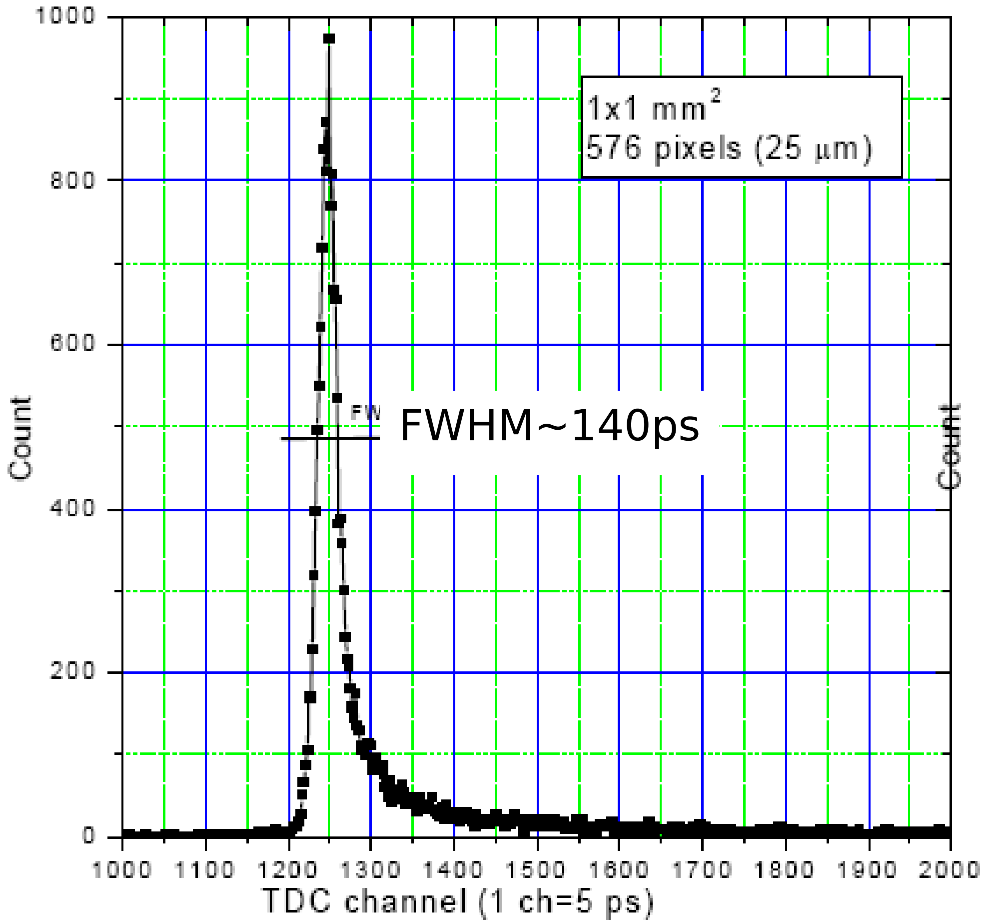

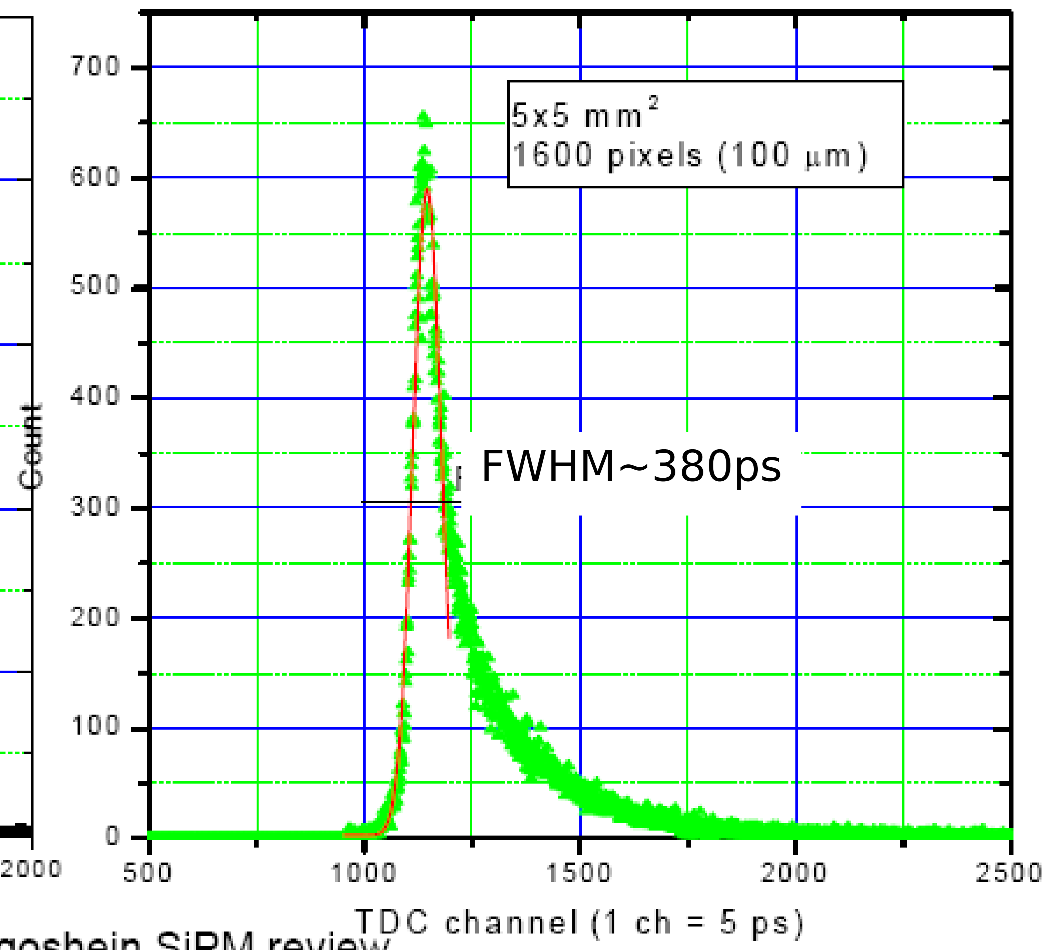

B.Dolgoshein,SiPM review

SiPM signal: effect of C_{tot} and Z_{load}

SiPM – MePhI/Pulsar:
1600 cells (100x100μm²)
Area = 5x5 mm²
C_{tot}~ 160pF

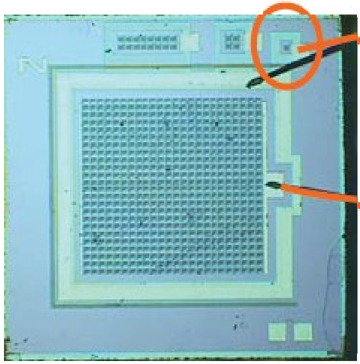

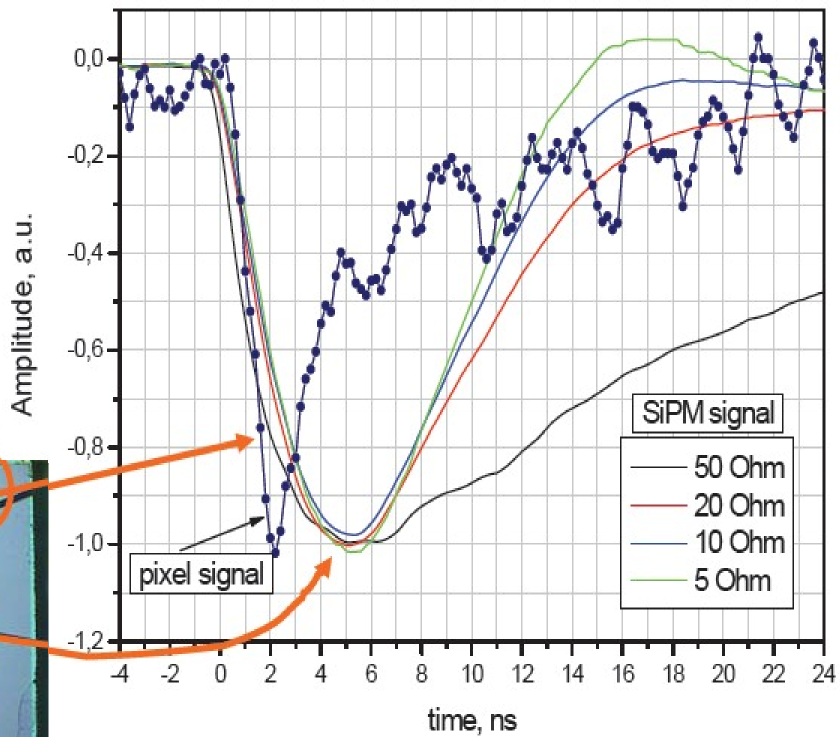

B.Dolgoshein and E.Popova
LIGHT07

Zin~50Ω
FWHM ~ 15ns

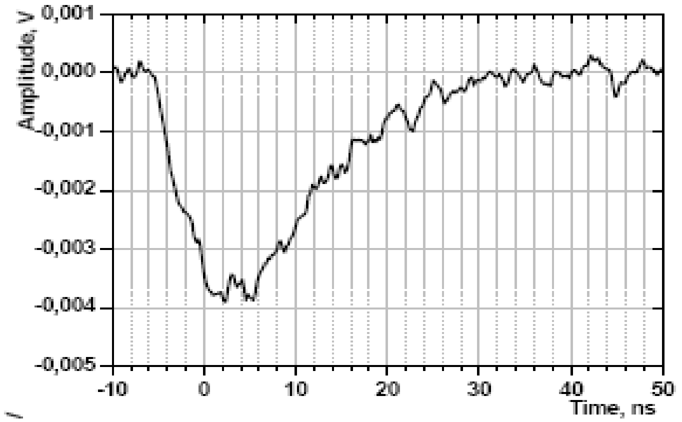

Zin~7Ω + shaper
FWHM ~ 2.5ns

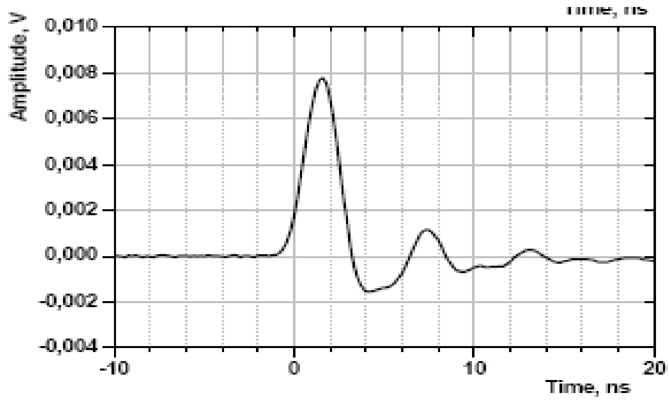

Trans-impedance amplifier

RPL model vs data: comparison ... not yet

Example of RPL simulation of pure electron injection in Si SPAD

Courtesy of C.H.Tan

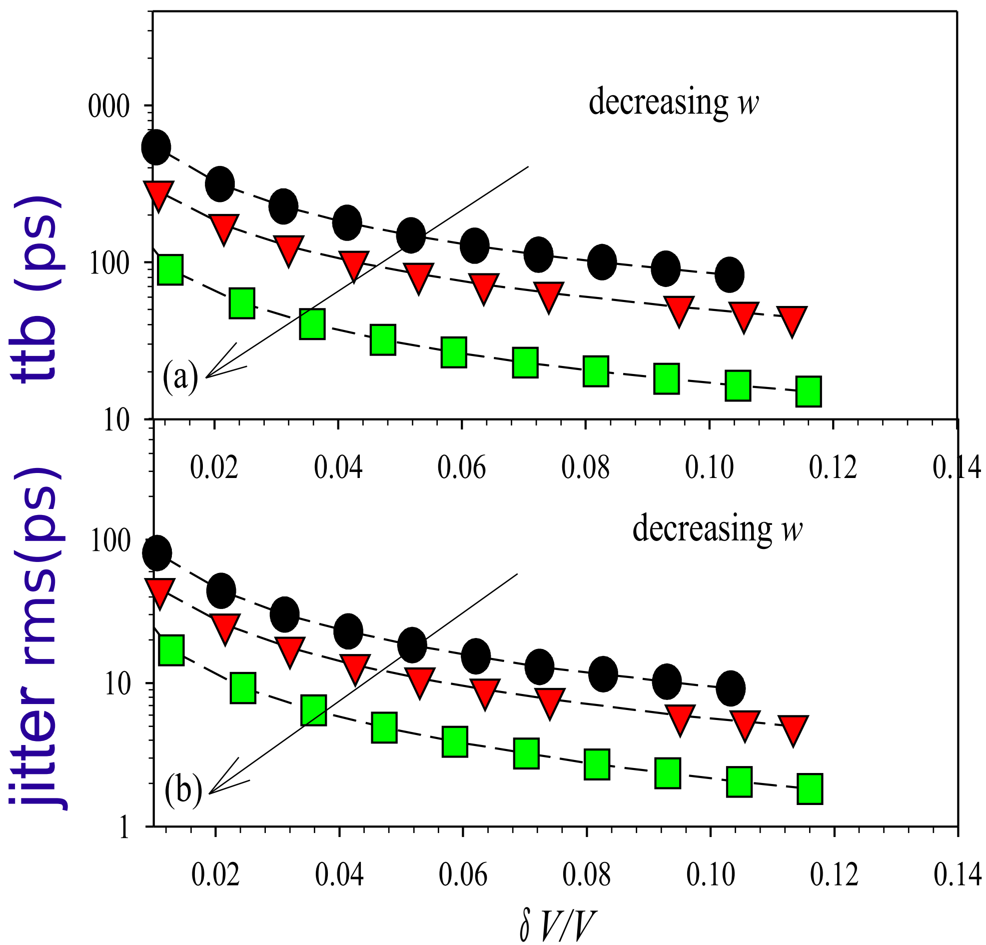

DATA
(DASIPM)

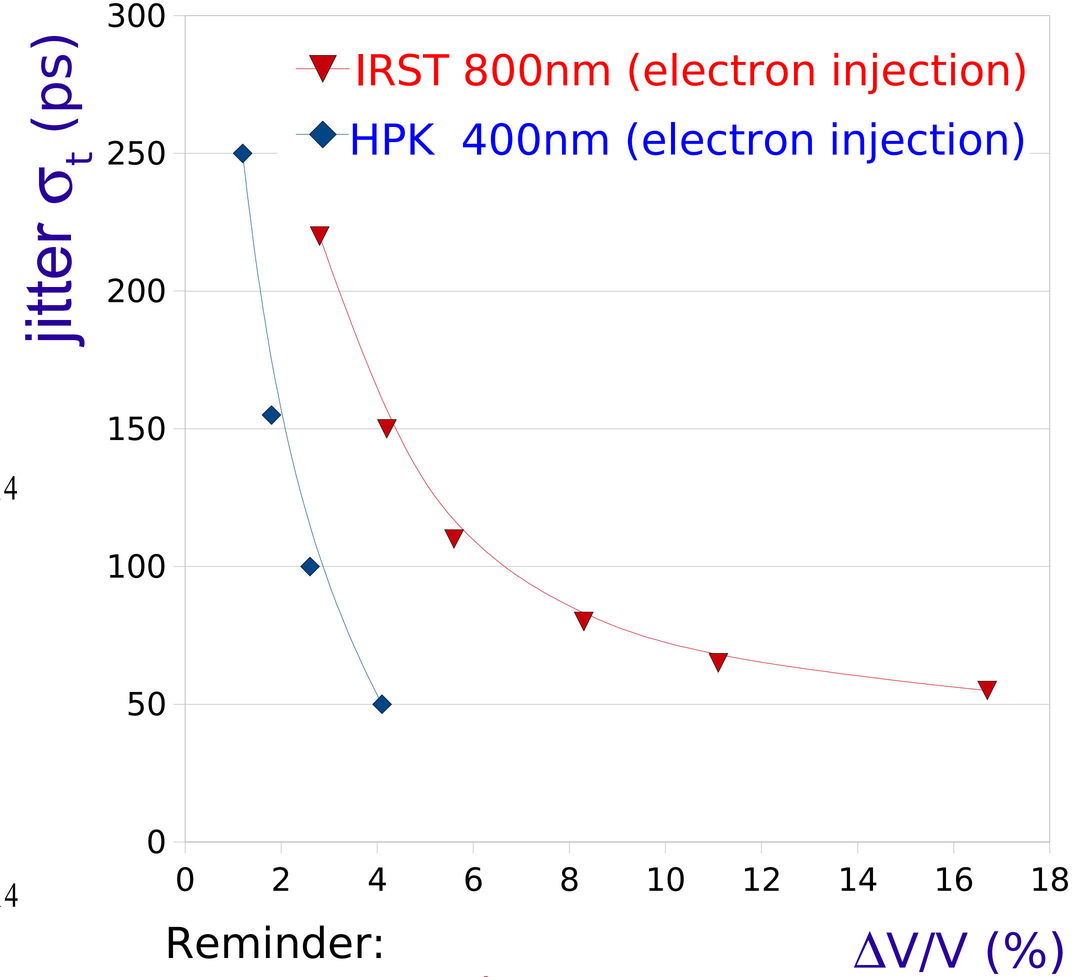

Reminder:
IRST structure is n on p
HPK structure is p on n

PDE

Photo-detection efficiency (PDE)

$$PDE = N_{pulses} / N_{photons} = QE \bullet P_{01} \bullet \varepsilon_{geom}$$

Carrier Photo-generation

(QE = probability for a photon to generate a carrier that reaches the high field region)

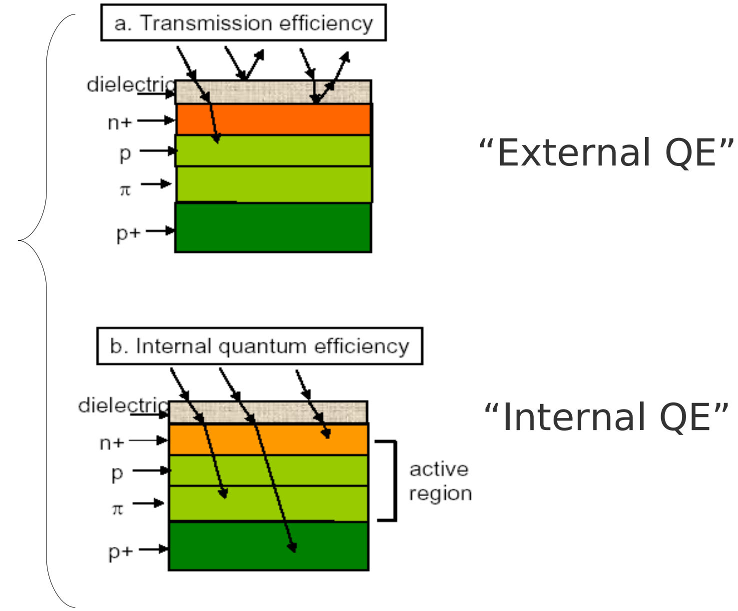

*

Avalanche triggering

(P_{01} = probability for a carrier traversing the high-field to generate the avalanche)

*

Geometrical fill factor

(ε = fraction of dead area due to structures between the cells, eg. guard rings, trenches)

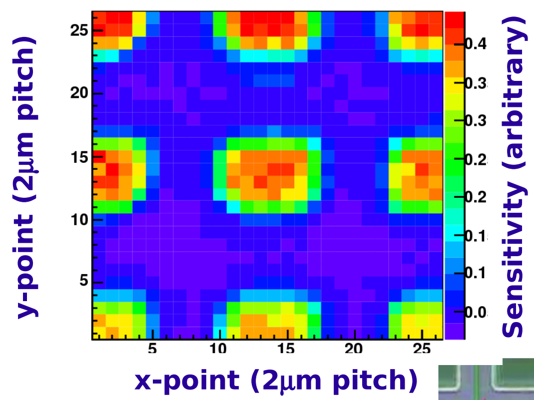

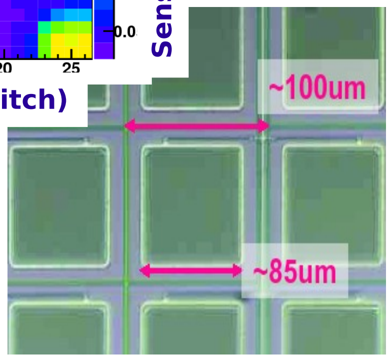

Hamamatsu SiPM close up

W.Oldham et al. IEEE TED (1972)

QE: Efficiency of a single cell

Two factors in QE:
(1) transmittance of the entrance window
(dielctric on top of silicon surface)
(2) probability of a photon inside to generate a e-h pair in the active layer (internal quantum efficiency)

Only the depleted region is fully active to efficiently photo-generate because of high recombination probability in the un-depleted regions.
Only a small layer ($\lambda_{diffsion} \sim \sqrt{D\tau_{recomb}}$) at the edge of un-depleted regions contributes to the photo-generation (critical for UV light)

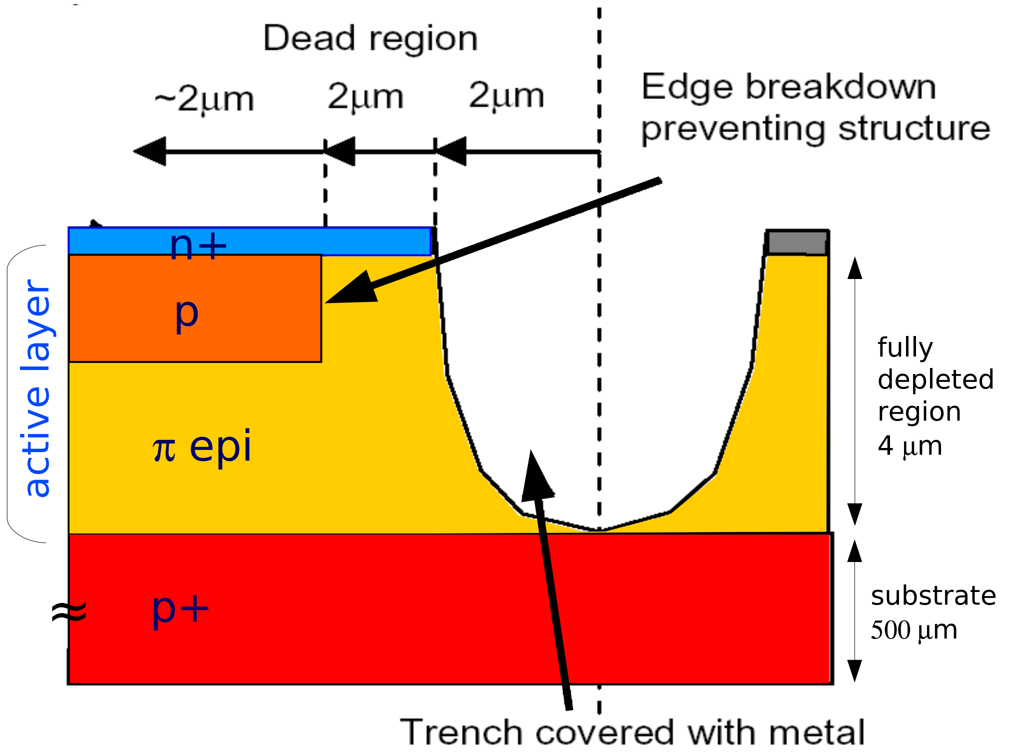

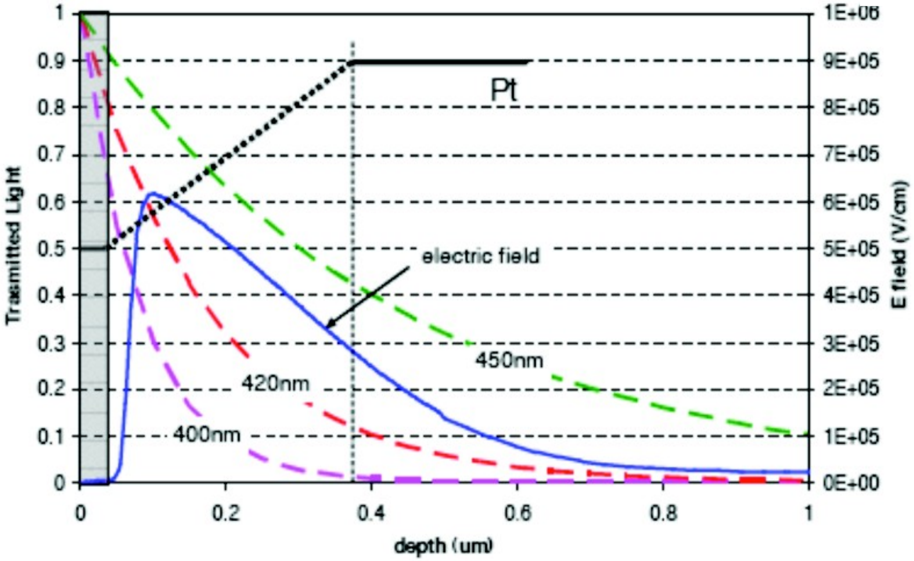

QE optimization

- Anti-reflective coating (ARC)
- Shallow junctions for short λ
- Thick epi layers for long λ

QE: Efficiency of a single cell

Direct access to internal QE and transmittance through ARC by measuring photo-voltaic regime (V_{bias}~ 0 V) the photon detection efficiency of a diode with the same n^+/p junction structure and same ARC

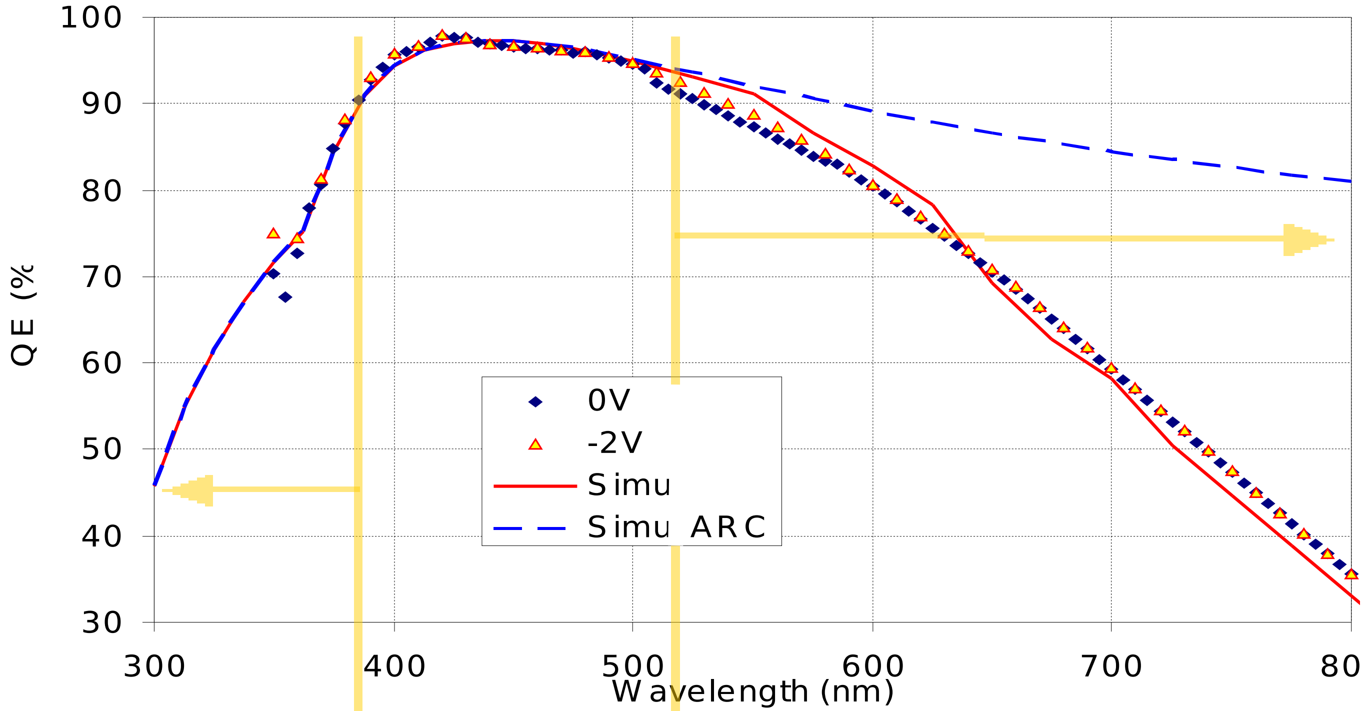

Reduced by ARC Transmittance

Reduced by the small π layer thickness

IRST devices

Avalanche trigger probability (P_{01})

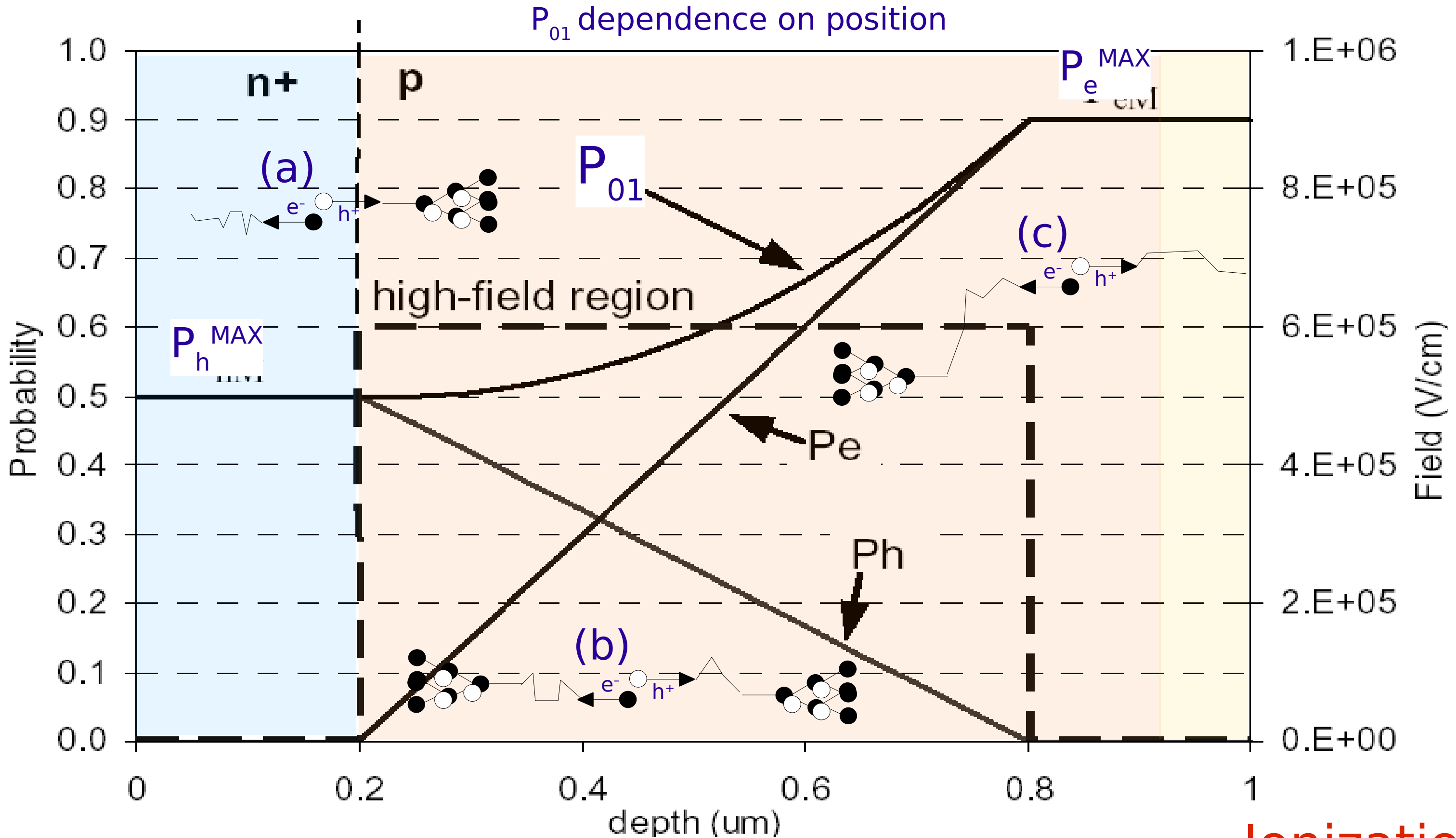

C.Piemonte
NIM A 568
(2006) 224

Example with constant high-field:
(a) only holes may trigger the avalanche
(b) both electrons and holes may trigger
(but in afraction of the high-field region)
(c) only electrons may trigger

Ionization rate in Silicon

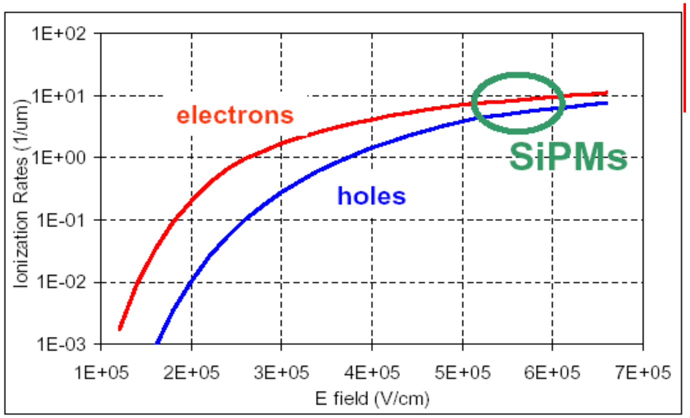

P_{01} optimization

- high over-voltage
- photo-generation in the p-side of the junction

Avalanche trigger probability (P_{01})

$P_{01} = PDE / QE / \varepsilon_{geom.}$

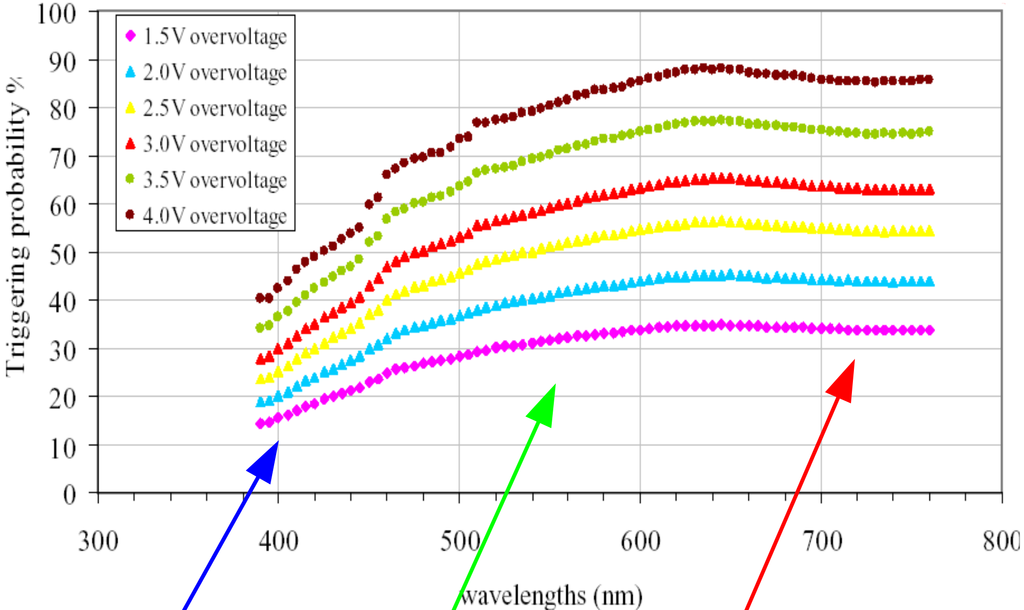

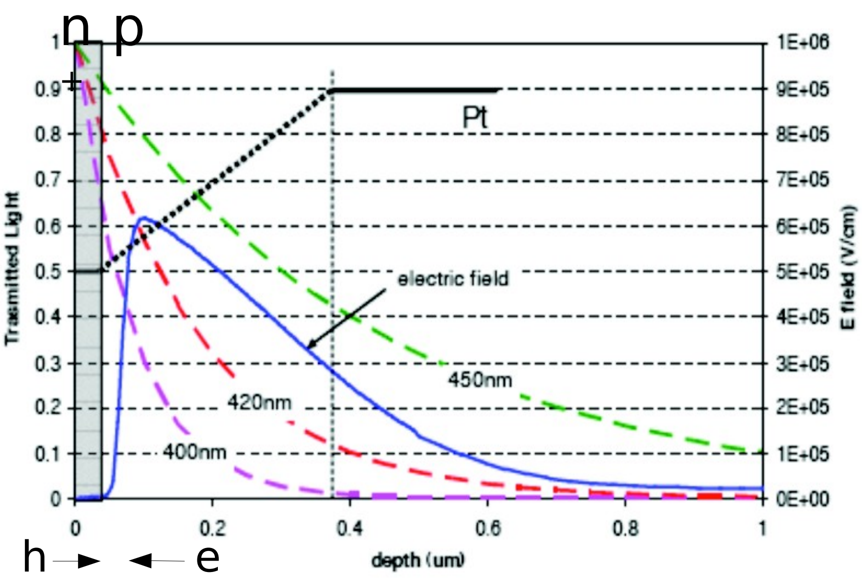

Only e⁻ cross the high E field region and trigger the avalanche

Both h⁺ and e⁻ might trigger the avalanche (but cross only a fraction of high field region)

Only h⁺ cross the high E field trigger the avalanche

IRST devices

PDE vs ΔV

"Statistics of Avalanche Current Buildup Time in Single-Photon Avalanche diodes"
C.H.Tan, J.S.Ng, G.J.Rees, J.P.R.David (Sheffield U.)
IEEE J.Quantum Electronics 13 (4) (2007) 906

RPL model Courtesy of C.H.Tan

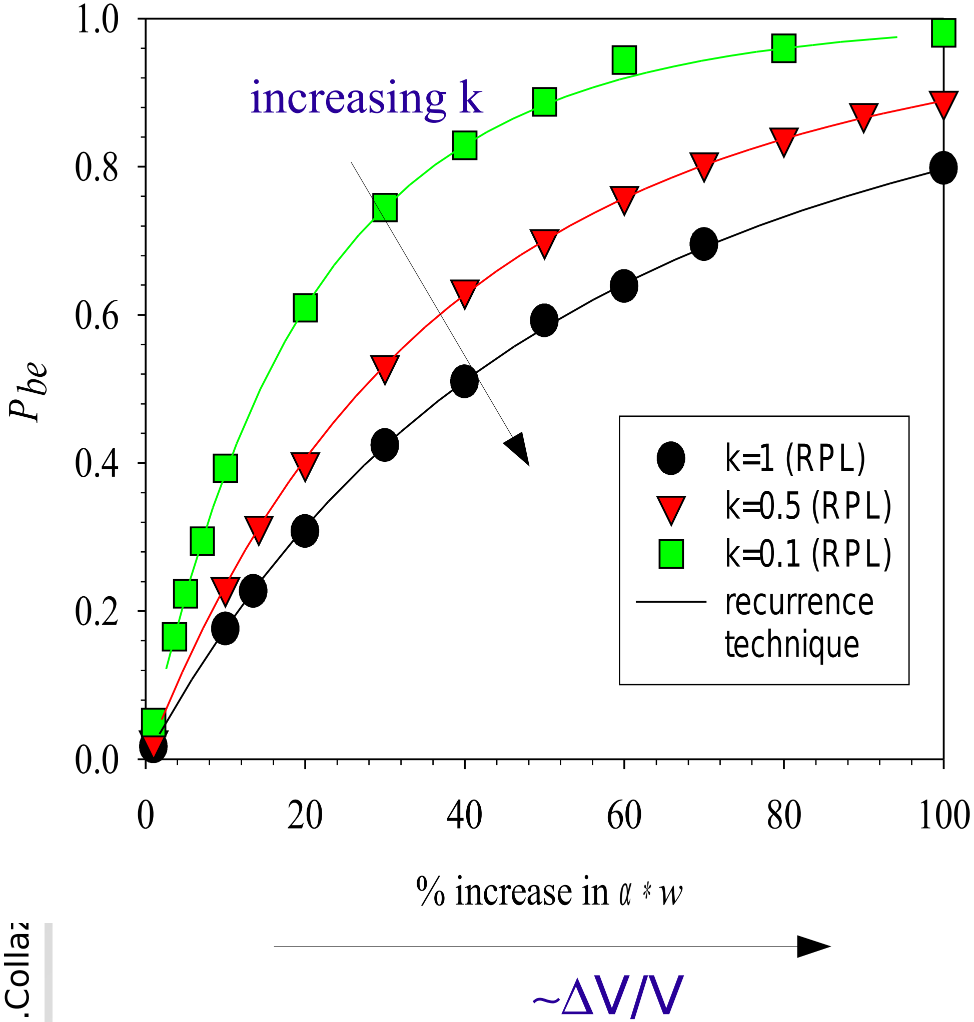

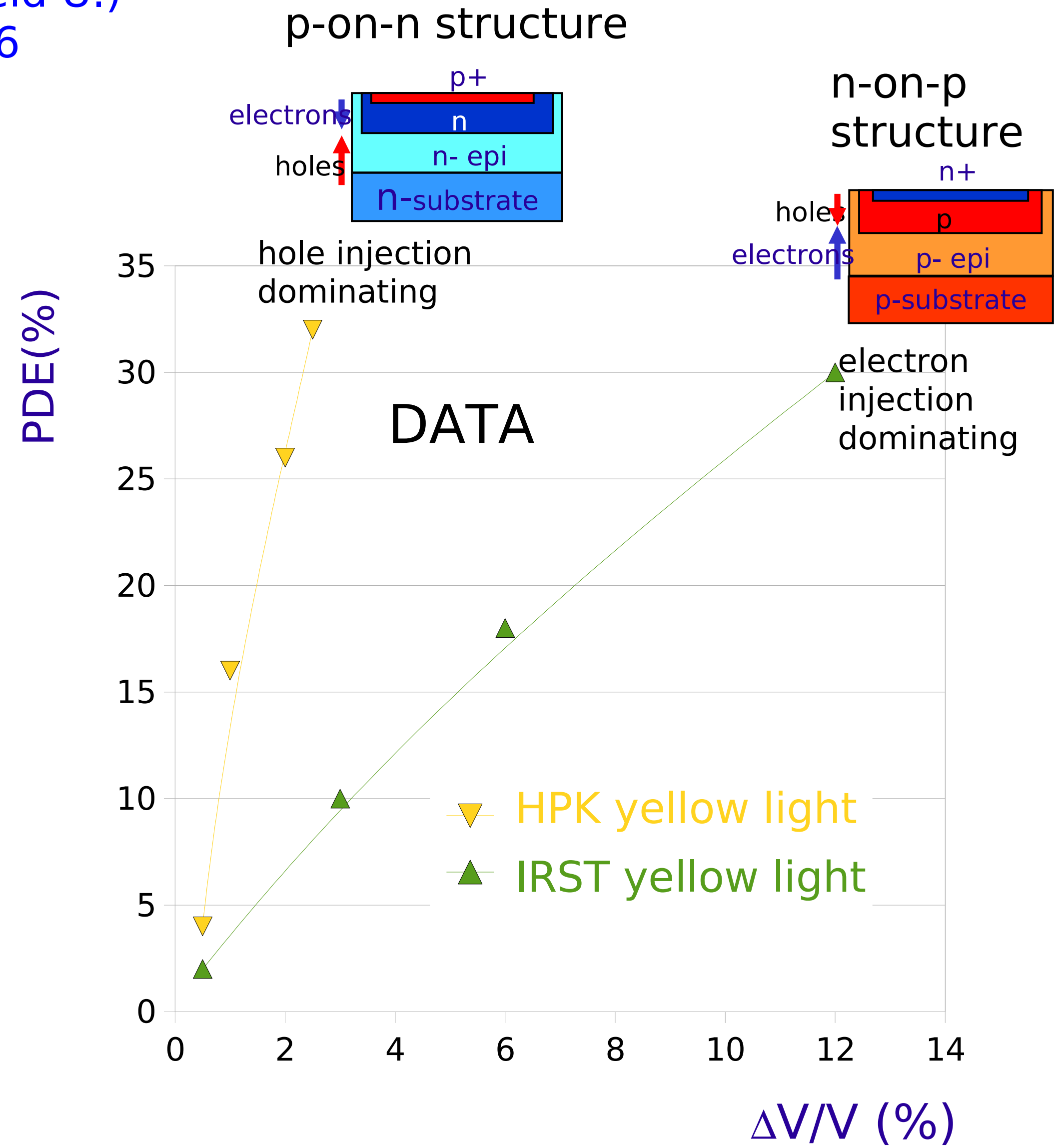

G.Collaz

PDE vs λ

N.Dinu et al. NIM A (2008) to be published

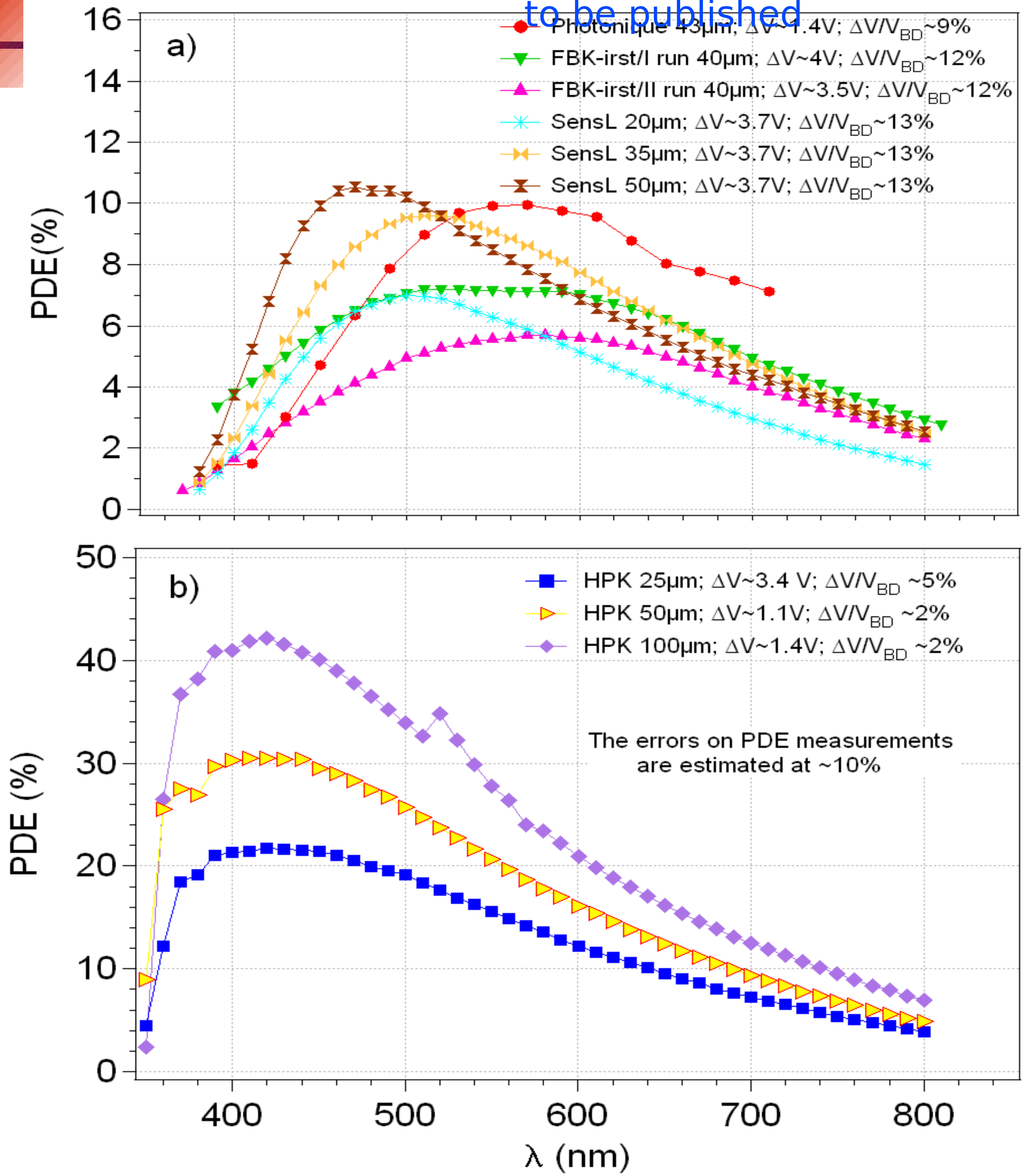

Fig. 5a) The PDE vs. λ of the Photonique, FBK-irst and SensL devices and b) HPK

n-on-p structures

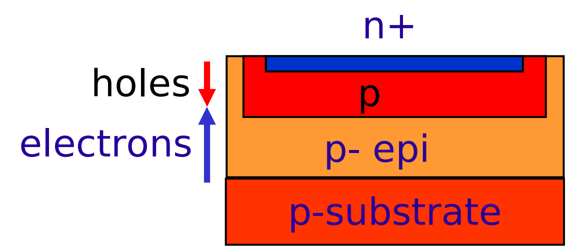

p-on-n structure

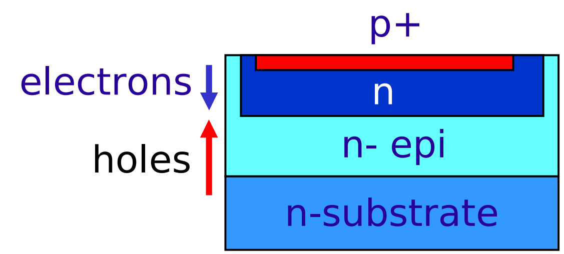

Note:
1) geometrical fill factor included
2) PDE in HPK catalog is 20%-30% more than the real PDE due to after-pulses and cross-talk

Radiation Hardness

Radiation damage: neutrons (0.1 -1 MeV)